Physics – Uspekhi **65** (9) 883 – 919 (2022)

REVIEWS OF TOPICAL PROBLEMS PACS numbers: 74.25.F –, **74.40. – n**, 74.78.Na

Superconducting quantum fluctuations in one dimension

A G Semenov, A D Zaikin

DOI: https://doi.org/10.3367/UFNe.2021.04.038962

Contents

Abstract. We review some recent developments in the field of quasi-one-dimensional superconductivity. We demonstrate that low temperature properties of superconducting nanowires are essentially determined by quantum fluctuations. Smooth (Gaussian) fluctuations of the superconducting phase (also associated with plasma modes propagating along a wire) may significantly affect the electron density of states in such nanowires and induce persistent current noise in superconducting nanorings. Further interesting phenomena, such as nonvanishing resistance and shot noise of the voltage in current-biased superconducting nanowires, are caused by non-Gaussian fluctuations of the order parameter — quantum phase slips (QPSs). Such phenomena may be interpreted in terms of the tunneling of fluxons playing the role of effective quantum 'particles' dual to Cooper pairs and obeying complicated full counting statistics, which reduces to the Poissonian one in the low frequency limit. We also demonstrate that QPS effects may be particularly pronounced in the thinnest wires and rings, where quantum phase slips remain unbound and determine a nonperturbative length scale L_c, beyond which the supercurrent gets suppressed by quantum fluctuations. Accordingly, for $T \to 0$, such nanowires should become insulating at scales exceeding L_c, whereas at shorter length scales they may still exhibit superconducting properties. We argue that certain nontrivial features associated with quantum fluctuations of the order parameter may be sensitive to a specific circuit topology and may be observed in structures like a system of capacitively coupled superconducting nanowires.

Keywords: superconductivity, low-dimensional systems, quantum fluctuations, quantum phase slips

A G Semenov [(1,2,*)], **A D Zaikin** [(1,2,†)]
[(1)] Lebedev Physical Institute,
Leninskii prosp. 53, 119991 Moscow, Russian Federation
[(2)] National Research University Higher School of Economics,
ul. Myasnitskaya 20, 101000 Moscow, Russian Federation
E-mail: [(*)]semenovag@lebedev.ru, [(†)]andrei.zaikin@kit.edu

Received 24 August 2020, revised 5 March 2021
Uspekhi Fizicheskikh Nauk **192** (9) 945 – 983 (2022)
Translated by A G Semenov

1. Introduction

The important role of fluctuations in a reduced dimension is widely known. Of special interest are fluctuation effects in low dimensional superconductors whose properties — in contrast to bulk structures — cannot in general be adequately described by means of the standard Bardeen–Cooper–Schrieffer (BCS) mean field theory. Fluctuations are most strongly pronounced in ultrathin superconducting wires, causing a large number of intriguing physical phenomena. Over recent decades, these phenomena have attracted a great

deal of attention of numerous researchers worldwide and have been discussed in detail in a number of recent books and review papers (see, e.g., [1–6]).

Can superconductivity also survive in structures of lower dimension, or do fluctuations disrupt any supercurrent in such systems? The answer to these questions are of both fundamental interest and practical importance due to rapidly progressing miniaturization of superconducting nanocircuits. According to a well-known theorem [7, 8], fluctuations destroy the true long-range order in low dimensional superconductors. With this in mind, one could attempt to conclude that low dimensional conductors cannot exhibit superconducting properties.

This conclusion, however, would be somewhat premature, because any generic superconducting system has a finite size in which case phase coherence can be preserved, at least to a certain extent. For instance, two-dimensional structures undergo Berezinskii–Kosterlitz–Thouless (BKT) phase transition [9–11] as a result of which the decay of correlations in space changes from exponential at fairly high temperatures to power law at lower T. This result implies that at low temperatures long range phase coherence does survive in samples of a finite size, and, hence, generic two-dimensional films can and do become superconducting.

Likewise, the general theorem [7, 8] does not yet allow one to make any definite conclusion about the presence or absence of superconductivity in quasi-one-dimensional wires of a finite length employed in any realistic experiment. Moreover, as we will see below, in the presence of quantum fluctuations, superconducting properties of such structures may crucially depend on a particular experimental configuration, which makes the whole situation even more complicated.

The superconducting state of a quasi-one-dimensional metallic wire can be described by means of a complex order parameter $\Delta(x) = |\Delta(x)| \exp[i\varphi(x)]$, where x is the coordinate along such a wire. Both thermal and quantum fluctuations cause deviations in the modulus as well as the phase of this order parameter from their equilibrium values. Such fluctuations can be divided into two different types: (i) small (Gaussian) fluctuations of the order parameter and (ii) non-Gaussian fluctuations, i.e., so-called *phase slips*. Both of these types of fluctuations are schematically illustrated in Fig. 1.

The effect of Gaussian superconducting fluctuations can be treated in a straightforward manner by expanding the exact gauge invariant expression for the effective action of a superconductor [12–14] in the fluctuating part of the order parameter $\Delta(x)$. In this way, one can, for example, derive the (negative) correction to the mean field (BCS) value of the order parameter Δ_0. In particular, at $T \to 0$, $\Delta = \Delta_0 - \delta\Delta_0$ is found with [15]

$$\frac{\delta\Delta_0}{\Delta_0} \sim \frac{1}{g_\xi} \sim \mathrm{Gi}_{1D}^{3/2} . \tag{1}$$

Here,

$$g_\xi = \frac{R_q}{R_\xi} \tag{2}$$

is dimensionless conductance, $R_q = 2\pi/e^2 \simeq 25.8\ \mathrm{k\Omega}$ is the quantum resistance unit, R_ξ is the normal state resistance of the wire segment of a length equal to the superconducting coherence length ξ, and Gi_{1D} is the so-called Ginzburg number in one dimension [3].

Note that in Eqn (1) fluctuations of both the phase and the absolute value of the order parameter make contributions of the same order. This estimate demonstrates that, at low temperatures, order parameter suppression due to Gaussian fluctuations in superconducting nanowires remains weak as long as $g_\xi \gg 1$, and, in full accordance with general expectations, it becomes important only for extremely thin wires with $\mathrm{Gi}_{1D} \sim 1$ and $g_\xi \sim 1$.

It is also important to emphasize that, even if the absolute value $|\Delta|$ does not fluctuate, the superconducting phase φ can still do so. In the limit $g_\xi \gg 1$, phase fluctuations in superconducting wires can be essentially decoupled from those of $|\Delta|$. Such phase fluctuations are controlled by the dimensionless admittance

$$g = \frac{R_q}{Z_w} , \tag{3}$$

where $Z_w = \sqrt{\mathcal{L}_{kin}/C}$ is the wire impedance, $\mathcal{L}_{kin} = 1/(\pi\sigma_N \Delta s)$ and C are, respectively, the kinetic wire inductance (times length) and the geometric wire capacitance (per length), $\sigma_N = 2e^2 \nu_F D$ is the normal state Drude conductance of the wire, ν_F is the density of states at the Fermi level, and s is the wire cross section. Such phase fluctuations are intimately related to sound-like plasma modes [16] (so-called Mooij–Schön modes), which can propagate along superconducting wires with velocity $v = 1/\sqrt{\mathcal{L}_{kin} C}$. The dimensionless impedance $g \propto \sqrt{s}$ constitutes another important parameter which, along with $g_\xi \propto s$, also accounts for Gaussian superconducting fluctuations in ultrathin nanowires.

Let us now turn to non-Gaussian fluctuations of the order parameter produced by phase slips. A nontrivial fluctuation of this kind corresponds to the temporal suppression of $|\Delta(x)|$ down to zero at some point $x = x_0$ inside the wire, as shown in Fig. 1b. As soon as the modulus of the order parameter $|\Delta(x_0)|$ vanishes, the phase $\varphi(x_0)$ becomes unrestricted and can jump by the value $2\pi n$, where n is any integer. After this process, the modulus $|\Delta(x_0)|$ gets restored, the phase becomes single valued again, and the system returns to its initial state, accumulating the net phase shift $2\pi n$. Provided such phase slip events are sufficiently rare, one can restrict n to $n = \pm 1$ and totally disregard fluctuations with $|n| \geqslant 2$.

Phase slips may have a strong impact on the behavior of sufficiently thin superconducting wires. For instance, as was first pointed out by Little [17], quasi-one-dimensional wires made of a superconducting material can acquire a finite resistance below the superconducting critical temperature T_C of a bulk material due to the mechanism of thermally activated phase slips (TAPSs). This mechanism works as follows.

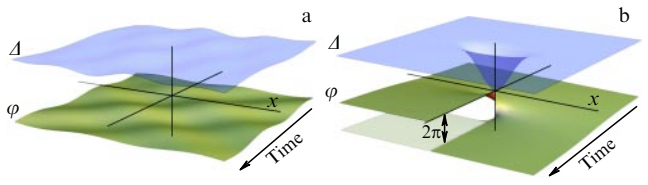

Figure 1. Schematics of small fluctuations of the order parameter (a) and the phase slip process (b) in superconducting nanowires. During the latter process, the absolute value of order parameter Δ gets locally and temporarily suppressed due to thermal and/or quantum fluctuations, while its phase φ undergoes a jump by $\pm 2\pi$.

According to the Josephson relation, each phase jump by $\delta\varphi = \pm 2\pi$ implies a positive or negative voltage pulse $\delta V = \dot{\varphi}/2e$. In the absence of any bias current, the net average numbers of positive ($n = +1$) and negative ($n = -1$) phase slips are equal; thus, the net voltage drop across the wire remains zero. Applying current $I \propto |\Delta|^2 \nabla\varphi$, a nonzero phase gradient is created along the wire, making 'positive' phase slips prevail over 'negative' ones. Hence, the net voltage drop V due to TAPS differs from zero, i.e., thermal fluctuations cause nonzero resistance $R = V/I$ of superconducting wires even below T_C.

A quantitative theory of this TAPS phenomenon was initially worked out by Langer and Ambegaokar [18], who employed the standard Ginzburg–Landau equations and evaluated the TAPS rate within the exponential accuracy. A more accurate analysis of the TAPS rate, including the pre-exponential factor, was performed by McCumber and Halperin [19], who employed the so-called time-dependent Ginzburg–Landau (TDGL) equations. More recently, it was realized that the TDGL-based approach is not sufficiently accurate to account for the effect of quantum fluctuations and, hence, to correctly determine the pre-exponent in the expression for the TAPS rate. Appropriate modifications of the LAMH (Langer–Ambegaokar–McCumber–Halperin) theory have been worked out [15] employing the general effective action approach [12–14].

This theory predicts that the TAPS creation rate and, hence, resistance of a superconducting wire R below T_C are determined by the activation exponent

$$R(T) \propto \exp\left(-\frac{\delta F}{T}\right), \tag{4}$$

where δF is the free energy difference or, in other words, an effective potential barrier which the system should overcome in order to create a phase slip. The height of this potential barrier is determined by the superconducting condensation energy for that part of the wire where superconductivity is destroyed by thermal fluctuations. At temperatures close to T_C, Eqn (4) yields appreciable resistivity, which was indeed detected in experiments [20, 21] performed on small superconducting whiskers with typical diameters in the range of ~ 0.5 μm. Close to T_C, the experimental results fully confirm the activation behavior of $R(T)$ expected from Eqn (4). However, as the temperature is lowered further below T_C, the number of TAPSs inside the wire decreases exponentially, and no measurable wire resistance is predicted by Eqn (4).

Recent progress in the nanolithographic technique has allowed the fabrication of samples with much smaller diameters down to ~ 10 nm or even below. In such systems, one can consider a possibility of phase slips occurring, not only due to thermal, but also due to *quantum* fluctuations in the superconducting order parameter. The physical picture describing such quantum phase slips (QPSs) is qualitatively similar to that of TAPSs (Fig. 1b), except the order parameter $|\Delta(x)|$ gets virtually suppressed due to the process of quantum tunneling rather than thermal activation. As a result, the superconducting phase again experiences jumps by $\delta\varphi = \pm 2\pi$.

Following standard quantum mechanical arguments, one can expect that the probability of such a tunneling process has to be controlled by the exponent $\sim \exp(-\delta F/\omega_0)$, i.e., temperature T must be replaced by some attempt frequency ω_0 in the activation exponent (4). This is because the order parameter field $\Delta(x)$ now tunnels under the barrier δF rather than overcoming it by thermal activation. Since this tunneling process should obviously persist down to $T = 0$, we arrive at a fundamentally important conclusion that such nanowires should demonstrate a nonvanishing resistivity down to the lowest temperatures. This effect was predicted and investigated theoretically in [12, 14] and received its convincing experimental confirmation in [22–26].

According to the present theory, quantum phase slip effects are controlled by the QPS amplitude per unit wire length [14]

$$\gamma_{\mathrm{QPS}} = b\left(\frac{g_\xi \Delta}{\xi}\right) \exp(-a g_\xi), \tag{5}$$

where, as before, Δ is the superconducting order parameter, and $a \sim 1$ and $b \sim 1$ are numerical prefactors. It follows immediately from Eqn (5) that — provided parameter g_ξ is not too large — QPS effects in superconducting nanowires (similarly to Gaussian fluctuations) are pronounced and need to be properly accounted for. Conversely, by choosing the dimensionless conductance g_ξ sufficiently large, one can suppress both these types of fluctuations in the superconducting order parameter.

Note that, although the dimensionless admittance g (3) does not enter directly into the QPS amplitude (5), it nevertheless plays an important role in the physics of quantum phase slips, because, as we already pointed out, it accounts for Mooij–Schön plasma modes propagating along the wire. Different quantum phase slips interact by exchanging such plasmons and, hence, parameter g controls the strength of inter-QPS interactions. By reducing the wire diameter, g is also reduced, and we eventually arrive at the superconductor–insulator quantum phase transition [12] that occurs at $T \to 0$. In other words, quantum fluctuations may drive a superconducting nanowire not only into a resistive but also into an insulating state.

Thus, we conclude that the same dimensionless parameters (2) and (3) which account for small fluctuations in the order parameter also essentially control the physics of quantum phase slips. These two parameters will play a central role in our further considerations.

The main purpose of this paper is to review some recent developments in the field. In doing so, we will merely emphasize fundamental aspects of the phenomena under consideration, focusing our attention on recent advances in the theory of quantum fluctuations in superconducting nanowires and nanorings. Wherever necessary, we will also briefly indicate relevant experiments and possible applications of the effects in question.

The structure of our review paper is as follows. In Section 2, we will analyze the effect of small (Gaussian) quantum fluctuations in the phase of the order parameter on the electron density of states in ultrathin superconducting wires. The same type of fluctuations causing supercurrent noise in superconducting nanorings will be addressed in Section 3. Section 4 will be devoted to the important issue of phase–charge duality in superconducting nanowires and nanorings in the presence of quantum phase slips. The effect of quantum phase slips on both the supercurrent and its fluctuations in superconducting nanorings will be investigated in Section 5. Voltage fluctuations in superconducting nanowires, such as shot noise associated with quantum phase slips, will be described in Section 6. In Section 7, we will outline a theory of full counting statistics for quantum phase slips. Topology-

controlled quantum phase transitions and superconducting fluctuation effects will be analyzed in Section 8. In Section 9, we will address several interesting phenomena associated with quantum phase slips in capacitively coupled superconducting nanowires. The paper concludes with a short summary in Section 10.

2. Quantum phase fluctuations and local density of states

Let us consider a long superconducting wire with sufficiently small diameter $\sim\sqrt{s}<\xi$ attached to two big superconducting reservoirs, as displayed in Fig. 2. The superconducting properties of the wire are described by the order parameter field $\Delta(x,t)=|\Delta(x,t)|\exp(\mathrm{i}\varphi(x,t))$, which depends both on the coordinate along the wire x and on time t. The wire remains in thermodynamic equilibrium at low enough temperature $T\ll|\Delta|$, and its parameters are chosen such that one can safely ignore fluctuations in the absolute value of the order parameter, which is set to be independent of both x and t, i.e., $|\Delta(x,t)|=\Delta$. As we already described above, this situation can be achieved provided the dimensionless conductance g_ξ remains very large, $g_\xi\gg1$.

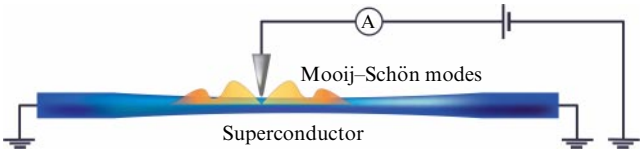

Figure 2. Narrow superconducting wire together with a circuit which could be employed for DOS measurements.

On the other hand, we will allow for fluctuations of the phase variable $\varphi(x,t)$ along the wire and keep the dimensionless impedance g not very large. Our main goal in this section is to demonstrate that such fluctuations can affect and significantly alter the local electron density of states (DOS) of superconducting nanowires. The physical origin of this effect is directly related to the presence of Mooij–Schön plasma modes propagating along the wire and forming an effective environment for electrons inside the system. As will be demonstrated below, interaction between electrons and such plasma modes can lead to substantial modifications and smearing of the local electron DOS inside superconducting nanowires [27].

2.1 Green's functions in the presence of phase fluctuations

In order to proceed, we will note that, typically, the motion of electrons in metallic nanowires is diffusive, implying that the elastic electron mean free path ℓ in such wires is much smaller than the superconducting coherence length ξ. This electron motion can be described quasiclassically with the aid of the standard approach based on the Keldysh version of the Usadel equations [28, 29]

$$\left[\partial_t\sigma_3-\mathrm{i}\check{\Delta}+\mathrm{i}e\check{V}\hat{1},\check{G}\right]-\frac{D}{2}\,\hat{\partial}\left[\check{G},\hat{\partial}\check{G}\right]=0 \tag{6}$$

for the quasiclassical electron Green–Keldysh matrix function

$$\check{G}=\begin{pmatrix}\hat{G}^{\mathrm{R}} & \hat{G}^{\mathrm{K}}\\ 0 & \hat{G}^{\mathrm{A}}\end{pmatrix},$$

which also obeys the normalization condition $\check{G}^2=\check{1}$. Both retarded and advanced 2×2 Green's functions are 2×2 matrices in the Nambu space

$$\hat{G}^{\mathrm{R,A}}=\begin{pmatrix}G^{\mathrm{R,A}} & F^{\mathrm{R,A}}\\ \tilde{F}^{\mathrm{R,A}} & -G^{\mathrm{R,A}}\end{pmatrix},$$

whereas the Keldysh matrix has the form $\hat{G}^{\mathrm{K}}=\hat{G}^{\mathrm{R}}\hat{h}-\hat{h}\hat{G}^{\mathrm{A}}$, where $\hat{h}$ is the matrix distribution function. In Eqn (6), we showed the covariant spatial derivative $\hat{\partial}(\ldots)=\partial_x(\ldots)+\mathrm{i}e\left[\check{A}_x\sigma_3,(\ldots)\right]$, $[a,b]=ab-ba$ denotes the commutator, V and A are the scalar and vector potentials of the electromagnetic field, $D=v_{\mathrm{F}}\ell/3$ is the diffusion coefficient, $\tau_{1,2,3}$ and $\sigma_{1,2,3}$ stand for the Pauli matrices, respectively, in Keldysh and Nambu spaces, and $\check{\Delta}$ is the superconducting order parameter matrix.

The electron DOS $\nu(E,x)$ is related to the quasiclassical Green's functions in a simple way as

$$\nu(E,x)=\nu_{\mathrm{F}}\,\mathrm{tr}\,\frac{\sigma_3}{4}\left(G^{\mathrm{R}}(E,x)-G^{\mathrm{A}}(E,x)\right), \tag{7}$$

where ν_{F} stands for DOS in a normal metal at the Fermi level and

$$\check{G}(E,x)=\int\mathrm{d}(t-t')\exp\left[\mathrm{i}E(t-t')\right]\check{G}(t,t',x). \tag{8}$$

It will be convenient for us to perform the rotation in the Keldysh space expressing initial field variables, e.g., the phase of the order parameter $\varphi_{\mathrm{F,B}}$ on the forward and backward branches of the Keldysh time contour in terms of their classical and quantum components $\varphi_+=(\varphi_{\mathrm{F}}+\varphi_{\mathrm{B}})/2$, $\varphi_-=\varphi_{\mathrm{F}}-\varphi_{\mathrm{B}}$. We also define the matrices

$$\check{\varphi}=\begin{pmatrix}\varphi_+ & \dfrac{\varphi_-}{2}\\ \dfrac{\varphi_-}{2} & \varphi_+\end{pmatrix}. \tag{9}$$

Employing the gauge transformation

$$e\check{V}\to\check{\Phi}\equiv e\check{V}+\frac{\dot{\check{\varphi}}}{2}, \tag{10}$$

$$e\check{A}_x\to\check{\mathcal{A}}\equiv e\check{A}_x-\frac{\partial_x\check{\varphi}}{2}, \tag{11}$$

$$\Delta_\pm\to|\Delta|_\pm, \tag{12}$$

we expel the phase of the order parameter from $\Delta(x,t)$ and get

$$\check{G}(t,t',x)=\exp\left[\frac{\mathrm{i}}{2}\check{\varphi}(t,x)\sigma_3\right]\check{\tilde{G}}(t,t',x)\times\exp\left[-\frac{\mathrm{i}}{2}\check{\varphi}(t',x)\sigma_3\right],$$

where $\check{\tilde{G}}$ obeys Eqn (6) combined with Eqns (10)–(12). In the next subsection, we will show that one can safely put gauge invariant combinations $\mathcal{A}\to0$ and $\Phi\to0$ and choose $\check{\tilde{G}}$ equal to the Green's function $\check{\Lambda}$ of a uniform superconductor in thermodynamic equilibrium, i.e.,

$$\check{\tilde{G}}=\check{\Lambda}=\begin{pmatrix}\Lambda^{\mathrm{R}} & \Lambda^{\mathrm{K}}\\ 0 & \Lambda^{\mathrm{A}}\end{pmatrix}, \tag{13}$$

where

$$\Lambda^{\mathrm{R}}_\epsilon=\frac{1}{\sqrt{(\epsilon+\mathrm{i}0)^2-\Delta^2}}\begin{pmatrix}\epsilon & \Delta\\ -\Delta & -\epsilon\end{pmatrix}, \tag{14}$$

$\Lambda^{\rm A} = -\sigma_3(\Lambda^{\rm R})^\dagger\sigma_3$ and

$$\Lambda^{\rm K}_\epsilon = \Lambda^{\rm R}_\epsilon F_\epsilon - F_\epsilon \Lambda^{\rm A}_\epsilon\,, \quad F_\epsilon = \tanh\left(\frac{\epsilon}{2T}\right). \tag{15}$$

Then, we obtain

$$\check{G}(t,t',x) \simeq \exp\left[\frac{\rm i}{2}\check{\varphi}(t,x)\sigma_3\right]\check{\Lambda}(t-t') \times \exp\left[-\frac{\rm i}{2}\check{\varphi}(t',x)\sigma_3\right], \tag{16}$$

where $\check{\Lambda}(t-t')$ is the inverse Fourier transform of $\check{\Lambda}_\epsilon$.

2.2 Effective action for phase fluctuations

In order to evaluate any physical observable, one needs to average the corresponding variable over all possible phase configurations. This can be done by means of the path integral technique employing an effective action $S_{\rm eff}$ which controls phase fluctuations in our system at sufficiently low energies. This action was microscopically derived and analyzed elsewhere [1, 2, 13, 14]. Here, we recover this action from simple symmetry arguments.

It is well known that global U(1) symmetry is broken in a superconductor, whereas local gauge symmetry remains preserved. Within this picture, the phase of the order parameter plays the role of a Goldstone boson, implying that the action should be constructed from the gauge invariant quantities $\mathcal{A}$ and Φ rather than from the phase derivatives only. The simplest appropriate form of the action then reads

$$S_{\rm le}[\varphi,V,A_x] = S_{\rm em}[V,A_x] + \int {\rm d}t \int {\rm d}x\,\left[\zeta_1(2eV+\dot{\varphi})^2 - \zeta_2(\partial_x\varphi - 2eA_x)^2\right], \tag{17}$$

where $S_{\rm em}[V,A_x]$ is action for the electromagnetic field and $\zeta_{1,2}$ are some constants. In the case of a quasi-one-dimensional wire, we have

$$S_{\rm em}[V,A_x] = \frac{1}{2}\int {\rm d}t \int {\rm d}x\left[CV^2 - \frac{A_x^2}{\mathcal{L}}\right], \tag{18}$$

where C is the capacitance per unit wire length and $\mathcal{L}$ is the geometric inductance times unit length. The constants $\zeta_{1,2}$ can be identified by evaluating the response to static fields V and A_x with the result

$$\zeta_1 = \frac{v_{\rm F}s}{4}\,, \qquad \zeta_2 = \frac{1}{8e^2\mathcal{L}_{\rm kin}}\,. \tag{19}$$

Integrating out the electromagnetic potentials, we arrive at the effective action for the phase variable

$$S_{\rm eff}[\varphi] = \int {\rm d}t \int {\rm d}x\left[\frac{v_{\rm F}sC}{4(C+2e^2v_{\rm F}s)}\,\dot{\varphi}^2 - \frac{1}{8e^2(\mathcal{L}+\mathcal{L}_{\rm kin})}(\partial_x\varphi)^2\right]. \tag{20}$$

In the case of interest to us, diffusive metallic wires with a diameter of the order of the superconducting coherence length $\xi = \sqrt{D/\Delta}$, we find $C \ll 2e^2v_{\rm F}s$ and $\mathcal{L} \ll \mathcal{L}_{\rm kin}$. We then obtain

$$S_{\rm eff}[\varphi] = \frac{C}{8e^2}\int {\rm d}t \int {\rm d}x\left[\dot{\varphi}^2 - \frac{1}{C\mathcal{L}_{\rm kin}}(\partial_x\varphi)^2\right]. \tag{21}$$

Following the same route, fluctuations of the variables Φ and $\dot{\varphi}$ can be linked to each other. From the equations of motion, we get

$$\Phi = \frac{C}{C+2e^2v_{\rm F}s}\,\dot{\varphi} \approx \frac{1}{4E_Cv_{\rm F}s}\,\dot{\varphi} \ll \dot{\varphi}\,, \tag{22}$$

and, hence, the effects related to weak ($\propto \Phi$) penetration of the fluctuating electric field inside the wire can be safely ignored [13, 14]. Here and below, $E_C = e^2/(2C)$ stands for the charging energy of a unit wire length. As usual, magnetic effects related to fluctuations in $\mathcal{A}$ can also be disregarded in the nonrelativistic limit considered here.

For the sake of completeness, let us also comment on the differences between the superconducting metal considered here and a neutral superfluid. In the latter situation, there is no interaction with the electromagnetic field which can be formally achieved by taking the limit $\mathcal{L} \to 0$ and $C \to \infty$, i.e., the opposite condition $C \gg 2e^2v_{\rm F}s$ is realized. Accordingly, the gauge transformation trick would not work anymore in this case. This fact constitutes a clear manifestation of the fundamental difference between the situations of global and local gauge symmetry breaking.

2.3 Density of states

In order to evaluate the electron DOS, we need to average Green's function (16) over all possible phase configurations. This averaging is conveniently accomplished by means of the path integral technique, which yields

$$\langle\check{G}\rangle_\varphi(t-t') = \int D\varphi\,\exp\left({\rm i}S^{\rm K}_{\rm eff}[\varphi]\right)\check{G}(t,t',x)\,, \tag{23}$$

where $S^{\rm K}_{\rm eff}[\varphi]$ is the effective Keldysh action which accounts for phase fluctuations in a superconducting wire. As we demonstrated above, at low enough energies, it can be written in the form

$$S^{\rm K}_{\rm eff}[\varphi] = \frac{1}{16E_C}\,{\rm tr}\left[\begin{pmatrix}\varphi_+ & \varphi_-\end{pmatrix}\mathcal{V}^{-1}\begin{pmatrix}\varphi_+\\ \varphi_-\end{pmatrix}\right], \tag{24}$$

where

$$\mathcal{V} = \begin{pmatrix}\mathcal{V}^{\rm K} & \mathcal{V}^{\rm R}\\ \mathcal{V}^{\rm A} & 0\end{pmatrix} \tag{25}$$

is the equilibrium Keldysh matrix propagator describing plasma modes and

$$\mathcal{V}^{\rm R,A}(\omega,k) = \frac{1}{(\omega\pm{\rm i}0)^2 - (vk)^2}\,, \tag{26}$$

$$\mathcal{V}^{\rm K}(\omega,k) = \frac{1}{2}\left(\mathcal{V}^{\rm R}(\omega,k) - \mathcal{V}^{\rm A}(\omega,k)\right)\coth\left(\frac{\omega}{2T}\right). \tag{27}$$

Making use of the structure of $\check{\Lambda}$ in the Nambu space and performing Gaussian integration, we get

$$\begin{aligned} \nu(E) &= \nu_{\rm F}\int {\rm d}(t-t')\exp\left[{\rm i}E(t-t')\right]\,{\rm tr}\left\langle\frac{\tau_3\sigma_3}{4}\right. \\ &\quad\left.\times\exp\left[\frac{\rm i}{2}\,\check{\varphi}(t,x)\sigma_3\right]\check{\Lambda}(t-t')\exp\left[-\frac{\rm i}{2}\,\check{\varphi}(t',x)\sigma_3\right]\right\rangle_\varphi \\ &= \nu_{\rm F}\int {\rm d}t\,\exp({\rm i}Et)\,{\rm tr}\left[\frac{\tau_3\sigma_3}{4}\,\tau_a\check{\Lambda}(t)\tau_b\mathcal{B}^{ab}(t)\right], \end{aligned} \tag{28}$$

where $a, b = \{0, 1\}$, $\tau_0 \equiv \hat{1}$,

$$\mathcal{B}(t) = \begin{pmatrix} \mathcal{B}^{\mathrm{K}}(t) & \mathcal{B}^{\mathrm{R}}(t) \\ \mathcal{B}^{\mathrm{A}}(t) & 0 \end{pmatrix} = \exp\left[2\mathrm{i}E_C\left(\mathcal{V}^{\mathrm{K}}(t) - \mathcal{V}^{\mathrm{K}}(0)\right)\right] \times \begin{pmatrix} \cos\left[E_C\left(\mathcal{V}^{\mathrm{R}}(t) - \mathcal{V}^{\mathrm{A}}(t)\right)\right] & \mathrm{i}\sin\left(E_C\mathcal{V}^{\mathrm{R}}(t)\right) \\ \mathrm{i}\sin\left(E_C\mathcal{V}^{\mathrm{A}}(t)\right) & 0 \end{pmatrix}, \quad (29)$$

$$\mathcal{V}(t) \equiv \mathcal{V}(t, 0) = \int \frac{\mathrm{d}\omega\,\mathrm{d}k}{(2\pi)^2} \exp(-\mathrm{i}\omega t)\,\mathcal{V}(\omega, k)\,. \quad (30)$$

Note that Eqn (28) accounts for all emission and absorption processes of multiple plasmons in our system via an auxiliary propagator $\mathcal{B}$. This propagator obeys the standard causality requirements and satisfies the bosonic fluctuation-dissipation theorem (FDT), because plasmons remain in thermodynamic equilibrium (cf. Eqn (27)).

Employing this theorem and taking traces both in Keldysh and in Nambu spaces, from Eqn (28) we obtain

$$\begin{aligned}\langle\nu\rangle_{\varphi}(E) &= \frac{\nu_{\mathrm{F}}}{4}\int \mathrm{d}t\,\exp(-\mathrm{i}Et)\,\mathrm{tr}\Big[\sigma_3\big(\Lambda^{\mathrm{R}}(t) - \Lambda^{\mathrm{A}}(t)\big)\mathcal{B}^{\mathrm{K}}(t) \\ &\quad + \sigma_3\Lambda^{\mathrm{K}}(t)\big(\mathcal{B}^{\mathrm{R}}(t) - \mathcal{B}^{\mathrm{A}}(t)\big)\Big] \\ &= \int \frac{\mathrm{d}\epsilon}{2\pi}\,\nu_{\mathrm{BCS}}(\epsilon)\mathcal{B}^{\mathrm{K}}(E-\epsilon)(1 + F_\epsilon F_{E-\epsilon})\,, \end{aligned} \quad (31)$$

where $\nu_{\mathrm{BCS}}(\epsilon)$ is the BCS density of states in a bulk superconductor.

Since, for $\epsilon \gtrsim E + 2T$, the combination $1 + F_\epsilon F_{E-\epsilon}$ decays as $\propto \exp[(E-\epsilon)/T]$, the electron DOS at subgap energies is suppressed by the factor $\sim \exp[(E-\Delta)/T]$, and at $T \to 0$ the superconducting gap Δ is not affected by Mooij–Schön plasmons at all.

Evaluating $\mathcal{B}^{\mathrm{K}}$ in Eqn (29), we find

$$\mathcal{B}^{\mathrm{K}}(t) = \exp\left[-\frac{1}{g}\int_0^{\omega_{\mathrm{c}}} \mathrm{d}\omega\,\frac{1-\cos(\omega t)}{\omega}\coth\left(\frac{\omega}{2T}\right)\right] \times \cos\left[\frac{1}{g}\int_0^{\omega_{\mathrm{c}}} \mathrm{d}\omega\,\frac{\sin(\omega t)}{\omega}\right], \quad (32)$$

where an exponential high frequency cutoff at $\omega_{\mathrm{c}} \sim \Delta$ is implied. This cutoff procedure is consistent with the fact that the effective action (24)–(27) remains applicable only at energies well below the superconducting gap.

Equation (32) provides a lot of useful information about the effect of phase fluctuations on the DOS. For instance, the identity

$$\int \mathrm{d}E\left(\nu(E) - \nu_{\mathrm{BCS}}(E)\right) = 0 \quad (33)$$

(which follows directly from the condition $\mathcal{B}^{\mathrm{K}}(t=0) = 1$) implies that phase fluctuations can only redistribute the electron states among different energies without affecting the energy integrated DOS. In the low temperature limit $T \to 0$, Eqn (32) reduces to

$$\mathcal{B}^{\mathrm{K}}(t) = \left(\frac{\sinh(\pi T t)}{\pi T t}\sqrt{1 + (\omega_{\mathrm{c}}t)^2}\right)^{-1/g} \times \cos\left(\frac{\arctan(\omega_{\mathrm{c}}t)}{g}\right). \quad (34)$$

It is also instructive to evaluate the Fourier transform of Eqn (32) $\mathcal{B}^{\mathrm{K}}_{\omega}$. After some algebra, we obtain [27]

$$\mathcal{B}^{\mathrm{K}}_{\omega} \simeq \cosh\left(\frac{\omega}{2T}\right)\left(\frac{2\pi T}{\omega_{\mathrm{c}}}\right)^{1/g}\frac{\left|\Gamma\left[1/(2g) + \mathrm{i}\omega/(2\pi T)\right]\right|^2}{2\pi T\Gamma(1/g)}\,, \quad (35)$$

where ω remains well below the superconducting gap Δ, and $\Gamma(x)$ is the Euler gamma function. At low frequencies $\omega \ll T$, Eqn (35) reduces further to

$$\mathcal{B}^{\mathrm{K}}_{\omega} \simeq \frac{1}{g\omega_{\mathrm{c}}}\left(\frac{2\pi T}{\omega_{\mathrm{c}}}\right)^{1/g}\frac{2\pi T}{\omega^2 + (\pi T/g)^2}\,, \quad (36)$$

whereas, for the frequency interval $T \ll \omega \ll \Delta$, we find

$$\mathcal{B}^{\mathrm{K}}_{\omega} \simeq \frac{\pi}{\omega_{\mathrm{c}}\Gamma(1/g)}\left(\frac{\omega}{\omega_{\mathrm{c}}}\right)^{1/g-1}. \quad (37)$$

Making use of the above expressions, at energies in the vicinity of the superconducting gap Δ, we arrive at the following result for the electron DOS:

$$\nu(\Delta + \omega) = \frac{\nu_{\mathrm{F}}\sqrt{\Delta}}{\sqrt{2}}\left(\frac{2\pi T}{\Delta}\right)^{1/g}\sum_{k=0}^{\infty}\frac{\Gamma(k+1/g)}{k!\Gamma(1/g)} \times \mathrm{Re}\left(\frac{\exp\left[-\mathrm{i}\pi/(2g)\right]}{\sqrt{\omega + 2\mathrm{i}\pi T\left[1/(2g) + k\right]}}\right). \quad (38)$$

The energy dependent DOS $\nu(E)$ for superconducting nanowires in the presence of phase fluctuations is also displayed in Fig. 3 at different temperatures and two different values of the parameter g. We observe that at $T \neq 0$ the BCS singularity at $E \to \Delta$ is smeared due to interactions between Mooij–Schön plasmons and electrons propagating inside the wire. For the same reason, the electron DOS at subgap energies $0 < E < \Delta$ remains nonzero at any nonzero T, i.e.,

$$\nu(E) \propto \exp\left(\frac{E-\Delta}{T}\right). \quad (39)$$

We also note that, at bigger values of g, the function $\nu(E)$ demonstrates a nonmonotonic behavior at energies slightly above the gap (Fig. 3a), whereas, at smaller g, the DOS decreases monotonically with decreasing energy at all E not far from the gap (Fig. 3b). In the zero temperature limit $T \to 0$ and for $E - \Delta \ll \Delta$, we obtain

$$\nu(E) \simeq \frac{\nu_{\mathrm{F}}\sqrt{\pi}\theta(E-\Delta)}{\sqrt{2}\Gamma(1/2 + 1/g)}\left(\frac{E-\Delta}{\Delta}\right)^{1/g-1/2}. \quad (40)$$

This result demonstrates that, while at $E < \Delta$ the electron DOS at $T = 0$ vanishes at all values of g, the behavior of $\nu(E)$ (40) at overgap energies differs, depending on the dimensionless conductance g. For relatively thicker wires with $g > 2$, the DOS singularity at $E \to \Delta$ survives, becoming progressively weaker with decreasing g. In contrast, for thinner wires with $g \leqslant 2$, the DOS singularity is washed out completely due to intensive phase fluctuations and $\nu(E)$ tends to zero at $E \to \Delta$ as a power law (40). This behavior is also illustrated in Fig. 3c.

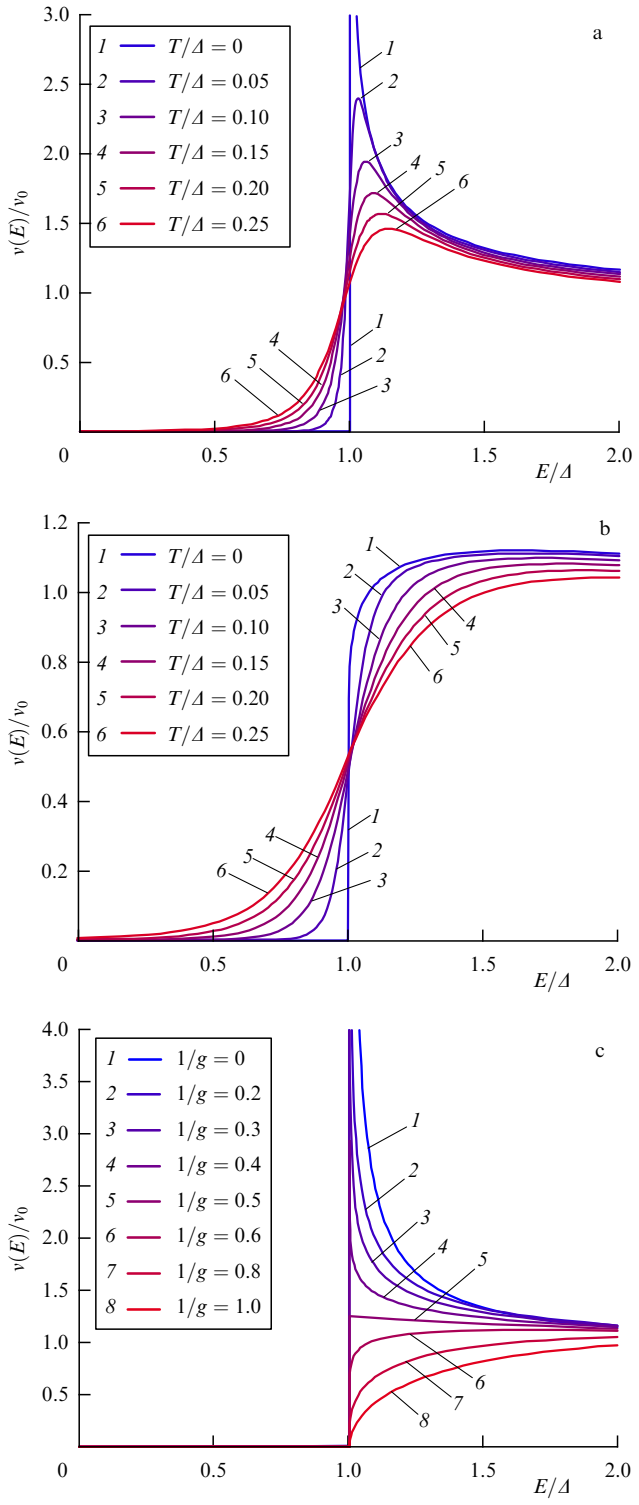

Figure 3. Normalized energy dependent electron DOS $\nu(E)/\nu_F$ for superconducting nanowires at different temperatures and two values of $g = 5$ (a) and $g = 1.67$ (b) as well as at $T = 0$ and different values of g (c). Energy E and temperature T are expressed in units of Δ.

2.4 Summary and comparison with experiments

To summarize, we demonstrated that *local* properties of superconducting nanowires, such as the electron density of states, can be sensitive to phase fluctuations in such nanowires. At this stage, we intentionally restricted our analysis to the effect of small phase fluctuations associated with low energy sound-like plasma modes propagating along a wire and forming an effective quantum dissipative environment for electrons inside the wire.

The coupling strength between electrons inside the wire and such an effective plasmon environment is controlled by the dimensionless parameter g. For relatively thick wires with $g \gg 1$ or, equivalently, provided the wire impedance Z_w remains much smaller than the quantum resistance unit R_q, phase fluctuations weakly affect the electron DOS except in the immediate vicinity of the superconducting gap Δ. For larger values $Z_w \sim R_q$, the effect of phase fluctuations becomes strong and has to be treated nonperturbatively as $1/g$ at all energies.

At any nonzero T, the electron DOS depends on temperature and substantially deviates from that derived from the standard BCS theory. In particular, at $T > 0$, the BCS square-root singularity in DOS at $E = \Delta$ gets totally smeared, and $\nu(E)$ differs from zero at subgap energies as well (cf. Eqn (39)). This behavior can be interpreted in terms of a depairing effect due to the interaction between electrons and Mooij–Schön plasmons. We also note that our results are consistent with the phenomenological Dynes formula [30]

$$\nu(E) \simeq \nu_F \,\mathrm{Re}\left(\frac{E + \mathrm{i}\Gamma}{\sqrt{(E+\mathrm{i}\Gamma)^2 - \Delta^2}}\right), \tag{41}$$

describing smearing of the BCS singularity in the DOS in the immediate vicinity of the superconducting gap.

At $T = 0$ and subgap energies, the electron DOS vanishes as in the BCS theory, while the BCS singularity in the DOS at $E \to \Delta$ becomes weaker for any finite $g > 2$ and eventually disappears for $g \leqslant 2$.

The local electron DOS in superconducting nanowires can be probed in a standard manner by performing a tunneling experiment, as is also illustrated in Fig. 2. Attaching a normal or superconducting electrode to our wire and measuring the differential conductance of the corresponding tunnel junction, direct access to the energy dependent electron DOS of a superconducting nanowire is obtained. For instance, in the case of a normal electrode at $T \to 0$ and $eV > \Delta$, we find

$$\frac{\mathrm{d}I}{\mathrm{d}V} \propto \nu(eV) \propto \left(V - \frac{\Delta}{e}\right)^{1/g-1/2}. \tag{42}$$

This power law dependence of the differential conductance resembles the one encountered in small normal tunnel junctions at low voltages $\mathrm{d}I/\mathrm{d}V \propto V^{2/g_N}$ [31], where g_N is the dimensionless conductance of normal leads. In fact, both dependence (42) and the zero bias anomaly in normal metallic junctions [31] are caused by Coulomb interaction and are controlled by the impedance of the corresponding effective electromagnetic environment.

Experiments similar to that described above were performed with both thicker ($\sqrt{s} > 40$ nm) and ultrathin ($\sqrt{s} < 35$ nm) titanium nanowires [32]. While the shape of $I-V$ curves measured for thicker wires agrees well with the standard BCS-like DOS, qualitatively different behavior was found in thinner nanowires. Namely, upon decreasing the wire diameter, (i) smaller and smaller values of the superconducting gap Δ in titanium were observed and (ii) progressively stronger smearing of the gap singularity was detected. Observation (i) is consistent with theoretical results [15] predicting suppression of the order parameter by quantum fluctuations. Indeed, as the inverse dimensionless

conductance $1/g_\xi$ increases with decreasing wire diameter, the order parameter suppression becomes more pronounced (cf. Eqn (1)), as was indeed observed in experiments [32].

Observed effect (ii) can be interpreted in terms of theoretical predictions [27] outlined in this section. For instance, the experimentally detected temperature dependence of the nonvanishing DOS tail at subgap energies [32] agrees well with our Eqn (39). We conclude that experimental observations [32] clearly support our theory, thus, also serving as an independent confirmation of the existence of Mooij–Schön plasmons in superconducting nanowires. Earlier, such plasma modes were also detected within a different experimental scheme in Ref. [33].

3. Gaussian phase fluctuations in superconducting rings

Let us now consider a somewhat different configuration for which small (Gaussian) fluctuations of the superconducting phase variable $\varphi(x,t)$ also yield interesting physical effects. We will consider a superconducting wire with cross section s closed in the form of a ring of radius R pierced by an external magnetic flux Φ_x (Fig. 4). As before, the wire is assumed to be thick enough (implying that $g_\xi \gg 1$) to be able to fully ignore fluctuations of the absolute value of the order parameter field $|\Delta(x,\tau)|$, where x is now the coordinate along the ring and τ is the imaginary time, $0 \geqslant \tau \geqslant \beta \equiv 1/T$. In this case, one can construct a complete description of fluctuation effects.

3.1 Grand partition function

It will be convenient for us to define the grand partition function of our system $\mathcal{Z}$, which can be expressed via the following path integral over the superconducting phase variable $\varphi(x,\tau)$:

$$\mathcal{Z} = \sum_{m,n} \int \mathcal{D}\varphi \, \exp\left[-\frac{\lambda}{2\pi} \int \mathrm{d}x \, \mathrm{d}\tau \left(v(\partial_x \varphi)^2 + v^{-1}(\partial_\tau \varphi)^2 \right) \right], \tag{43}$$

where we introduced an effective coupling constant $\lambda \equiv g/8$ [12]. According to our assumptions, this partition function includes only small fluctuations of the superconducting phase φ described by the imaginary time version of the effective action (24) in the exponent of Eqn (43).

The path integral (43) should be supplemented by proper boundary conditions, which should keep track of (a) the periodicity of the phase variable φ in space–time, (b) the fact that the phase is defined up to $2\pi m$, where m is an arbitrary integer (the so-called winding number), and (c) the magnetic flux Φ_x piercing the ring. Putting all these requirements together, we obtain

$$\varphi(x,0) = \varphi(x,\beta) + 2\pi m \,, \quad \varphi(L,\tau) = \varphi(0,\tau) + 2\pi(\phi_x + n) \,. \tag{44}$$

Here, $L = 2\pi R$ is the ring perimeter, $\phi_x = \Phi_x/\Phi_0$, and $\Phi_0 = \pi c/e$ is the superconducting flux quantum. Combining Eqns (43) and (44), after a simple calculation we find

$$\mathcal{Z} = \sum_{n=-\infty}^{\infty} \exp\left[-\beta E_n(\phi_x)\right] = \sqrt{\frac{2\pi T}{E_R}} \, \vartheta_3\left[\pi\phi_x, \exp\left(-\frac{2\pi^2 T}{E_R} \right) \right], \tag{45}$$

where

$$E_n(\phi_x) = \frac{E_R}{2}(n + \phi_x)^2 \tag{46}$$

are the flux-dependent energy levels of the ring, $\vartheta_3(u,q)$ is the third Jacobi theta function, and

$$E_R = \frac{4\pi\lambda v}{L} = \frac{\pi^2 v_\mathrm{F} D \Delta s}{R} \,. \tag{47}$$

In the limit $T \to 0$, the supercurrent $I(\phi_x)$ flowing around the ring in its ground state is obtained by means of a well-known simple formula

$$I(\phi_x) = \frac{\partial E(\Phi_x)}{\partial \Phi_x} \,, \tag{48}$$

where $E(\Phi_x) = \min_n E_n(\phi_x)$ is the ground-state energy of the ring, which is periodic in Φ_x with the period Φ_0. Hence, supercurrent I is also periodic in Φ_x, being defined as

$$I(\phi_x) = \frac{eE_R}{\pi} \frac{\partial}{\partial \phi_x} \min_n (n + \phi_x)^2 \,. \tag{49}$$

The supercurrent flowing across the ring can also be expressed in terms of the phase variable by means of the relation

$$I(\tau) = \frac{eE_R}{2\pi^2} \left(\varphi(L,\tau) - \varphi(0,\tau) \right). \tag{50}$$

Combining Eqn (50) with the second Eqn (44), in the zero temperature limit, we again recover the expression for the expectation value of the current operator $I(\phi_x) = \langle I(\tau) \rangle$.

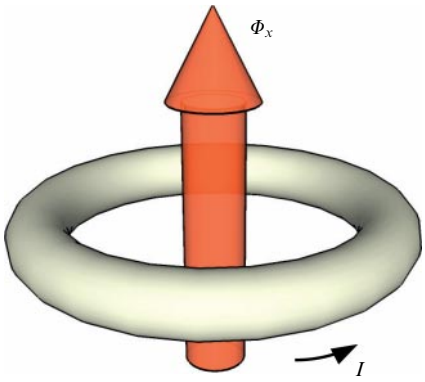

Figure 4. Superconducting ring threaded by magnetic flux Φ_x.

3.2 Coherent fluctuations of supercurrent

Fluctuations in the phase should in general cause fluctuations in the supercurrent flowing inside the ring. It turns out that, under the conditions formulated above, we can derive formally exact expressions for all current correlators in our problem. Employing Eqn (50), it is straightforward to demonstrate that none of these correlators depend on time and can be expressed through the derivatives of the theta

function $\vartheta_3^{(k,0)}$ as [34]

$$\begin{aligned}\big\langle \hat{I}(\tau_1)\dots\hat{I}(\tau_k)\big\rangle &= \left(\frac{eE_R}{\pi}\right)^k \frac{\sum_{n=-\infty}^{\infty}(n+\phi_x)^k \exp\left[-\beta E_n(\phi_x)\right]}{\sum_{n=-\infty}^{\infty}\exp\left[-\beta E_n(\phi_x)\right]} \\ &= \sum_{n=0}^{2n\leqslant k}\frac{(-eT)^k k!}{n!(k-2n)!}\left(\frac{E_R}{2\pi^2 T}\right)^n \\ &\times \frac{\vartheta_3^{(k-2n,0)}\big(\pi\phi_x, \exp\left(-2\pi^2 T/E_R\right)\big)}{\vartheta_3\big(\pi\phi_x, \exp\left(-2\pi^2 T/E_R\right)\big)}\,. \end{aligned} \tag{51}$$

At $T\to 0$, this expression obviously yields

$$\big\langle I^k(\tau)\big\rangle = \big\langle I(\tau)\big\rangle^k \tag{52}$$

for all integers $k\geqslant 0$. Equation (52) implies that *no supercurrent fluctuations can occur in the ground state of superconducting rings*. This observation is fully consistent with general theorem [35] stating that no persistent current fluctuations can occur at $T=0$ provided the current operator commutes with the total Hamiltonian of the ring. Sufficiently thick superconducting rings where QPS effects can be totally disregarded represent an example of this physical situation.

Supercurrent fluctuations, however, may and do occur at nonzero temperatures. Below, let us focus our attention on the supercurrent noise, the power spectrum of which reads

$$S_\omega = \int \mathrm{d}t\, \exp\left(\mathrm{i}\omega t\right) S(t)\,, \tag{53}$$

where

$$S(t) = \frac{1}{2}\big\langle \hat{I}(t)\hat{I}(0) + \hat{I}(0)\hat{I}(t)\big\rangle - \langle\hat{I}\rangle^2 \tag{54}$$

and $\hat{I}(t) = \exp\left(\mathrm{i}t\hat{H}\right)\hat{I}\exp\left(-\mathrm{i}t\hat{H}\right)$ is the current operator in the Heisenberg representation and $\hat{H}$ is the system Hamiltonian. In order to evaluate the above current–current correlation function, it will be convenient for us to also define the irreducible Matsubara correlator

$$\Pi(\tau) = T\sum_k \exp\left(-\mathrm{i}\omega_k\tau\right)\Pi_{\mathrm{i}\omega_k} = \big\langle \hat{I}_{\mathrm{M}}(\tau)\hat{I}_{\mathrm{M}}(0)\big\rangle - \langle\hat{I}\rangle^2\,, \tag{55}$$

where $\hat{I}_{\mathrm{M}} = \exp\left(\tau\hat{H}\right)\hat{I}\exp\left(-\tau\hat{H}\right)$ is the current operator in the Matsubara representation and $\omega_k = 2\pi kT$ is the Matsubara frequency. It is also important that, from the expression for the imaginary time correlator (55), one can directly recover the real time PC noise power spectrum

The quantities $S(t)$ and $\Pi(\tau)$ defined respectively in Eqns (54) and (55) can be related to each other through the appropriate analytic continuation procedure combined with the fluctuation-dissipation theorem. Expressing both correlators in terms of the exact eigenstates E_m of the system Hamiltonian $\hat{H}|m\rangle = E_m|m\rangle$, we find

$$\begin{aligned} S_\omega &= 2\pi P\delta(\omega) + \frac{\pi}{\mathcal{Z}}\sum_{m\neq n}\left|\langle m|\hat{I}|n\rangle\right|^2 \\ &\times\left[\exp\left(-\beta E_n\right) + \exp\left(-\beta E_m\right)\right]\delta(\omega+E_n-E_m)\,, \end{aligned} \tag{56}$$

$$\Pi_{\mathrm{i}\omega_k} = \beta P\delta_{k,0} + \frac{1}{\mathcal{Z}}\sum_{m\neq n}\left|\langle m|\hat{I}|n\rangle\right|^2 \frac{\exp\left(-\beta E_m\right) - \exp\left(-\beta E_n\right)}{\mathrm{i}\omega_k + E_n - E_m}\,, \tag{57}$$

where

$$P = \frac{1}{\mathcal{Z}}\sum_n \left|\langle n|\hat{I}|n\rangle\right|^2 \exp\left(-\beta E_n\right) - I^2 \tag{58}$$

defines the zero-frequency contribution and

$$I = \mathcal{Z}^{-1}\sum_n \langle n|\hat{I}|n\rangle\exp\left(-\beta E_n\right)$$

is the expectation value for the current. With the aid of the above general expressions, we easily arrive at the relation

$$\mathrm{Im}\left[\left(\Pi_{\mathrm{i}\omega_k} - \beta P\delta_{k,0}\right)\big|_{\mathrm{i}\omega_k\to\omega+\mathrm{i}0}\right] = \tanh\left(\frac{\omega}{2T}\right)S_\omega\,. \tag{59}$$

Equation (59) enables us to recover the current noise power spectrum S_ω directly from the imaginary time analysis.

It follows from Eqns (56) and (58) that, in the zero temperature limit (i) $P\equiv 0$, i.e., zero frequency, the supercurrent noise vanishes identically, and (ii) at nonzero frequencies, this noise also vanishes provided the current operator commutes with the system Hamiltonian $\hat{H}$.

At nonzero temperatures, the supercurrent noise power does not vanish, having a peak at zero frequency,

$$S_\omega = 2\pi P\delta(\omega)\,, \tag{60}$$

where, from Eqn (51), we find [34]

$$\begin{aligned} P &= e^2T^2\left[\frac{E_R}{\pi^2 T} + \frac{\vartheta_3^{(2,0)}\big(\pi\phi_x, \exp\left(-2\pi^2T/E_R\right)\big)}{\vartheta_3\big(\pi\phi_x, \exp\left(-2\pi^2T/E_R\right)\big)}\right] \\ &- e^2T^2\left[\frac{\vartheta_3^{(1,0)}\big(\pi\phi_x, \exp\left(-2\pi^2T/E_R\right)\big)}{\vartheta_3\big(\pi\phi_x, \exp\left(-2\pi^2T/E_R\right)\big)}\right]^2. \end{aligned} \tag{61}$$

In the low and high temperature limits, this expression reduces to

$$P\approx\begin{cases} \dfrac{2e^2E_R^2}{\pi^2}\exp\left(-\dfrac{E_R}{2T}\right)\cosh\left(\dfrac{\pi I(\phi_x)}{eT}\right), & T\ll E_R\,, \\ \dfrac{e^2E_RT}{\pi^2} - 8e^2T^2\exp\left(-\dfrac{2\pi^2T}{E_R}\right)\cos\left(2\pi\phi_x\right), & T\gg E_R\,, \end{cases} \tag{62}$$

where $I(\phi_x)$ is defined in Eqn (49). Also, one can note that, in the absence of phase slips, P can be related to the second derivative of free energy $\mathcal{F}$ over the flux

$$P = \frac{e^2TE_R}{\pi^2} - T\frac{\partial^2\mathcal{F}}{\partial\Phi_x^2} \tag{63}$$

and thus to the difference between the Drude and Meissner weights of the system [36, 37].

Dependence (61) is also depicted in Fig. 5 for different values of the magnetic flux. We observe that at sufficiently low temperatures the magnitude of PC fluctuations can be tuned by the external flux ϕ_x, hence indicating the coherent nature of such fluctuations. At higher temperatures, quantum coherence is destroyed and $P(T)\propto T$ becomes practically independent of ϕ_x.

The above picture remains applicable as long as the ring is sufficiently thick and one can essentially ignore quantum fluctuations of the absolute value of the order parameter field. However, upon decreasing the wire diameter $\sim\sqrt{s}$, typically

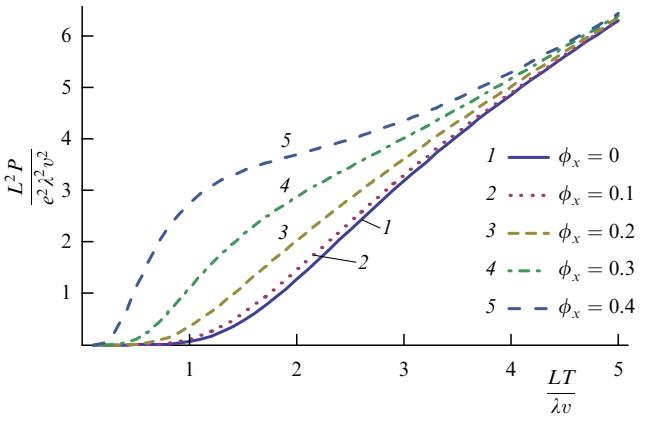

Figure 5. Temperature dependent zero frequency supercurrent fluctuations in superconducting rings at different values of magnetic flux ϕ_x.

to values in the 10-nm range, one eventually reaches the regime in which quantum fluctuations of $|\Delta(x)|$ gain importance and may strongly modify the low temperature behavior of the system. This regime of strong quantum fluctuations in superconducting nanowires and nanorings will be considered in the forthcoming sections.

4. Quantum phase slips and phase–charge duality

As we already discussed, at low temperatures, the most significant non-Gaussian quantum fluctuations in superconducting nanowires are quantum phase slips. Provided such a wire is sufficiently thin, quantum fluctuations may yield temporal local suppression of the absolute value of the superconducting order parameter field $\Delta(x) = |\Delta(x)| \exp[\mathrm{i}\varphi(x)]$ at different points along the wire. As soon as the modulus of the order parameter $|\Delta(x)|$ in the point x vanishes, the phase $\varphi(x)$ becomes unrestricted and can jump by the value $\pm 2\pi$. After this process, the modulus $|\Delta(x)|$ gets restored, the phase becomes single valued again, and the system returns to its initial state, accumulating the net phase shift $\pm 2\pi$.

Loosely speaking, each QPS event involves suppression of the order parameter *inside* the phase slip core and a winding of the superconducting phase *around* this core. This process can also be viewed as quantum tunneling of the order parameter field through an effective potential barrier. As the phase φ changes in time, according to the Josephson relation $V = \dot{\varphi}/2e$, each QPS event causes a voltage pulse inside the wire, thus essentially influencing the system electrodynamics.

An important property of superconducting nanowires is so-called phase–charge duality. This property will be substantially explored below in this section. Note that, earlier, duality between the phase and the charge variables was extensively discussed for ultrasmall Josephson junctions [31, 38–41]. In particular, it was demonstrated that, under a certain duality transformation, the effective actions for Josephson tunnel junctions in the phase and in the charge representations are *exactly* transformed into each other. Furthermore, in the absence of a shunt resistor, one can describe the Josephson junction in terms of an effective Hamiltonian for a 'quantum particle' in the periodic potential in the (quasi)-charge space. Within this picture, charge q and flux Φ are canonically conjugate variables exactly analogous to the momentum and coordinate variables in quantum mechanics. For more details on this issue, we refer the reader to book [1] and review paper [41].

Later on, it was pointed out in [42] that all the same arguments remain applicable for short superconducting nanowires in the presence of quantum phase slips, whose properties are exactly dual to those of Josephson junctions. For this reason, a short superconducting nanowire was named a *QPS junction* [42]. Note that 'Josephson-junction-like' duality arguments are strictly applicable only to sufficiently short nanowires, i.e., as long as the coordinate dependence of both the phase and the charge variables can be ignored and the QPS junction can be effectively treated as a zero-dimensional object. It turns out that one can also modify and extend these arguments further to the case of long superconducting nanowires. This task can be accomplished either by means a rigorous path integral analysis [34] or in terms of simple quantum mechanical operator manipulations [43]. Both methods will be outlined below.

4.1 Phase–charge duality in the operator formalism

We first consider a more intuitive operator approach. As before, we are going to deal with a uniform superconducting wire of length L and cross section s. The effective Hamiltonian of the wire can be expressed in a simple form:

$$\hat{H}_{\mathrm{eff}} = \int_0^L \mathrm{d}x \left[\frac{\hat{Q}^2(x)}{2C} + \frac{1}{2\mathcal{L}_{\mathrm{kin}}} \left(\frac{\partial_x \hat{\varphi}(x)}{2e} \right)^2 \right], \tag{64}$$

where $\hat{Q}(x)$ and $\hat{\varphi}(x)$ are canonically conjugate local charge and phase operators obeying the commutation relations

$$\left[\hat{Q}(x), \hat{\varphi}(x') \right] = -2\mathrm{i}e\delta(x - x'). \tag{65}$$

Employing Hamiltonian (64), one should arrive at results exactly equivalent to those derived, for example, within the effective action approach based on Eqn (24) or (43).

At this stage, we will assume that our superconducting wire is isolated from any external circuit, in which case the current at its end points $x = 0$ and $x = L$ vanishes, and, hence, we can define the boundary conditions for the phase in the form

$$\partial_x \hat{\varphi}(0) = \partial_x \hat{\varphi}(L) = 0. \tag{66}$$

Employing the Fourier series expansion, we get

$$\begin{aligned} \hat{\varphi}(x) &= \hat{\varphi}_0 + \sqrt{\frac{2}{L}} \sum_{n=1}^{\infty} \hat{\varphi}_n \cos\left(\frac{\pi n x}{L} \right), \\ \hat{Q}(x) &= \frac{\hat{Q}_0}{L} + \sqrt{\frac{2}{L}} \sum_{n=1}^{\infty} \hat{Q}_n \cos\left(\frac{\pi n x}{L} \right), \end{aligned} \tag{67}$$

where

$$\left[\hat{Q}_0, \hat{\varphi}_0 \right] = -2\mathrm{i}e, \qquad \left[\hat{Q}_m, \hat{\varphi}_n \right] = -2\mathrm{i}e\delta_{mn}. \tag{68}$$

Let us now introduce the following (dual) operators:

$$\begin{aligned} \hat{\Phi}(x) &= \frac{\partial_x \hat{\varphi}(x)}{2e}, \\ \hat{\chi}(x) &= -\frac{\pi}{e} \int_x^L \mathrm{d}x' \, \hat{Q}(x') + \frac{\pi(L - x)}{eL} \int_0^L \mathrm{d}x' \, \hat{Q}(x'), \end{aligned} \tag{69}$$

which can also be expressed as

$$\hat{\Phi}(x) = -\sqrt{\frac{\pi^2}{2e^2L^3}}\sum_{n=1}^{\infty} n\hat{\varphi}_n \sin\left(\frac{\pi n x}{L}\right), \qquad \hat{\chi}(x) = \sqrt{\frac{2L}{e^2}}\sum_{n=1}^{\infty}\frac{\hat{Q}_n}{n}\sin\left(\frac{\pi n x}{L}\right). \tag{70}$$

These new canonically conjugate operators obey the commutation relations

$$\left[\hat{\Phi}(x), \hat{\chi}(x')\right] = -\mathrm{i}\Phi_0\delta(x-x') \tag{71}$$

and obvious boundary conditions

$$\hat{\Phi}(0) = \hat{\Phi}(L) = 0\,, \qquad \hat{\chi}(0) = \hat{\chi}(L) = 0\,. \tag{72}$$

Substituting the relations

$$\partial_x\hat{\varphi}(x) = 2e\hat{\Phi}(x)\,, \qquad \hat{Q}(x) = \frac{\hat{Q}_0}{L} + \frac{e}{\pi}\,\partial_x\hat{\chi}(x) \tag{73}$$

into Eqn (64), we obtain

$$\hat{H}_{\mathrm{eff}} = \frac{\hat{Q}_0^2}{2LC} + \hat{H}_{\mathrm{TL}}\,, \tag{74}$$

where

$$\hat{H}_{\mathrm{TL}} = \int_0^L \mathrm{d}x\left[\frac{\hat{\Phi}^2}{2\mathcal{L}_{\mathrm{kin}}} + \frac{1}{2C}\left(\frac{\partial_x\hat{\chi}}{\Phi_0}\right)^2\right] \tag{75}$$

is the Hamiltonian for a transmission line formed by a superconducting wire.

The above analysis does not yet include the effect of QPS. In order to account for the QPS contribution to the wire Hamiltonian, let us first define the phase field configurations as

$$\hat{\varphi}(x)|\varphi(x)\rangle = \varphi(x)|\varphi(x)\rangle \tag{76}$$

and bear in mind that the phase of the superconducting order parameter is a compact variable implying that, for example, the field configurations $\varphi(x)$ and $\varphi(x) + 2\pi$ correspond to the same quantum state of our system. Furthermore, in the absence of QPS, i.e., provided the absolute value of the order parameter $|\Delta(x,t)|$ does not fluctuate, the states φ and $\tilde{\varphi}(x) = \varphi(x) + 2\pi\theta(x-x_1)$ (where $0 < x_1 < L$ and $\theta(x)$ is the Heaviside step function equal to 0 for $x \leqslant 0$ and to 1 for $x > 0$) are also physically indistinguishable. For instance, the supercurrent operator $\hat{I}$ proportional to the combination $|\Delta|^2\exp[-\mathrm{i}\hat{\varphi}(x)]\partial_x\exp[\mathrm{i}\hat{\varphi}(x)]$ remains the same in both cases.

Let us now slightly modify the step function, making it continuous by effectively smearing it at the scale of the superconducting coherence length ξ. We substitute $\theta(x) \to \theta_\xi(x)$, where field configuration $\tilde{\varphi}_\xi(x) = \varphi(x) + 2\pi\theta_\xi(x-x_1)$, on the one hand, remains very close to $\tilde{\varphi}(x)$ and, on the other hand, is now physically distinguishable from the latter. The QPS process can be interpreted as quantum tunneling between these two different (though very close to each other) phase configurations.

Making use of the fact that any shift by a constant phase does not change the state of our system, without loss of generality, we may set $\hat{\varphi}_0|\psi\rangle = 0$ for any system state $|\psi\rangle$. This condition applies for quantum dynamics controlled by Hamiltonian (64), and it is also maintained in the presence of quantum phase slips. Hence, we conclude that the QPS process corresponds to quantum tunneling of the phase between the states $\varphi(x)$ and

$$\varphi'(x) = \varphi(x) + 2\pi\theta_\xi(x-x_1) - 2\pi\int_0^L \mathrm{d}x\,\theta_\xi(x-x_1)\,. \tag{77}$$

In the operator language, this tunneling process can be denoted as $\hat{U}_\xi(x_1)|\varphi(x)\rangle = |\varphi'(x)\rangle$, where the operator $\hat{U}_\xi(x_1)$ can be established with the aid of the commutation relations. It reads

$$\hat{U}_\xi(x_1) = \exp\left[\frac{\mathrm{i}\pi}{e}\int_0^L \mathrm{d}x\left(\hat{Q}(x) - \frac{\hat{Q}_0}{L}\right)\theta_\xi(x-x_1)\right]. \tag{78}$$

As a result, the part of the Hamiltonian which explicitly accounts for the QPS contribution takes the form

$$\hat{H}_{\mathrm{QPS}} = -\gamma_{\mathrm{QPS}}\int_0^L \mathrm{d}x_1\,\cos\left[\frac{\pi}{e}\int_0^L \mathrm{d}x\left(\hat{Q}(x) - \frac{\hat{Q}_0}{L}\right)\theta_\xi(x-x_1)\right].$$

Setting $\xi \to 0$ now and making use of the second Eqn (73), we obtain

$$\hat{H}_{\mathrm{QPS}} = -\gamma_{\mathrm{QPS}}\int_0^L \mathrm{d}x\,\cos\left(\hat{\chi}(x)\right). \tag{79}$$

The above analysis can be easily generalized in order to include the effect of an external circuit. Let us consider one example of an external circuit displayed in Fig. 6. The system consists of a superconducting nanowire and a capacitance C_0 (which also includes the wire capacitance C) switched in parallel to this wire. The right end of the wire ($x = L$) is grounded as shown in the figure. The voltage $V(t)$ at its left end $x = 0$ can be measured by a detector. The whole system is biased by an external current $I = V_x/R_x$.

The system depicted in Fig. 6 can be described by means of the effective Hamiltonian in the mixed phase–charge representation:

$$\hat{H} = \hat{H}_{\mathrm{SW}} + \frac{\hat{Q}_0^2}{2C_0} - \frac{I\hat{\varphi}}{2e}\,, \tag{80}$$

where the term

$$\hat{H}_{\mathrm{SW}} = \hat{H}_{\mathrm{TL}} + \hat{H}_{\mathrm{QPS}} \tag{81}$$

defined by Eqns (75) and (79) accounts for the superconducting nanowire. The last two terms in Eqn (80) describe, respectively, the charging energy (which also includes the

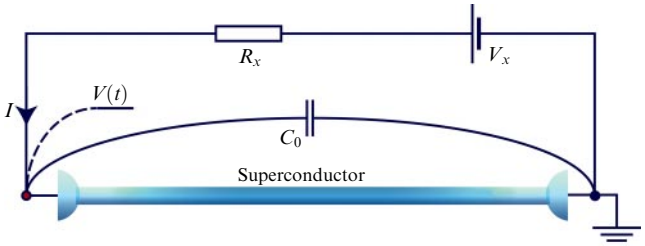

Figure 6. Superconducting circuit embedded in an external circuit.

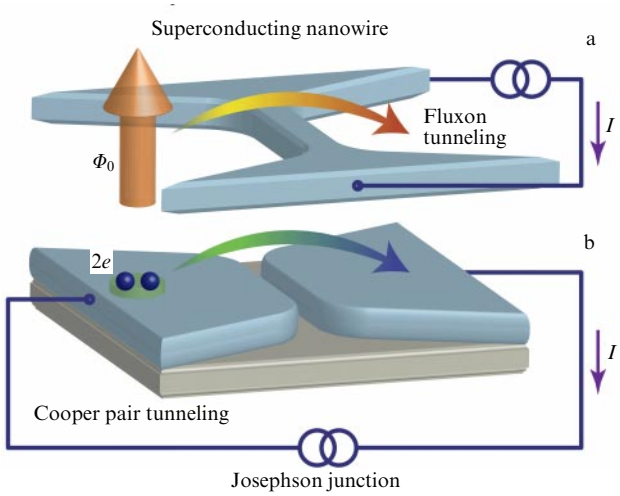

Figure 7. Dual tunneling processes for (a) a quantum fluxon (that tunnels through a superconducting nanowire) and (b) a Cooper pair (which tunnels across a Josephson junction).

first term on the right-hand side of Eqn (74)) and the potential energy tilt produced by an external current I. The operator $\hat{\varphi} \equiv \hat{\varphi}(0)$ corresponds to the phase of the superconducting order parameter field $\Delta(x,t)$ at $x = 0$. Here, we also set $\hat{\varphi}(L) \equiv 0$.

Let us now take a quick look at Fig. 7 where we display two complementary superconducting devices. One of them is an arbitrarily long superconducting nanowire surrounded by a vacuum or an insulator (Fig. 7a). In the device depicted in Fig. 7b, the superconductor is interchanged with the vacuum/insulator, thus forming a spatially extended Josephson junction between two superconductors. As we just demonstrated, the superconducting nanowire in Fig. 7 is described by Hamiltonian (81), whereas the Hamiltonian corresponding to a Josephson junction (of length L) in Fig. 7 is well known to have the form (see, e.g., [44])

$$\hat{H}_{\rm JJ} = \int_0^L {\rm d}x \left[\frac{\hat{\mathcal{Q}}^2(x)}{2C_{\rm J}} + \frac{1}{2\mathcal{L}_{\rm J}} \left(\frac{\partial_x \hat{\phi}(x)}{2e} \right)^2 \right] - \frac{j_C}{2e} \int_0^L {\rm d}x \, \cos\left(\hat{\phi}(x)\right), \tag{82}$$

where $\hat{\mathcal{Q}}(x)$ and $\hat{\phi}(x)$ are the local charge and phase difference operators, $C_{\rm J}$ and $\mathcal{L}_{\rm J}$ represent, respectively, the Josephson junction capacitance and inductance per unit junction length, and, finally, j_C is the Josephson critical current density. We observe that, under the transformation of the operators

$$\hat{\Phi}(x) \leftrightarrow \hat{\mathcal{Q}}(x), \qquad \hat{\chi}(x) \leftrightarrow \hat{\phi}(x), \tag{83}$$

Hamiltonians $\hat{H}_{\rm SW}$ (defined by Eqns (75) and (79)) and $\hat{H}_{\rm JJ}$ (82) are *exactly dual* to each other provided we interchange

$$\Phi_0 \leftrightarrow 2e, \qquad \gamma_{\rm QPS} \leftrightarrow \frac{j_C}{2e}, \qquad \mathcal{L}_{\rm kin} \leftrightarrow C_{\rm J}, \qquad C \leftrightarrow \mathcal{L}_{\rm J}. \tag{84}$$

The above duality transformations, on the one hand, interchange magnetic and charging energies in these two Hamiltonians (cf. Eqn (75) and the first line in Eqn (82)) and, on the other hand, establish a correspondence between the term (79) describing the effect of QPS and the Josephson coupling energy on the second line in Eqn (82) that accounts for Cooper pair tunneling across the junction.

We conclude that the tunneling of a Cooper pair with charge $2e$ between two superconductors is a dual process to a QPS event that can be viewed as tunneling of a quantum fluxon (i.e., the flux quantum Φ_0) across a superconducting wire, as illustrated in Fig. 7. Indeed, we note that Hamiltonian (79) contains a linear combination of creation ($\exp(i\hat{\chi})$) and annihilation ($\exp(-i\hat{\chi})$) operators for the flux quantum Φ_0. Each QPS event corresponds to the net phase jump by 2π associated with voltage pulse $\delta V = \dot{\varphi}/2e$ and magnetic flux $\int |\delta V(t)| \, {\rm d}t = \pi/e \equiv \Phi_0$ passing through the wire in the direction normal to its axis.

Also, the physical meaning of the quantum field $\chi(x,t)$ is transparent: it is proportional to the total electric charge $q(x,t)$ that has passed through the point x up to the time moment t, i.e., $q(x,t) = \chi(x,t)/\Phi_0$. Accordingly, the local current $I(x,t)$ and the local charge density $\rho(x,t)$ are defined as

$$I(x,t) = \frac{\partial_t \chi(x,t)}{\Phi_0}, \qquad \rho(x,t) = -\frac{\partial_x \chi(x,t)}{\Phi_0}, \tag{85}$$

thereby satisfying the continuity equation.

The property of phase–charge duality in superconducting nanowires was confirmed and illustrated in a number of experiments. For instance, tunneling of magnetic flux quanta through such nanowires was detected in experiments [45, 46]. The insulating behavior of these nanowires as well as Bloch steps (dual to Shapiro ones) on their $I-V$ curves were also discussed and reported experimentally [47–50]. A phase–charge duality-based single-charge transistor and charge quantum interference device were demonstrated in Refs [51, 52], respectively. The duality property also enables one to investigate the possibility of employing superconducting nanowires for creating a QPS-based standard of electric current [48, 53].

4.2 Path integral analysis

We now turn to a more formal path integral analysis. For pedagogical purposes and also for reasons which will be clear below in the next section, we will now consider a closed ring (with perimeter $L = 2\pi R$ and cross section s) made of a thin superconducting wire. The configuration remains essentially the same as that already treated in Section 3 (e.g., we again assume that the magnetic flux Φ_x pierces the ring) with only one important difference: we now allow for quantum phase slips. We will perform the whole calculation for the ring geometry and at the very end of it we will explain how to apply our results to superconducting wires with open ends and/or attached to an external circuit.

In order to proceed, we will again make use of the expression for the grand partition function $\mathcal{Z}$ (43) that accounts for the ring geometry as well as for an external magnetic flux inside the ring. It is also important to bear in mind that Eqn (43) remains valid only at length and time scales exceeding, respectively, the superconducting coherence length $\xi \sim \sqrt{D/\Delta}$ and the inverse gap Δ^{-1}, i.e., outside the QPS core where only superconducting phase fluctuations may occur. Within the semiclassical approximation, it suffices to take into account all relevant saddle point configurations of the phase variable φ which satisfy the equation

$$(\partial_\tau^2 + v^2 \partial_x^2)\varphi(x,\tau) = 0. \tag{86}$$

Apart from trivial solutions of this equation (linear in τ and x), nontrivial ones exist which correspond to virtual phase jumps by $\pm 2\pi$ at various points of a superconducting ring where the magnitude of the order parameter gets locally (at spatial scales $x_0 \sim \xi$) and temporarily (within the time interval $\tau_0 \sim 1/\Delta$) suppressed by quantum fluctuations. These quantum topological objects can be viewed as vortices in space-time and just represent quantum phase slips. For sufficiently long wires or large rings and outside the QPS core $|x| > x_0, |\tau| > \tau_0$ (whose position in space-time can be chosen, e.g., at $x = 0$ and $\tau = 0$), the saddle point solution $\tilde{\varphi}(x, \tau)$ corresponding to a single QPS event should satisfy the identity

$$\partial_x \partial_\tau \tilde{\varphi} - \partial_\tau \partial_x \tilde{\varphi} = 2\pi \delta(\tau, x)\,, \tag{87}$$

implying that, after a wind around the QPS center, the phase should change by 2π. This saddle point solution has the form [14]

$$\tilde{\varphi}(x, \tau) = -\arctan\left(\frac{x}{v\tau}\right). \tag{88}$$

Configurations $\varphi^{qps}(x, \tau)$ consisting of an arbitrary number of quantum phase slips can be treated analogously. Our goal here is to effectively sum up the contributions to the partition function $\mathcal{Z}$ (43) from all possible QPS configurations. This goal can be conveniently accomplished with the aid of the approach involving the so-called duality transformation. Let us express the general solution of Eqn (86) in the form

$$\varphi^{sp}(x, \tau) = a_m \tau + b_n x + \varphi^{qps}(x, \tau)\,, \tag{89}$$

where a_m and b_n are some constants fixed by the boundary conditions. We also introduce the vorticity field $\varpi(x, \tau)$ by means of the relations

$$v\,\partial_x \varpi = \partial_\tau \varphi^{qps}\,, \quad \partial_\tau \varpi = -v\,\partial_x \varphi^{qps}\,. \tag{90}$$

This field is single-valued, obeying the equation

$$\partial_\tau^2 \varpi + v^2 \partial_x^2 \varpi = -2\pi v \sum_j \nu_j\, \delta(x - x_j)\delta(\tau - \tau_j)\,, \tag{91}$$

where x_j and τ_j denote, respectively, the space and time coordinates of the jth phase slip, while $\nu_j = \pm 1$ is its topological charge corresponding to a phase jump by $\pm 2\pi$. It follows from boundary conditions (44) that the vorticity field derivatives are periodic functions in both space and time, implying, in turn, that $\sum_j \nu_j = 0$.

Let us define the function

$$\varpi^{qps}(x, \tau) = \frac{\beta L v}{2\pi} \sum_{|m|+|n|>0} \frac{\exp\left(2\pi \mathrm{i} m\tau/\beta + 2\pi \mathrm{i} n x/L\right)}{m^2 L^2 + n^2 v^2 \beta^2}\,. \tag{92}$$

One can verify that the function

$$\varpi(x, \tau) = \sum_j \nu_j\, \varpi^{qps}(x - x_j, \tau - \tau_j) \tag{93}$$

satisfies Eqn (91), and, by virtue of the duality relations (90), it yields the saddle point configuration φ^{qps}. Combining boundary conditions (44) with the above equations, we find

$$\varphi^{qps}(L, \tau) - \varphi^{qps}(0, \tau) = -\frac{1}{v}\int_0^L \mathrm{d}x\, \partial_\tau \varpi(x, \tau)$$
$$= 2\pi \sum_j \nu_j \left(\theta(\tau - \tau_j) + \frac{\tau_j}{\beta}\right), \tag{94}$$

$$\varphi^{qps}(x, \beta) - \varphi^{qps}(x, 0) = v\int_0^\beta \mathrm{d}\tau\, \partial_x \varpi(x, \tau)$$
$$= -2\pi \sum_j \nu_j \left(\theta(x - x_j) + \frac{x_j}{L}\right) \tag{95}$$

and, hence,

$$a_m = \frac{2\pi}{\beta}\left(m + \sum_j \nu_j \frac{x_j}{L}\right), \tag{96}$$

$$b_n = \frac{2\pi}{L}\left(n + \phi_x - \sum_j \nu_j \frac{\tau_j}{\beta}\right). \tag{97}$$

We also note that, for each of the above saddle point configurations, the expression for the current (50) takes the form

$$I(\tau) = \frac{4ev\lambda}{L}\left(n + \phi_x + \sum_j \nu_j\, \theta(\tau - \tau_j)\right). \tag{98}$$

Let us now carry out the summation over all possible saddle point configurations. Expanding the partition function in powers of γ_{QPS}, we get

$$\mathcal{Z}\big[J(\tau)\big] = \sum_{N=0}^{\infty} \frac{1}{N!} \sum_{\nu_1, \ldots, \nu_N = \pm 1} \delta_{\sum_j \nu_j, 0} \int \mathrm{d}x_1\, \mathrm{d}\tau_1 \ldots \mathrm{d}x_N\, \mathrm{d}\tau_N$$
$$\times \sum_{m,n=-\infty}^{\infty} \exp\left[-\frac{\lambda}{2\pi}\left(\frac{\beta L}{v}\, a_m^2 + \beta L v b_n^2\right)\right]\left(\frac{\gamma_{\mathrm{QPS}}}{2}\right)^N$$
$$\times \exp\left[-\frac{\lambda}{2\pi}\int \mathrm{d}x\, \mathrm{d}\tau\, \left(v(\partial_x \varpi)^2 + v^{-1}(\partial_\tau \varpi)^2\right) + \mathrm{i}\int \mathrm{d}\tau\, J(\tau) I(\tau)\right]. \tag{99}$$

Here, $J(\tau)$ is the source variable which we introduced for future purposes. Rewriting the sum over m, n with the aid of the relations

$$\sum_{m=-\infty}^{\infty} \exp\left(-\frac{\lambda\beta L}{2\pi v}\, a_m^2\right)$$
$$\sim \sum_{m=-\infty}^{\infty} \exp\left(-\frac{\pi v \beta m^2}{2\lambda L} + 2\pi \mathrm{i} m \sum_j \nu_j \frac{x_j}{L}\right), \tag{100}$$

$$\sum_{n=-\infty}^{\infty} \exp\left[-\frac{\lambda\beta v L}{2\pi}\, b_n^2 + \frac{4\mathrm{i}ev\lambda(n + \phi_x)}{L}\int \mathrm{d}\tau\, J(\tau)\right]$$
$$\sim \sum_{n=-\infty}^{\infty} \exp\left[-\frac{\pi L}{2\lambda\beta v}\left(n - \frac{2ev\lambda}{\pi L}\int \mathrm{d}\tau\, J(\tau)\right)^2 + 2\pi \mathrm{i} n \phi_x\right.$$
$$\left. - 2\pi \mathrm{i}\left(n - \frac{2ev\lambda}{\pi L}\int \mathrm{d}\tau\, J(\tau)\right)\sum_j \nu_j \frac{\tau_j}{\beta}\right], \tag{101}$$

employing the Kronecker delta-function representation $\delta_{m,n} = \int_0^{2\pi} \mathrm{d}z \exp\left[\mathrm{i}z(m - n)\right]/(2\pi)$, and formally inserting

the path integral over the ϖ-field, we find

$$\mathcal{Z}[J(\tau)] \sim \sum_{N=0}^{\infty} \frac{1}{N!} \sum_{v_1,\ldots,v_N=\pm 1} \int_0^{2\pi} \frac{\mathrm{d}z}{2\pi} \int \mathrm{d}x_1\, \mathrm{d}\tau_1 \ldots \mathrm{d}x_N\, \mathrm{d}\tau_N$$
$$\times \sum_{m,n=-\infty}^{\infty} \exp\left[2\pi \mathrm{i} n\phi_x - \frac{\pi v \beta m^2}{2\lambda L} - \frac{\pi L}{2\lambda\beta v}\left(n - \frac{2ev\lambda}{\pi L}\int \mathrm{d}\tau\, J(\tau)\right)^2\right] \left(\frac{\gamma_{\mathrm{QPS}}}{2}\right)^N$$
$$\times \exp\left[2\pi \mathrm{i} m \sum_j v_j \frac{x_j}{L} - 2\pi \mathrm{i}\left(n - \frac{2ev\lambda}{\pi L}\int \mathrm{d}\tau\, J(\tau)\right) \sum_j v_j \frac{\tau_j}{\beta}\right]$$
$$\times \int \mathcal{D}\varpi \exp\left[-\frac{\lambda}{2\pi}\int \mathrm{d}x\, \mathrm{d}\tau \left(v(\partial_x \varpi)^2 + v^{-1}(\partial_\tau \varpi)^2\right)\right]$$
$$\times \exp\left[\mathrm{i}z \sum_j v_j + \frac{4\mathrm{i}ev\lambda}{L} \sum_j v_j \int \mathrm{d}\tau\, J(\tau)\theta(\tau - \tau_j)\right]$$
$$\times \delta\left(\partial_\tau^2 \varpi + v^2 \partial_x^2 \varpi + 2\pi v \sum_j v_j \delta(x - x_j)\delta(\tau - \tau_j)\right), \quad (102)$$

where the functional delta-function follows from Eqn (91). Expressing this delta-function via the integral over the dual field $\eta(x,\tau)$ with the periodic boundary conditions and evaluating the gaussian integral over ϖ, from Eqn (102) we get

$$\mathcal{Z}[J(\tau)] \sim \sum_{N=0}^{\infty} \frac{1}{N!} \sum_{v_1,\ldots,v_N=\pm 1} \int_0^{2\pi} \frac{\mathrm{d}z}{2\pi} \int \mathrm{d}x_1\, \mathrm{d}\tau_1 \ldots \mathrm{d}x_N\, \mathrm{d}\tau_N$$
$$\times \sum_{m,n=-\infty}^{\infty} \exp\left[2\pi \mathrm{i} n\phi_x - \frac{\pi v \beta m^2}{2\lambda L} - \frac{\pi L}{2\lambda\beta v}\left(n - \frac{2ev\lambda}{\pi L}\int \mathrm{d}\tau\, J(\tau)\right)^2\right] \left(\frac{\gamma_{\mathrm{QPS}}}{2}\right)^N$$
$$\times \exp\left[2\pi \mathrm{i} m \sum_j v_j \frac{x_j}{L} - 2\pi \mathrm{i}\left(n - \frac{2ev\lambda}{\pi L}\int \mathrm{d}\tau\, J(\tau)\right) \sum_j v_j \frac{\tau_j}{\beta}\right]$$
$$\times \int \mathcal{D}\eta \exp\left[-\frac{\pi v}{2\lambda}\int \mathrm{d}x\, \mathrm{d}\tau \left((\partial_\tau \eta)^2 + v^2(\partial_x \eta)^2\right)\right]$$
$$\times \exp\left[2\pi \mathrm{i} v \sum_j v_j \eta(x_j, \tau_j) + \mathrm{i}z \sum_j v_j + \frac{4\mathrm{i}ev\lambda}{L} \sum_j v_j \int \mathrm{d}\tau\, J(\tau)\theta(\tau - \tau_j)\right]. \quad (103)$$

Introducing now the field

$$\chi(x,\tau) = -\frac{2\pi m x}{L} + \frac{2\pi\tau}{\beta}\left(n - \frac{2ev\lambda}{\pi L}\int \mathrm{d}\tau\, J(\tau)\right) - 2\pi v \eta(x,\tau) - z - \frac{4ev\lambda}{L}\int \mathrm{d}\tau'\, J(\tau')\theta(\tau' - \tau), \quad (104)$$

which obeys the boundary conditions

$$\chi(x,\beta) - \chi(x,0) = 2\pi n, \qquad \chi(0,\tau) - \chi(L,\tau) = 2\pi m, \quad (105)$$

we obtain

$$\mathcal{Z}[J(\tau)] \sim \sum_{m,n=-\infty}^{\infty} \exp(2\pi \mathrm{i} n\phi_x) \times \int^{mn} \mathcal{D}\chi \exp\left\{-S_{\mathrm{eff}}[\chi(x,\tau), J(\tau)]\right\} \quad (106)$$

with the effective action

$$S_{\mathrm{eff}} = \frac{1}{8\pi\lambda v}\int_0^\beta \mathrm{d}\tau \int_0^L \mathrm{d}x \left[\left(\partial_\tau \chi(x,\tau) - \frac{4ev\lambda J(\tau)}{L}\right)^2 + v^2\left(\partial_x \chi(x,\tau)\right)^2\right] - \gamma_{\mathrm{QPS}}\int_0^\beta \mathrm{d}\tau \int_0^L \mathrm{d}x \cos\left(\chi(x,\tau)\right). \quad (107)$$

These expressions define the generating functional and the effective action for superconducting nanorings in the dual representation. In other words, our original problem of a nanoring with quantum phase slips was exactly mapped onto a sine-Gordon model on a torus. Equations (106), (107) keep track of interactions between different QPSs and serve as a convenient starting point for an analysis of the ground state properties of superconducting nanorings, which will be carried out in Section 5.

In the absence of the source $J(\tau) \to 0$, the effective action (107) turns out to be exactly dual to that for spatially extended quasi-one-dimensional Josephson barriers described by Hamiltonian (82), i.e., we again arrive at the duality transformations (83) and (84) already derived within the operator formalism for superconducting nanowires. In particular, the Josephson phase $\phi(x,\tau)$ in the latter model is dual to the field $\chi(x,\tau)$ (104).

Finally, we point out that all the above arguments developed for superconducting nanorings equally apply to nanowires with open ends. In that case, one should set $\phi_x = 0$, $J = 0$, and abandon the second boundary condition (44). Removing the summation over n in Eqn (43) and repeating all the same steps, one again arrives at the sine-Gordon action (107) (with $J(\tau) = 0$) describing a superconducting nanowire of length L in the presence of quantum phase slips.

5. Superconducting nanorings with quantum phase slips

In Section 3, we already considered some quantum coherent effects associated with fluctuations in the phase variable in superconducting rings threaded by a magnetic flux. That analysis was performed for sufficiently thick rings, thus enabling us to fully disregard QPS effects. Our main goal here is to include quantum phase slips into our consideration.

According to the existing microscopic theory [1, 2, 5, 12, 14], QPSs represent quantum coherent objects[1] which may significantly affect not only transport but also equilibrium ground state properties of superconducting nanowires and nanorings. The coherent nature of quantum phase slips was also demonstrated in a number of experiments [45, 46, 52]. A fundamental manifestation of a quantum coherent ground state is the possibility of a nonvanishing supercurrent flowing around a superconducting ring pierced by an external magnetic flux. Provided such a ring is sufficiently thin, as displayed on the left side of Fig. 8, quantum phase slips proliferate and may drastically modify both the supercurrent magnitude and its dependence on the magnetic flux [2, 5, 34]. Below, we will also demonstrate that quantum phase slips

[1] For this very reason, the notion of 'coherent quantum phase slips' sometimes used in the literature is to a large extent tautological. No such objects as 'incoherent quantum phase slips' (or, by duality, "incoherent Cooper pairs") exist in Nature. At the same time, quantum tunneling of both fluxons and Copper pairs can, of course, be made incoherent, provided, for example, enough extra dissipation is added to the system.

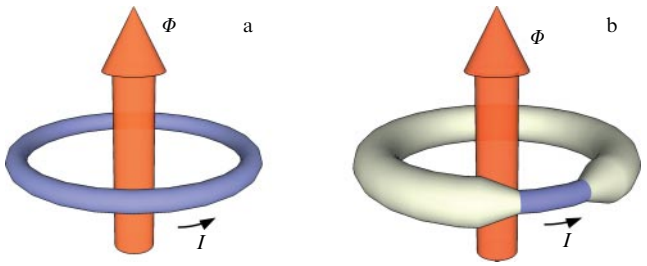

Figure 8. (a) Quantum phase slip ring, i.e., an ultrathin superconducting ring threaded by an external magnetic flux. (b) Quantum phase slip junction embedded in a thick superconducting ring.

cause nonvanishing supercurrent noise [54], which otherwise would be totally absent in the limit $T \to 0$ (see Section 3).

All the same phenomena can also occur in rings consisting of thicker and thinner parts, as shown in Fig. 8b. In this case, QPS effects are negligible in a thicker part of the ring and may only occur in its thinner part, which is named a *quantum phase slip junction* [42]. It was proposed to employ such QPS junctions as central elements of so-called quantum phase slip flux qubits [55].

Bearing in mind that QPS effects are basically the same in uniform superconducting nanorings and QPS junctions (see Fig. 8), in what follows, we will merely address only the former systems. In order to distinguish them from thicker superconducting rings (where QPS effects are negligible) and, on the other hand, to stress their similarity to QPS junctions, we will denote such systems as *quantum phase slip rings*.

5.1 Supercurrent in quantum phase slip rings

In order to proceed, we will make use of the effective action (107) derived in the previous section. At low enough temperatures $T \ll v/L$ and provided the ring perimeter $L = 2\pi R$ remains sufficiently small, we can ignore the spatial dependence of the field χ and, hence, ignore the term $v^2(\partial_x\chi)^2$ in the effective action (107). Then, our problem reduces to a zero-dimensional one with an effective Hamiltonian [35, 36]

$$\hat{H} = \frac{E_R}{2}(\hat{\phi} - \phi_x)^2 + U_0\big(1 - \cos(\hat{\chi})\big) \tag{108}$$

describing a fictitious quantum particle on a ring in the presence of the cosine external potential. Here, we identify [54]

$$E_R = \frac{\pi^2 N_0 D\Delta s}{R} \sim \frac{g_\xi \Delta\xi}{R}\,, \tag{109}$$

$$U_0 = 2\pi R\gamma_{\rm QPS} \sim \frac{g_\xi \Delta R}{\xi}\exp(-ag_\xi)\,. \tag{110}$$

The average value of the supercurrent I flowing across the ring can be obtained by means of the standard formula

$$I = -\frac{e}{\pi\beta}\frac{\partial \ln \mathcal{Z}}{\partial\phi_x}\,. \tag{111}$$

In the zero dimensional limit described by the effective Hamiltonian (108) and at low temperatures $T \to 0$, Eqn (111) reduces to

$$I = \frac{e}{\pi}\frac{\partial E_0(\phi_x)}{\partial\phi_x}\,, \tag{112}$$

where $E_0(\phi_x)$ is the flux-dependent ground state energy. For smaller rings with $U_0 \ll E_R$, we have

$$E_0(\phi_x) = \frac{E_R}{2\pi^2}\arcsin^2\left[\left(1 - \frac{\pi^2}{2}\left(\frac{U_0}{E_R}\right)^2\right)\sin(\pi\phi_x)\right], \tag{113}$$

i.e., the ground state energy is almost parabolic except in the vicinity of the crossing points $\phi_x = 1/2 + n$, where the gap to the first excited energy band $\delta E_{01} = U_0$ opens up due to level repulsion. Accordingly, not too close to the points $\phi_x = 1/2 + n$, the supercurrent is not affected by QPS and is again defined by Eqn (49).

For larger U_0, the bandwidth shrinks, while the gaps become bigger. In the limit $U_0 \gg E_R$, i.e., for

$$R \gg R_{\rm c} \sim \xi\exp\left(\frac{ag_\xi}{2}\right), \tag{114}$$

we obtain [2, 5]

$$I = I_0\sin(2\pi\phi_x)\,, \qquad I_0 \sim eE_R^{1/4}U_0^{3/4}\exp\left(-\frac{R}{R_{\rm c}}\right). \tag{115}$$

This result demonstrates that quantum phase slips yield exponential suppression of the supercurrent even at $T = 0$ provided the ring radius R exceeds the critical value $R_{\rm c}$ (114).

Let us now generalize our analysis by including the spatial derivative term $v^2(\partial_x\chi)^2$ in Eqn (107) or, in other words, by taking into account logarithmic interactions between quantum phase slips described by the sine-Gordon effective action. This task can be accomplished by means of the standard Berezinskii–Kosterlitz–Thouless (BKT) renormalization group (RG) approach [11]. Adapting the corresponding RG equations to our problem, we get

$$\frac{{\rm d}\zeta}{{\rm d}\ln\Lambda} = (2 - \lambda)\zeta\,, \qquad \frac{{\rm d}\lambda}{{\rm d}\ln\Lambda} = -32\pi^2\zeta^2\lambda^2K(\lambda)\,, \tag{116}$$

where $\zeta = \gamma_{\rm QPS}\Lambda^2$ is the dimensionless coupling parameter, Λ is the renormalization scale, and $K(\lambda)$ is some nonuniversal function (which depends on the renormalization scheme) equal to one at the quantum BKT phase transition point $\lambda = 2$, which separates superconducting (ordered) phase $\lambda > 2$ with bound QPS–anti-QPS pairs and disordered phase $\lambda < 2$ with unbound QPS [12].

Starting renormalization at the shortest scale $\Lambda \sim \xi_{\rm c} = (\xi^2 + v^2/\Delta^2)^{1/2}$, we, as usual, proceed to bigger scales. Within the first order perturbation theory in ζ, it suffices to ignore weak renormalization of the parameter λ. Then, the solution of Eqns (116) takes the simple form $\gamma_{\rm QPS}(\Lambda) = \gamma_{\rm QPS}(\xi_{\rm c}/\Lambda)^\lambda$. Our RG procedure should be stopped at the scale corresponding to the ring perimeter $\Lambda \sim L = 2\pi R$. As a result, we arrive at the renormalized QPS amplitude

$$\tilde{\gamma}_{\rm QPS} = \gamma_{\rm QPS}\left(\frac{\xi_{\rm c}}{L}\right)^\lambda. \tag{117}$$

This result allows us to conclude that inter-QPS interaction effects remain weak and can be disregarded only for very small values of

$$\lambda \ll \frac{1}{\ln(L/\xi_{\rm c})}\,. \tag{118}$$

This inequality, in turn, may severely restrict both the wire length and cross section values at which the system can still be

treated as effectively zero-dimensional and analyzed by means of simplified Hamiltonian (108).

Substituting the renormalized QPS amplitude (117) instead of the bare one into Eqn (110), we again reproduce the same expressions for the supercurrent, now with $\gamma_{\rm QPS} \to \tilde{\gamma}_{\rm QPS}$. As before, for smaller rings with $R \ll \tilde{R}_{\rm c}$ and at $T \to 0$, the current is defined by Eqn (49) at all values of the flux except for $\phi_x \approx 1/2 + n$, where QPS effects with the effective rate (117) become significant. The critical radius $\tilde{R}_{\rm c}$ is now determined by the condition $E_R \sim 2\pi\tilde{\gamma}_{\rm QPS}$, which yields

$$\tilde{R}_{\rm c} \sim \xi \exp\left(\frac{a g_\xi}{2-\lambda}\right)\left(\frac{\xi}{\xi_{\rm c}}\right)^{\lambda/(2-\lambda)}, \tag{119}$$

where λ is not supposed to exceed 2. In the opposite limit of bigger rings $R \gg \tilde{R}_{\rm c}$, we again reproduce Eqn (115), where now

$$I_0 \sim e\left(\frac{\xi_{\rm c}}{\xi}\right)^{3\lambda/4} g_\xi \Delta \left(\frac{R}{\xi}\right)^{1/2-3\lambda/4} \exp\left[-\frac{3a g_\xi}{4} - \left(\frac{R}{\tilde{R}_{\rm c}}\right)^{1-\lambda/2}\right]. \tag{120}$$

We observe that the critical radius $\tilde{R}_{\rm c}$ (119) increases with increasing λ and eventually diverges at the quantum BKT phase transition point $\lambda = 2$. In the ordered phase $\lambda > 2$, QPSs are bound in 'neutral' pairs and, hence, become practically irrelevant. In this case, the supercurrent is determined by Eqn (49) for any value of R.

5.2 Supercurrent noise in quantum phase slip rings

Let us now analyze fluctuations in supercurrent in QPS rings. Taking the derivatives of the generating functional $\mathcal{Z}[J(\tau)]$ over the source variable $J(\tau)$ and setting this variable equal to zero afterwards, we obtain

$$I \equiv \langle I(\tau)\rangle = -\frac{{\rm i}e}{\pi}\left\langle \partial_\tau \chi(x,\tau)\right\rangle, \tag{121}$$

whereas the irreducible Matsubara current–current correlator (55) now reads

$$\Pi(\tau_1-\tau_2) = \frac{4e^2\lambda v}{\pi L}\,\delta(\tau_1-\tau_2) - \frac{e^2}{\pi^2 L^2}\int {\rm d}x_1\,{\rm d}x_2\left\langle \partial_{\tau_1}\chi(x_1,\tau_1)\partial_{\tau_2}\chi(x_2,\tau_2)\right\rangle - I^2. \tag{122}$$

One can also decompose the source variable as $J(\tau) = J_0 + \partial_\tau J_1(\tau)$ and perform a shift under the functional integral

$$\mathcal{Z}\left[J_0 + \partial_\tau J_1(\tau)\right] = \sum_{mn}\exp\left(2\pi {\rm i} n\phi_x + 2eJ_0 n - \frac{2e^2 v\lambda J_0^2\beta}{\pi L}\right) \times \int^{mn}\mathcal{D}\chi\,\exp\left[-S_{\rm eff}\left(\chi(x,\tau) + \frac{4ev\lambda J_1(\tau)}{L}, 0\right)\right]. \tag{123}$$

Expanding both sides in powers of J_0 and $J_1(\tau)$, we again recover Eqn (111) for the current and arrive at the following exact relations:

$$\int {\rm d}\tau\,\Pi(\tau) = \frac{4e^2\lambda v}{\pi L}\left(1 + \frac{L}{4\pi\lambda\beta v}\frac{\partial^2 \ln \mathcal{Z}}{\partial\phi_x^2}\right), \tag{124}$$

$$\Pi''(\tau) = -\frac{16\gamma_{\rm QPS}e^2\lambda^2 v^2}{L^2}\int {\rm d}x\left\langle \cos\left(\chi(x,\tau_1)\right)\right\rangle\delta(\tau) + \frac{16\gamma_{\rm QPS}^2 e^2\lambda^2 v^2}{L^2}\int {\rm d}x_1\,{\rm d}x_2\left\langle \sin\left(\chi(x_1,\tau)\right)\sin\left(\chi(x_2,0)\right)\right\rangle. \tag{125}$$

Let us restrict our attention to the low temperature limit $T \to 0$. We are going to evaluate the imaginary time current–current correlator (55), (122) and then carry out its analytic continuation to real times. Setting $R \ll \tilde{R}_{\rm c}$ and proceeding perturbatively in $\gamma_{\rm QPS}$, in the leading approximation, Eqn (125) can be reduced to the form

$$\Pi''(\tau) = \frac{8\gamma_{\rm QPS}^2 e^2\lambda^2 v^2}{L}\int {\rm d}x\left\langle \cos\left(\chi(x,\tau)-\chi(0,0)\right)\right\rangle_0 - \frac{8\gamma_{\rm QPS}^2 e^2\lambda^2 v^2}{L}\,\delta(\tau)\int {\rm d}\tau_1\,{\rm d}x\left\langle \cos\left(\chi(x,\tau_1)-\chi(0,0)\right)\right\rangle_0, \tag{126}$$

where averaging $\langle\ldots\rangle_0$ is now performed with the noninteracting effective action

$$S_0 = \frac{1}{8\pi\lambda v}\int_0^\beta {\rm d}\tau\int_0^L {\rm d}x\left((\partial_\tau\chi)^2 + v^2(\partial_x\chi)^2\right). \tag{127}$$

The task at hand is to evaluate the correlation function

$$\left\langle \exp\left[{\rm i}\left(\chi(x,\tau)-\chi(0,0)\right)\right]\right\rangle_0 = \sum_{m,n=-\infty}^{\infty}\exp\left(2\pi {\rm i} n\phi_x\right) \times \int^{mn}\mathcal{D}\chi\,\exp\left[{\rm i}\left(\chi(x,\tau)-\chi(0,0)\right) - S_0\right], \tag{128}$$

which can be rewritten through the zero topological sector $m = n = 0$ as

$$\left\langle \exp\left[{\rm i}\left(\chi(x,\tau)-\chi(0,0)\right)\right]\right\rangle_0 = \frac{1}{\mathcal{Z}_0}\frac{\int^{00}\mathcal{D}\chi\,\exp\left[-S_0 + {\rm i}\left(\chi(x,\tau)-\chi(0,0)\right)\right]}{\int^{00}\mathcal{D}\chi\,\exp\left(-S_0\right)} \times \sum_{mn}\exp\left[-\frac{2\pi g v\beta(\phi_x+m+\tau/\beta)^2}{L} - \frac{\pi\beta v n^2}{2\lambda L} + \frac{2\pi {\rm i} n x}{L}\right], \tag{129}$$

where

$$\mathcal{Z}_0 = \sum_{mn}\exp\left[-\frac{2\pi\lambda v\beta(m+\phi_x)^2}{L} - \frac{\pi\beta v n^2}{2\lambda L}\right]. \tag{130}$$

Performing Gaussian integration in Eqn (129), we obtain

$$\left\langle \exp\left[{\rm i}\left(\chi(x,\tau)-\chi(0,0)\right)\right]\right\rangle_0 = \frac{\exp\left[G(x,\tau)-G(0,0)\right]}{\mathcal{Z}_0} \times \sum_{mn}\exp\left(-\frac{2\pi g v\beta(\phi_x+m+\tau/\beta)^2}{L} - \frac{\pi\beta v n^2}{2\lambda L} + \frac{2\pi {\rm i} n x}{L}\right), \tag{131}$$

where $G(x,\tau)$ is the noninteracting Green's function (with subtracted zero mode) obeying the equation

$$(-\partial_\tau^2 - v^2\partial_x^2)G(x,\tau) = 4\pi\lambda v\left(\delta(\tau)\delta(x) - 1\right) \tag{132}$$

with periodic boundary conditions. The solution of this equation reads

$$G(x,\tau)-G(0,0)=\frac{2\pi\lambda v\tau^2}{\beta L}-\lambda\sum_{m=-\infty}^{\infty}\ln\left\{\frac{\cosh\left[2\pi v(\tau+\beta m)/L\right]-\cos\left(2\pi x/L\right)}{\cosh\left[2\pi v(\beta m)/L\right]-1}\right\}. \tag{133}$$

The divergent term with $m=0$ in this sum is regularized by means of the replacement $G(0,0)\to G(x_0,\tau_0)$, which is appropriate since the above expressions do apply only at the space and time scales exceeding $x_0\sim\xi$ and $\tau_0\sim 1/\Delta$, respectively. With this in mind, we obtain the $m=0$ term in the form

$$\sim\ln\left[\frac{\cosh\left(2\pi v\tau/L\right)-\cos\left(2\pi x/L\right)}{4\pi^2\xi_c^2/L^2}\right]. \tag{134}$$

In the zero temperature limit, the above equations yield

$$\left\langle\cos\left(\chi(x,\tau)-\chi(0,0)\right)\right\rangle_0=\left(\frac{4\pi^2\xi_c^2}{L^2}\right)^{\lambda}\times\frac{\cosh\left(4\pi\lambda v\phi_x\tau/L\right)}{\left[\cosh\left(2\pi v\tau/L\right)-\cos\left(2\pi x/L\right)\right]^{\lambda}}. \tag{135}$$

Integrating this expression over x, we get

$$\int_0^L dx\left\langle\cos\left(\chi(\tau,x)-\chi(0,0)\right)\right\rangle_0=L\left(\frac{2\pi^2\xi_c^2}{L^2}\right)^{\lambda}\times\sum_{n=0}^{\infty}\frac{\Gamma(n+1/2)\Gamma(\lambda+n)}{\sqrt{\pi}\Gamma(\lambda)\Gamma^2(n+1)}\frac{\cosh\left(4\pi\lambda v\phi_x\tau/L\right)}{\cosh^{2n+2\lambda}(\pi v\tau/L)}, \tag{136}$$

where again $\Gamma(x)$ is the gamma function. Performing now the Fourier transformation in Eqn (136) with the aid of the relation

$$\begin{aligned}\int_{-\infty}^{\infty}d\tau\,\exp\left(i\omega\tau\right)\frac{\cosh\left(4\pi\lambda v\phi_x\tau/L\right)}{\cosh^{2n+2\lambda}(\pi v\tau/L)}&=\frac{2^{2n+2\lambda}L}{4\pi v}\sum_{m=0}^{\infty}\frac{\Gamma(2\lambda+2n+m)(-1)^m}{\Gamma(2\lambda+2n)\Gamma(m+1)}\\&\times\left(\frac{1}{\lambda(1-2\phi_x)+n+m-iL\omega/(2\pi v)}\right.\\&+\frac{1}{\lambda(1+2\phi_x)+n+m-iL\omega/(2\pi v)}\\&+\frac{1}{\lambda(1-2\phi_x)+n+m+iL\omega/(2\pi v)}\\&\left.+\frac{1}{\lambda(1+2\phi_x)+n+m+iL\omega/(2\pi v)}\right)\end{aligned} \tag{137}$$

and combining the result with Eqn (126) after simple algebra, we arrive at the following expression:

$$\Pi_{i\omega}=\frac{8\gamma_{QPS}^2e^2\lambda^2v^2}{\Gamma^2(\lambda)}\left(\frac{8\pi^2\xi_c^2}{L^2}\right)^{\lambda}\sum_{k=0}^{\infty}\frac{\Gamma^2(\lambda+k)}{\Gamma^2(1+k)}\times\left[\frac{1}{\Omega_k(\phi_x)\left(\omega^2+\Omega_k^2(\phi_x)\right)}+\frac{1}{\Omega_k(-\phi_x)\left(\omega^2+\Omega_k^2(-\phi_x)\right)}\right], \tag{138}$$

where

$$\Omega_k(\phi_x)=\frac{2\pi\lambda v(1+2\phi_x)}{L}+\frac{4\pi vk}{L} \tag{139}$$

denotes the energy differences between the exited states and the ground state of our ring. Equation (139) applies for $-1/2<\phi_x\leqslant 1/2$. Outside this interval, $\Omega_k(\phi_x)$ should be continued periodically with the period equal to unity.

What remains is to perform an analytic continuation of Eqn (138) with the aid of Eqn (59). As a result, we obtain the expression for the supercurrent noise power spectrum at $T=0$:

$$\begin{aligned}\mathcal{S}_\omega=&\frac{4\pi\gamma_{QPS}^2e^2\lambda^2v^2}{\Gamma^2(\lambda)}\left(\frac{8\pi^2\xi_c^2}{L^2}\right)^{\lambda}\sum_{k=0}^{\infty}\frac{\Gamma^2(\lambda+k)}{\Gamma^2(1+k)}\\&\times\left[\frac{1}{\Omega_k^2(\phi_x)}\delta\left(\omega-\Omega_k(\phi_x)\right)+\frac{1}{\Omega_k^2(\phi_x)}\delta\left(\omega+\Omega_k(\phi_x)\right)\right.\\&+\frac{1}{\Omega_k^2(-\phi_x)}\delta\left(\omega-\Omega_k(-\phi_x)\right)\\&\left.+\frac{1}{\Omega_k^2(-\phi_x)}\delta\left(\omega+\Omega_k(-\phi_x)\right)\right].\end{aligned} \tag{140}$$

In accordance with general considerations [35, 56], the spectrum $\mathcal{S}_\omega$ depends periodically on the external magnetic flux ϕ_x and consists of sharp peaks at the frequencies Ω_k corresponding to the system eigenmodes. These features clearly illustrate the coherent nature of supercurrent noise.

The effect of inter-QPS interactions on supercurrent noise turns out to be richer than that of the average supercurrent value analyzed above. In contrast to the latter, fluctuations in the supercurrent cannot in general be correctly described by Hamiltonian (108), even if the renormalization of γ_{QPS} (117) is taken into account. This is because virtual tunneling of flux quanta across a superconducting wire in general leads to the creation of plasmon modes, thereby causing extra peaks with $k\neq 0$ in the supercurrent noise power spectrum (140). The simplest process of this kind is associated with the simultaneous creation of two plasmons with opposite momenta values propagating clockwise and counterclockwise around a ring. This process is illustrated in Fig. 9. Thus, by experimentally detecting these peaks, one can directly demonstrate the existence of Mooij–Schön plasma modes in superconducting nanorings.

Let us emphasize again that, owing to its coherent nature, supercurrent noise can be tuned by an external magnetic flux piercing the ring. Both the positions of the peaks and the magnitude of this noise essentially depend on ϕ_x. Here, we evaluated the dependence $\mathcal{S}_\omega(\phi_x)$ in the experimentally relevant limit $R<\tilde{R}_c$, in which case we can proceed perturbatively in the QPS rate γ_{QPS}. In the opposite limit

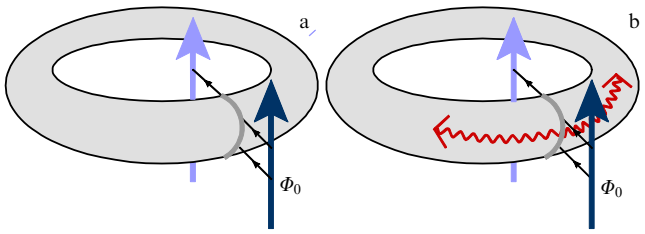

Figure 9. Schematic of the process of coherent flux tunneling (a) without and (b) with excitation of a pair of Mooij–Schön plasma modes.

$R > \tilde{R}_c$, supercurrent noise also has the form of sharp peaks, although its dependence on the magnetic flux becomes much weaker [54]. As follows from Eqn (140), in the immediate vicinity of level degeneracy points $\phi_x = \pm 1/2$, supercurrent fluctuations become strong, and our analysis perturbative in γ_{QPS} fails, even for $R \ll \tilde{R}_c$. In this case, it is necessary to account for level splitting and regularize the corresponding terms in Eqn (140) by substituting the value $\sim U_0$ instead of $\Omega_0(\phi_x)$ whenever the former exceeds the latter.

At nonzero temperatures, supercurrent noise is modified in two ways: (i) a zero frequency peak (61) appears which is not related to QPS and (ii) numerous extra QPS-related peaks at nonzero frequencies emerge (cf. (56)). At low enough T, quantum coherence is still maintained; however, with increasing temperature, the dependence on ϕ_x comes to be less pronounced and supercurrent noise eventually becomes incoherent.

Finally, we point out a certain physical similarity between the supercurrent noise studied here and that in superconducting weak links analyzed elsewhere [57–59]. In addition, in the latter case, the noise power spectrum depends on the phase difference across the weak link and has the form of peaks at both zero and nonzero frequencies. Similarly to our problem, at $T \to 0$, the zero frequency peak disappears, while all other peaks persist except in the limit of fully transparent barriers [57–59]. Unlike here, however, in the case of superconducting weak links, nonzero frequency peaks originate from subgap Andreev levels and are not related to quantum phase slips.

6. Shot noise from quantum phase slips

In Section 5, we demonstrated that quantum phase slips may strongly affect the equilibrium properties of superconducting nanorings and even cause supercurrent noise in the ground state of such systems. Here, we will continue studying QPS-generated noise in a different physical situation. To this end, we will get back to a thin superconducting wire embedded in an external circuit as shown in Fig. 6 (see Section 4.1).

Can such a superconducting wire generate voltage fluctuations? Furthermore, can this wire produce shot noise provided it is biased by an external current $I = V_x/R_x$? In posing these questions, we imply that temperature T and typical values of voltage, frequency, and all other relevant energy parameters remain well below superconducting gap Δ, i.e., the superconductor is either in or sufficiently close to its quantum ground state.

At first sight, positive answers to both these questions can be rejected on fundamental grounds, because a superconducting state is characterized by zero resistance. Hence, the system can sustain a nondissipative current below some critical value, and neither nonzero average voltage nor voltage fluctuations can be expected.

These simple considerations — although applicable to bulk superconductors — become obviously insufficient in the case of ultrathin superconducting wires because of the presence of quantum phase slips. As we already discussed in Section 4, each QPS event corresponds to the net phase jump by $\delta\varphi = \pm 2\pi$, implying positive or negative voltage pulse $\delta V = \dot{\varphi}/2e$ and tunneling of one magnetic flux quantum $\Phi_0 \equiv \pi/e = \int |\delta V(t)|\, dt$ across the wire perpendicular to its axis. This process is illustrated in the upper part of Fig. 7a. Biasing the wire by an external current I, one breaks the symmetry between positive and negative voltage pulses, making the former more likely than the latter. As a result, the net voltage drop V occurs across the wire, also implying nonzero resistance $R = V/I$, which may not vanish down to the lowest temperatures [12, 14]. Thus, according to, for example, the fluctuation-dissipation theorem (FDT), in the presence of QPS, one should also expect voltage fluctuations to occur in the system.

While these general arguments suggest a positive answer to the first of the above questions, they do not specifically address the issue of shot noise. Let us recall that two key prerequisites of shot noise are (see, e.g., Ref. [60]): (i) the presence of discrete charge carriers (e.g., electrons) in the system and (ii) the scattering of such carriers on disorder. As for superconducting nanowires, although discrete charge carriers — Cooper pairs — are certainly present there, they form a superconducting condensate flowing along the wire *without any scattering*. For this reason, the possibility of shot noise occurring in superconducting nanowires needs special analysis, which we are going to outline further below.

6.1 Keldysh technique and perturbation theory

An effective Hamiltonian $\hat{H}_{eff}$ for the structure depicted in Fig. 6 was already derived in Section 4.1 (see Eqn (74)). In order to proceed, we will follow Ref. [61] and employ the Keldysh path integral technique. As usual, we define our variables of interest on the forward and backward time branches of the Keldysh contour, i.e., we introduce the variables $\varphi_{F,B}(t)$ and $\chi_{F,B}(x,t)$. We also routinely define the 'classical' and 'quantum' variables, respectively, $\varphi_+(t) = (\varphi_F(t) + \varphi_B(t))/2$ and $\varphi_-(t) = \varphi_F(t) - \varphi_B(t)$ (and similarly for the χ-fields). Making use of the Josephson relation between the voltage and the phase, we can formally express the expectation value of the voltage operator across the superconducting wire in the form

$$\langle V(t_1)\rangle = \frac{1}{2e}\langle \dot{\varphi}_+(t_1)\exp(iS_{QPS})\rangle_0\,, \tag{141}$$

where

$$S_{QPS} = -2\gamma_{QPS}\int dt \int_0^L dx\, \sin(\chi_+)\sin\left(\frac{\chi_-}{2}\right), \tag{142}$$

$$\langle \ldots\rangle_0 = \int \mathcal{D}^2\varphi(t)\,\mathcal{D}^2\chi(x,t)\,(\ldots)\exp\left(iS_0[\varphi,\chi]\right) \tag{143}$$

implies averaging with the Keldysh effective action S_0 corresponding to the noninteracting Hamiltonian $\hat{H}_0 = \hat{H}_{eff} - \hat{H}_{QPS}$, where H_{QPS} is defined in Eqn (79). Similarly, for the symmetrized voltage–voltage correlator

$$\langle V(t_1)V(t_2)\rangle = \frac{1}{2}\left\langle \left(\hat{V}(t_1)\hat{V}(t_2) + \hat{V}(t_2)\hat{V}(t_1)\right)\right\rangle, \tag{144}$$

we obtain

$$\langle V(t_1)V(t_2)\rangle = \frac{1}{4e^2}\langle \dot{\varphi}_+(t_1)\dot{\varphi}_+(t_2)\exp(iS_{QPS})\rangle_0\,. \tag{145}$$

Equations (141) and (145) are formally exact expressions which we are now going to evaluate perturbatively in γ_{QPS}. In the zero order in γ_{QPS}, all averages can be handled exactly with the aid of the Green's functions

$$\begin{aligned} G^R_{ab}(X,X') &= -i\langle a_+(X)b_-(X')\rangle\,,\\ G^K_{ab}(X,X') &= -i\langle a_+(X)b_+(X')\rangle, \end{aligned} \tag{146}$$

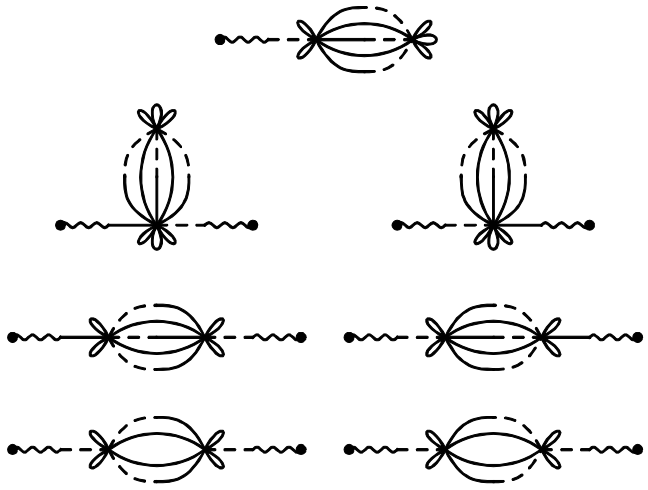

Figure 10. 'Candy' diagrams, which determine both average voltage (141) (upper diagram) and voltage noise (145) (six remaining diagrams) in the second order in $\gamma_{\rm QPS}$. Fields φ_+, χ_+, and χ_- in the propagators (146) are denoted by wavy, solid, and dashed lines, respectively.

where $a(X)$ and $b(X)$ denote one of the fields $\varphi(t)$ and $\chi(x,t)$. As both these fields are real, the advanced and retarded Green's functions obey the condition $G^{\rm A}_{ab}(\omega) = G^{\rm R}_{ba}(-\omega)$, and the Keldysh function $G^{\rm K}$ can be expressed in the form

$$G^{\rm K}_{ab}(\omega) = \frac{1}{2}\coth\left(\frac{\omega}{2T}\right)\left(G^{\rm R}_{ab}(\omega) - G^{\rm R}_{ba}(-\omega)\right). \tag{147}$$

Expanding Eqns (141) and (145) up to the second order in $\gamma_{\rm QPS}$ and performing all necessary averages, we evaluate the results in terms of Green's functions (146), expressing them in the form of 'candy' diagrams, displayed in Fig. 10. They involve four different propagators ($G^{\rm R,K}_{\chi\chi}$ and $G^{\rm R,K}_{\varphi\chi}$) and plenty of vertices originating from Taylor expansion of the cosine terms. Summing up all the diagrams in the same order in $\gamma_{\rm QPS}$, we arrive at the final expression containing the exponents of the Green's functions.

6.2 Current–voltage curve and voltage noise

Let us first re-derive the results [12] for the average voltage within the framework of our technique. We obtain

$$\langle V\rangle = \frac{{\rm i}\gamma^2_{\rm QPS}}{8e}\int_0^L {\rm d}x\int_0^L {\rm d}x'\left(\lim_{\omega\to 0}\omega G^{\rm R}_{\varphi\chi}(x;\omega)\right) \times\left(\mathcal{P}_{x,x'}(-I\Phi_0) - \mathcal{P}_{x,x'}(I\Phi_0)\right), \tag{148}$$

where $\mathcal{P}_{x,x'}(\omega) = P_{x,x'}(\omega) + \bar{P}_{x,x'}(\omega)$ and

$$P_{x,x'}(\omega) = \int_0^\infty {\rm d}t\,\exp({\rm i}\omega t)\exp\left[{\rm i}\mathcal{G}(x,x';t,0)\right], \tag{149}$$

$$\mathcal{G}(x,x';t,0) = G^{\rm K}_{\chi\chi}(x,x';t,0) - \frac{1}{2}G^{\rm K}_{\chi\chi}(x,x;t,t) - \frac{1}{2}G^{\rm K}_{\chi\chi}(x',x';0,0) + \frac{1}{2}G^{\rm R}_{\chi\chi}(x,x';t,0). \tag{150}$$

Bearing in mind that $\lim_{\omega\to 0}\omega G^{\rm R}_{\varphi\chi}(x;\omega) = 2\pi{\rm i}$, Eqn (148) can be cast in the form

$$\langle V\rangle = \Phi_0\left(\Gamma_{\rm QPS}(I\Phi_0) - \Gamma_{\rm QPS}(-I\Phi_0)\right), \tag{151}$$

where we identify $\Gamma_{\rm QPS}$ as

$$\Gamma_{\rm QPS}(\omega) = \frac{\gamma^2_{\rm QPS}}{4}\int_0^L {\rm d}x\int_0^L {\rm d}x'\,\mathcal{P}_{x,x'}(\omega). \tag{152}$$

Comparing result (151) with that found in Ref. [12], we immediately conclude that $\Gamma_{\rm QPS}(I\Phi_0)$ defines the quantum decay rate of the current state due to QPS. In [12], this rate was evaluated from the imaginary part of the free energy $\Gamma_{\rm QPS}(I\Phi_0) = 2\,{\rm Im}\,F$. Here, we derived the expression for $\Gamma_{\rm QPS}$ by means of the real time technique without employing the Im F-method [62].

Making use of the above results, evaluating the Green's functions (146), and keeping in mind the detailed balance condition

$$\mathcal{P}_{x,x'}(\omega) = \exp\left(\frac{\omega}{T}\right)\mathcal{P}_{x,x'}(-\omega), \tag{153}$$

we obtain

$$\langle V\rangle = \frac{\Phi_0 L v\gamma^2_{\rm QPS}}{4}\,\varsigma^2\left(\frac{I\Phi_0}{2}\right)\sinh\left(\frac{I\Phi_0}{2T}\right), \tag{154}$$

where

$$\varsigma(\omega) = \tau_0^{\lambda}(2\pi T)^{\lambda-1}\,\frac{\mathbb{\Gamma}\left(\lambda/2 - {\rm i}\omega/(2\pi T)\right)\mathbb{\Gamma}\left(\lambda/2 + {\rm i}\omega/(2\pi T)\right)}{\mathbb{\Gamma}(\lambda)}. \tag{155}$$

Here, for the sake of simplicity, we assumed that $v\tau_0 \sim x_0$. It is satisfactory to observe that the result (154), (155) matches that derived in Ref. [12] by means of the Im F-technique. A detailed analysis of the relation between the Im F-approach and the Keldysh technique employed here can be found in Ref. [63].

Let us now turn to the voltage–voltage correlator. Our perturbative analysis allows recovering three different contributions to the noise power spectrum, i.e.,

$$\mathcal{S}_\Omega = \int {\rm d}t\,\exp({\rm i}\Omega t)\left\langle V(t)V(0)\right\rangle = \mathcal{S}^{(0)}_\Omega + \mathcal{S}^r_\Omega + \mathcal{S}^a_\Omega. \tag{156}$$

The first of these contributions $\mathcal{S}^{(0)}_\Omega$ defines equilibrium voltage noise for a transmission line and has nothing to do with QPS. This contribution reads

$$\mathcal{S}^{(0)}_\Omega = \frac{{\rm i}\Omega^2\coth\left(\Omega/(2T)\right)}{16e^2}\left(G^{\rm R}_{\varphi\varphi}(\Omega) - G^{\rm R}_{\varphi\varphi}(-\Omega)\right). \tag{157}$$

The remaining two terms are due to QPS effects. The term $\mathcal{S}^r_\Omega$ is also proportional to $\coth\left(\Omega/(2T)\right)$ and contains the products of two retarded (advanced) Green's functions:

$$\mathcal{S}^r_\Omega = \frac{\gamma^2_{\rm QPS}\Omega^2\coth\left(\Omega/(2T)\right)}{16e^2}\int_0^L {\rm d}x\int_0^L {\rm d}x'\,{\rm Re}\Big[G^{\rm R}_{\varphi\chi}(x;\Omega) \times\left(\mathcal{F}_{x,x'}(\Omega)G^{\rm R}_{\varphi\chi}(x';\Omega) - \mathcal{F}_{x,x'}(0)G^{\rm R}_{\varphi\chi}(x;\Omega)\right)\Big], \tag{158}$$

where

$$\mathcal{F}_{x,x'}(\Omega) = -P_{x,x'}(\Omega + I\Phi_0) - P_{x,x'}(\Omega - I\Phi_0) + \bar{P}_{x,x'}(-\Omega + I\Phi_0) + \bar{P}_{x,x'}(-\Omega - I\Phi_0). \tag{159}$$

The remaining term $\mathcal{S}^a_\Omega$ contains the product of one retarded and one advanced Green's functions and scales with the combinations $\mathcal{C}_\pm = \coth\left((\Omega \pm I\Phi_0)/(2T)\right) - \coth\left(\Omega/(2T)\right)$ as

$$\mathcal{S}^a_\Omega = \frac{\gamma^2_{\rm QPS}\Omega^2}{32e^2}\int_0^L \mathrm{d}x \int_0^L \mathrm{d}x'\, G^{\rm R}_{\varphi\chi}(x;\Omega)G^{\rm R}_{\varphi\chi}(x';-\Omega) \times \left[\sum_\pm \mathcal{C}_\pm\left(\mathcal{P}_{x,x'}(\Omega \pm I\Phi_0) - \mathcal{P}_{x,x'}(-\Omega \mp I\Phi_0)\right)\right]. \quad (160)$$

Equations (156)–(160), together with the expressions for the Green's functions, fully account for the voltage noise power spectrum of a superconducting nanowire in the regime perturbative in $\gamma_{\rm QPS}$.

In the zero bias limit $I \to 0$, the term $\mathcal{S}^a_\Omega$ vanishes, and the equilibrium noise spectrum $\mathcal{S}_\Omega = \mathcal{S}^{(0)}_\Omega + \mathcal{S}^r_\Omega$ is determined from the FDT (see also [34]). At nonzero bias values, the QPS noise becomes nonequilibrium. In the zero frequency limit $\Omega \to 0$, the terms $\mathcal{S}^{(0)}_\Omega$ and $\mathcal{S}^r_\Omega$ vanish, and the voltage noise $\mathcal{S}_{\Omega\to 0} \equiv \mathcal{S}_0$ is determined solely by $\mathcal{S}^a_\Omega$. Then, from Eqn (160), we get [61]

$$\mathcal{S}_0 = \Phi_0^2\left(\Gamma_{\rm QPS}(I\Phi_0) + \Gamma_{\rm QPS}(-I\Phi_0)\right) = \Phi_0 \coth\left(\frac{I\Phi_0}{2T}\right)\langle V\rangle, \quad (161)$$

where $\langle V\rangle$ is specified in Eqns (151), (154). Combining (161) with (154) and (155), we obtain

$$\mathcal{S}_0 \propto \begin{cases} T^{2\lambda-2}, & T \gg I\Phi_0, \\ I^{2\lambda-2}, & T \ll I\Phi_0. \end{cases} \quad (162)$$

At higher temperatures $T \gg I\Phi_0$ (though still $T \ll \Delta_0$), Eqn (162) just describes equilibrium voltage noise $S_0 = 2TR$ of a linear Ohmic resistor $R = \langle V\rangle/I \propto T^{2\lambda-3}$ [12]. In the opposite low temperature limit $T \ll I\Phi_0$, it accounts for QPS-induced *shot noise* $\mathcal{S}_0 = \Phi_0\langle V\rangle$, obeying the *Poisson statistics* with an effective 'charge' equal to the flux quantum Φ_0. This result makes the physical origin of shot noise in superconducting nanowires transparent: it is produced by coherent tunneling of magnetic flux quanta Φ_0 across the wire (cf. also Fig. 7).

Another interesting limit is that of sufficiently high frequencies and/or long wires $v/L \ll \Omega \ll \Delta_0$. In this case, we obtain

$$\mathcal{S}^{(0)}_\Omega = \frac{\lambda}{8\pi e^2}\,\frac{\Omega\coth\left(\Omega/(2T)\right)}{(\Omega/2E_C)^2 + (\lambda/\pi)^2}. \quad (163)$$

Note that this contribution is independent of the wire length L. At low T and $\Omega/\lambda \gtrsim E_C = e^2/2C$, we have $\mathcal{S}^{(0)}_\Omega \propto 1/\Omega$, i.e., in a certain regime, the wire may generate $1/f$ voltage noise. Evaluating the QPS terms $\mathcal{S}^r_\Omega$ and $\mathcal{S}^a_\Omega$, we observe that the latter scales linearly with wire length L, whereas the former does not. Hence, the term $\mathcal{S}^r_\Omega$ can be disregarded in the long wire limit. For the remaining QPS term $\mathcal{S}^a_\Omega$, we get

$$\mathcal{S}^a_\Omega = \frac{L\lambda^2 v\gamma^2_{\rm QPS}}{8e^2}\left[\varsigma\left(\frac{I\Phi_0}{2} - \Omega\right) - \varsigma\left(\frac{I\Phi_0}{2} + \Omega\right)\right] \times \frac{\sinh\left(I\Phi_0/(2T)\right)\varsigma(I\Phi_0/2)}{\left((\Omega/2E_C)^2 + (\lambda/\pi)^2\right)\sinh\left(\Omega/(2T)\right)}. \quad (164)$$

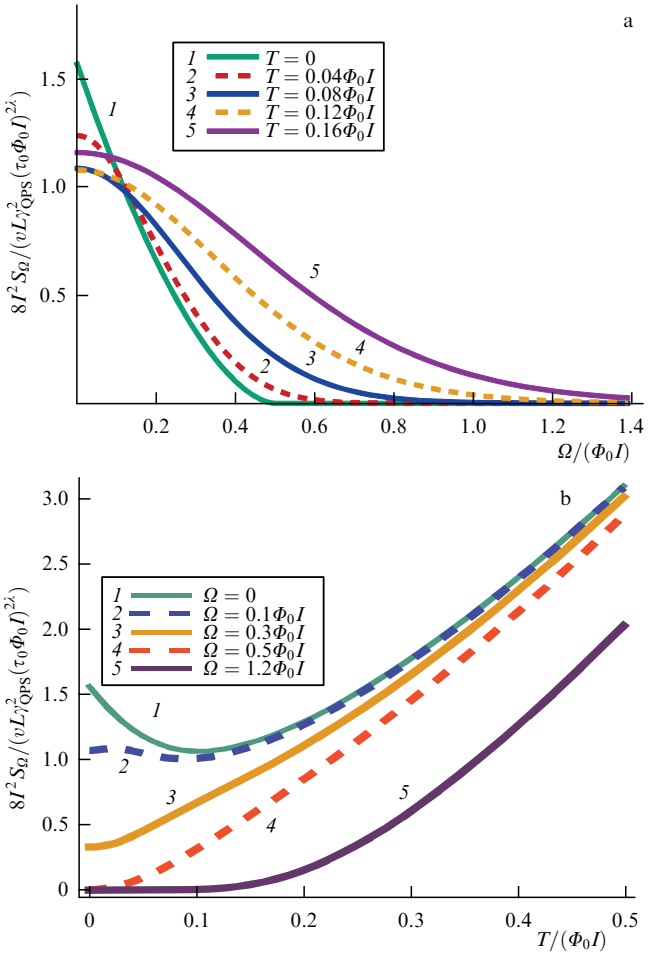

Figure 11. (a) Frequency dependence of QPS noise spectrum $\mathcal{S}_\Omega$ (164) at $\lambda = 2.7$, large E_C, and different values of T in the long wire limit. (b) $\mathcal{S}_\Omega$ as a function of T.

At $T \to 0$, from Eqn (164), we find

$$\mathcal{S}^a_\Omega \propto \begin{cases} I^{\lambda-1}\left(I - \dfrac{2\Omega}{\Phi_0}\right)^{\lambda-1}, & \Omega < \dfrac{I\Phi_0}{2}, \\ 0, & \Omega > \dfrac{I\Phi_0}{2}. \end{cases} \quad (165)$$

This result can be interpreted as follows. At $T = 0$, each QPS event excites (at least) two plasmons with total energy $E = I\Phi_0$ and zero total momentum propagating in opposite directions along the wire. One plasmon (whose energy equals $E/2$) gets dissipated at the grounded end of the wire, while the other one (also with energy $E/2$) reaches its opposite end, causing voltage fluctuations (it emits a photon) with frequency Ω measured by a detector. Clearly, at $T = 0$, this process is only possible at $\Omega < E/2$, in agreement with Eqn (165).

The result (164) is also illustrated in Fig. 11. At sufficiently small Ω (though we still keep $\Omega \gg v/L$), we observe a nonmonotonic dependence of $\mathcal{S}_\Omega$ on temperature, which serves as a clear manifestation of the quantum coherent nature of QPS noise.

To conclude our analysis of QPS-induced shot noise in superconducting nanowires, we point out that the approach employed here that is perturbative in $\gamma_{\rm QPS}$ is fully justified in the 'superconducting' regime, i.e., for not too thin wires with

$\lambda > 2$. In wires with $\lambda < 2$ (characterized by unbound QPS–anti-QPS pairs), the perturbation theory becomes unsuitable at quite low energies and large distances, since γ_{QPS} gets effectively renormalized to higher values (see, e.g., BKT-like RG equations (116)). Even in this case, however, our results may still remain applicable at relatively high temperatures, frequencies, and/or current values. In the low energy limit, long wires with $\lambda < 2$ show an insulating behavior, as follows from the exact solution to the corresponding sine-Gordon model [64]. This solution suggests that voltage fluctuations also become large in this limit.

Further interesting features of the shot noise of the voltage in superconducting nanowires under different measuring systems were analyzed in Refs [43, 63, 65, 66].

7. Full counting statistics of quantum phase slips

In order to fully describe voltage fluctuations in the system under consideration, it is generally necessary to evaluate all cumulants of the voltage operator. Various aspects of voltage fluctuation statistics were already discussed in the case of quasi-one-dimensional wires [15] and resistively shunted Josephson junctions [67, 68]. The authors of [15, 67, 68] restricted their analysis to thermal fluctuations and, hence, their results remain applicable only at sufficiently high temperatures. Here, in contrast, we will set up a fully quantum mechanical treatment of the problem that essentially operates with interacting quantum phase slips and allows us to fully describe full counting statistics of voltage fluctuations at any temperature down to $T \to 0$. In our further analysis, we will to a large extent follow Ref. [69].

As in Section 6.1, we can again make use of the Josephson relation between the voltage and the phase variables. Then, analogously to the averages in Eqns (141) and (145), we can express the general correlator of voltages in the form

$$\begin{aligned}\bigl\langle V(t_1)V(t_2)\dots V(t_n)\bigr\rangle \\ = \frac{1}{(2e)^n}\bigl\langle \dot\varphi_+(t_1)\dot\varphi_+(t_2)\dots\dot\varphi_+(t_n)\exp\left(\mathrm{i}S_{\mathrm{QPS}}\right)\bigr\rangle_0 .\end{aligned} \tag{166}$$

Here, we stress that Eqn (166) defines the symmetrized voltage correlators. For example, for $n = 2$, this equation is equivalent to Eqn (151), whereas for $n = 3$ one can verify that [63, 70]

$$\begin{aligned}\bigl\langle V(t_1)V(t_2)V(t_3)\bigr\rangle = \frac{1}{8}\Bigl\{\bigl\langle \hat V(t_1)\bigl(\mathcal{T}\hat V(t_2)\hat V(t_3)\bigr)\bigr\rangle \\ + \bigl\langle\bigl(\tilde{\mathcal{T}}\hat V(t_2)\hat V(t_3)\bigr)\hat V(t_1)\bigr\rangle + \bigl\langle \hat V(t_2)\bigl(\mathcal{T}\hat V(t_1)\hat V(t_3)\bigr)\bigr\rangle \\ + \bigl\langle\bigl(\tilde{\mathcal{T}}\hat V(t_1)\hat V(t_3)\bigr)\hat V(t_2)\bigr\rangle + \bigl\langle \hat V(t_3)\bigl(\mathcal{T}\hat V(t_1)\hat V(t_2)\bigr)\bigr\rangle \\ + \bigl\langle\bigl(\tilde{\mathcal{T}}\hat V(t_1)\hat V(t_2)\bigr)\hat V(t_3)\bigr\rangle + \bigl\langle \mathcal{T}\hat V(t_1)\hat V(t_2)\hat V(t_3)\bigr\rangle \\ + \bigl\langle \tilde{\mathcal{T}}\hat V(t_1)\hat V(t_2)\hat V(t_3)\bigr\rangle\Bigr\},\end{aligned} \tag{167}$$

where $\mathcal{T}$ and $\tilde{\mathcal{T}}$ are, respectively, the forward and backward time ordering operators.

7.1 Cumulant generating function

In order to proceed with our calculation of higher voltage correlators, it will be convenient for us to define the cumulant generating function

$$\mathcal{W}[J] = \ln\bigl(\mathcal{Z}[J]\bigr) = \ln\left\langle \exp\left(\mathrm{i}\int \mathrm{d}t\, J(t)V(t)\right)\right\rangle, \tag{168}$$

where

$$V = \frac{1}{\Phi_0 C}\left(\partial_x\chi\left(-\frac{L}{2}\right) - \partial_x\chi\left(\frac{L}{2}\right)\right) \tag{169}$$

is the voltage drop across a wire and $\langle\dots\rangle$ denotes the quantum average fulfilled with the total Hamiltonian of our system. Evaluating the Nth variational derivative of $\mathcal{W}[J]$ with respect to $J(t)$, the Nth cumulant of the voltage operator is recovered.

The function $\mathcal{Z}[J]$ can be conveniently derived with the aid of the Keldysh path integral technique already described in Section 6. Defining the voltage values V (169) on both forward and backward time branches of the Keldysh contour, respectively, V_{F} and V_{B}, and introducing, as before, 'classical' and 'quantum' variables $v_+ = (V_{\mathrm{F}} + V_{\mathrm{B}})/2$ and $v_- = V_{\mathrm{F}} - V_{\mathrm{B}}$, one can verify that the voltage cumulants of (166) are exactly equivalent to the cumulants of the 'classical' variable $v_+(t)$ in our path integral formalism. With this in mind, the function $\mathcal{Z}[J]$ can be expressed as

$$\mathcal{Z}[J] = \left\langle \exp\left(\mathrm{i}S_{\mathrm{QPS}}[\chi_+,\chi_-]\right)\exp\left(\mathrm{i}\int \mathrm{d}t\, J(t)v_+(t)\right)\right\rangle_0, \tag{170}$$

where S_{QPS} is defined in (142). Function (170) generates voltage correlators

$$\begin{aligned}\bigl\langle v_+(t_1)v_+(t_2)\dots v_+(t_n)\bigr\rangle \\ = \bigl\langle v_+(t_1)v_+(t_2)\dots v_+(t_n)\exp\left(\mathrm{i}S_{\mathrm{QPS}}\right)\bigr\rangle_0 .\end{aligned} \tag{171}$$

Let us eliminate the second exponent in Eqn (170) by making a linear substitution $\chi_i = \lambda_i + \tilde\chi_i$ and imposing the condition

$$\left\langle \tilde\chi_i \exp\left(\mathrm{i}\int \mathrm{d}t\, J(t)v_+(t)\right)\right\rangle_0 = 0, \tag{172}$$

implying that

$$\lambda_+(x,t) = \chi_0(x,t) - \int \mathrm{d}t'\, G^{\mathrm{K}}_{\chi^v}(x;t,t')J(t'), \tag{173}$$

$$\lambda_-(x,t) = -\int \mathrm{d}t'\, G^{\mathrm{A}}_{\chi^v}(x;t,t')J(t'). \tag{174}$$

Here, we denoted $\chi_0 \equiv \langle\chi_+\rangle_0$ and introduced both Keldysh and advanced Green's functions

$$G^{\mathrm{K}}_{\chi^v}(x;t,t') = -\mathrm{i}\bigl\langle \chi_+(x,t)v_+(t')\bigr\rangle_0, \tag{175}$$

$$G^{\mathrm{A}}_{\chi^v}(x;t,t') = -\mathrm{i}\bigl\langle \chi_-(x,t)v_+(t')\bigr\rangle_0 . \tag{176}$$

The latter function coincides with the transposed version of the retarded Green's function

$$G^{\mathrm{R}}_{\chi^v}(x;t,t') = -\mathrm{i}\bigl\langle \chi_+(x,t)v_-(t')\bigr\rangle_0 . \tag{177}$$

As a result of the above manipulations, we get

$$\begin{aligned}\mathcal{Z}[J] = \exp\left[-\frac{\mathrm{i}}{2}\int \mathrm{d}t\,\mathrm{d}t'\, J(t)G^{\mathrm{K}}_{vv}(t,t')J(t')\right] \\ \times\bigl\langle \exp\left(\mathrm{i}S_{\mathrm{QPS}}[\lambda_+ + \tilde\chi_+, \lambda_- + \tilde\chi_-]\right)\bigr\rangle_0 ,\end{aligned} \tag{178}$$

where Keldysh Green's function $G^{\rm K}_{vv}(t,t')$ is defined analogously to that in Eqn (175). The remaining average can be performed with the aid of Wick's theorem and expressed via two Green's functions,

$$G^{\rm K}_{\chi\chi}(x,x';t,t') = -{\rm i}\big\langle\tilde\chi_+(x,t)\tilde\chi_+(x',t')\big\rangle_0\,, \tag{179}$$

$$G^{\rm R}_{\chi\chi}(x,x';t,t') = -{\rm i}\big\langle\tilde\chi_+(x,t)\tilde\chi_-(x',t')\big\rangle_0\,, \tag{180}$$

while all $\langle\tilde\chi_-\tilde\chi_-\rangle_0$ type averages vanish identically due to causality.

Let us now evaluate the cumulant generating function by expanding $\mathcal{Z}[J]$ up to the second order in $\gamma_{\rm QPS}$. We obtain

$$\begin{aligned}\mathcal{W}[J] = &-\frac{\rm i}{2}\int {\rm d}t\,{\rm d}t'\,J(t)G^{\rm K}_{vv}(t,t')J(t')\\ &+{\rm i}\big\langle S_{\rm QPS}[\lambda_+ +\tilde\chi_+,\lambda_- +\tilde\chi_-]\big\rangle_0\\ &-\frac{1}{2}\big\langle S^2_{\rm QPS}[\lambda_+ +\tilde\chi_+,\lambda_- +\tilde\chi_-]\big\rangle_0\\ &+\frac{1}{2}\big\langle S_{\rm QPS}[\lambda_+ +\tilde\chi_+,\lambda_- +\tilde\chi_-]\big\rangle_0^2\,.\end{aligned} \tag{181}$$

Substituting now the QPS action $S_{\rm QPS}$ (142) into Eqn (181), we can verify that the first order contribution in $\gamma_{\rm QPS}$ vanishes, while the second order one takes the form

$$\begin{aligned}\mathcal{W}[J] \approx &-\frac{\rm i}{2}\int {\rm d}t\,{\rm d}t'\,J(t)G^{\rm K}_{vv}(t,t')J(t') + \gamma^2_{\rm QPS}\int_{-L/2}^{L/2}{\rm d}x\,{\rm d}x'\\ &\times\int {\rm d}t\int^t {\rm d}t'\,\big(P(x,x';t,t') - P(x',x;t',t)\big)\\ &\times\sin\big(\lambda_+(x,t)-\lambda_+(x',t')\big)\sin\left(\frac{\lambda_-(x,t)}{2}\right)\cos\left(\frac{\lambda_-(x',t')}{2}\right)\\ &-\frac{\gamma^2_{\rm QPS}}{2}\int_{-L/2}^{L/2}{\rm d}x\,{\rm d}x'\int {\rm d}t\int {\rm d}t'\,\big(P(x,x';t,t') + P(x',x;t',t)\big)\\ &\times\cos\big(\lambda_+(x,t)-\lambda_+(x',t')\big)\sin\left(\frac{\lambda_-(x,t)}{2}\right)\sin\left(\frac{\lambda_-(x',t')}{2}\right),\end{aligned} \tag{182}$$

where the function $P(x,x';t,t')$ is defined in

$$\begin{aligned}P(x,x';t,t') &= \left\langle\exp\left[{\rm i}\left(\tilde\chi_+(x,t)-\tilde\chi_+(x',t')\right.\right.\right.\\ &\left.\left.\left.-\frac{1}{2}\tilde\chi_-(x,t)-\frac{1}{2}\tilde\chi_-(x',t')\right)\right]\right\rangle_0 = \left\langle\exp\left[{\rm i}\left(\tilde\chi_+(x',t')\right.\right.\right.\\ &\left.\left.\left.-\tilde\chi_+(x,t)+\frac{1}{2}\tilde\chi_-(x,t)+\frac{1}{2}\tilde\chi_-(x',t')\right)\right]\right\rangle_0\\ &= \exp\left({\rm i}G^{\rm K}_{\chi\chi}(x,x';t,t') - \frac{\rm i}{2}\,G^{\rm K}_{\chi\chi}(x,x;t,t)\right.\\ &\left.-\frac{\rm i}{2}\,G^{\rm K}_{\chi\chi}(x',x';t',t') + \frac{\rm i}{2}\,G^{\rm R}_{\chi\chi}(x,x';t,t') - \frac{\rm i}{2}\,G^{\rm A}_{\chi\chi}(x,x';t,t')\right).\end{aligned} \tag{183}$$

Equation (182) enables us to directly evaluate all voltage correlators by taking variational derivatives of $\mathcal{W}$ with respect to $J(t)$. It follows immediately from Eqn (182) that in the absence of QPS all voltage cumulants except for the second one (describing Gaussian noise) vanish identically. We conclude, therefore, that at fairly low temperatures only quantum phase slips give rise to both shot noise of the voltage and all higher cumulants of the voltage operator in superconducting nanowires.

We also note that, in the case of a constant in time current bias I, we have $\chi_0(x,t) = I\Phi_0 t$ and the function P depends only on the time difference, i.e., $P(x,x';t,t') = P(x,x';t-t')$. This property will be employed in our subsequent calculations.

7.2 Voltage cumulants in the zero frequency limit

As a first step, let us make use of the above general results and evaluate all cumulants of the voltage operator in the zero frequency limit. As we already know, an instantaneous voltage value $V(t)$ fluctuates in time due to a sequence of voltage pulses produced by QPS. It is instructive to define the time average

$$\bar v = \frac{1}{\tau}\int_{-\tau/2}^{\tau/2}{\rm d}t\,V(t)\,, \tag{184}$$

where the time interval τ exceeds any relevant time scale for our problem. It is easy to demonstrate that the cumulants of $\bar v$ are identical to the corresponding cumulants of the voltage operator evaluated in the zero frequency limit. For instance, for the first two cumulants, we readily find

$$\langle\bar v\rangle = \big\langle V(t)\big\rangle = V(I)\,, \tag{185}$$

$$\big\langle\big(\bar v - \langle\bar v\rangle\big)^2\big\rangle = \frac{1}{\tau}\int {\rm d}t\,\big(\big\langle V(t)V(0)\big\rangle - V^2\big) = \frac{1}{\tau}\,\mathcal{S}_0(I)\,, \tag{186}$$

where $\mathcal{S}_\omega(I)$ is the frequency dependent voltage noise power for our wire, already evaluated in Section 6.

In order to derive the cumulant generating function for $\bar v$

$$w(j) = \ln\big\langle\exp({\rm i}j\bar v)\big\rangle\,, \tag{187}$$

it suffices to make use of Eqn (182) and set $J(t) = j/\tau$ for $-\tau/2 < t < \tau/2$ and $J(t) = 0$ otherwise. For quite large time intervals τ, the combination $\lambda_+(x,t) - \chi_0(x,t)$ becomes practically independent of both x and t, implying that $\lambda_+(x,t) - \lambda_+(x',t') \approx I\Phi_0(t-t')$. Employing the equation of motion

$$\big(\partial_t^2 - v^2\partial_x^2\big)\hat\chi(x,t) = 0\,, \tag{188}$$

we obtain

$$\lim_{\omega\to0}G^{\rm A}_{\chi v}(x;\omega) = \lim_{\omega\to0}G^{\rm R}_{v\chi}(x;\omega) = \Phi_0\,, \tag{189}$$

and, hence, we have $\lambda_-(x,t) \approx -\Phi_0 j/\tau$. As a result, we get

$$\begin{aligned}\frac{w(j)}{\tau} = &-\frac{{\rm i}j^2}{2\tau^2}\,G^{\rm K}_{vv}(0) - \frac{\gamma^2_{\rm QPS}}{2}\sin\left(\frac{\Phi_0 j}{\tau}\right)\int_{-L/2}^{L/2}{\rm d}x\,{\rm d}x'\\ &\times\int_0^\infty {\rm d}t\big(P(x,x';t) - P(x',x;-t)\big)\sin(I\Phi_0 t)\\ &-\gamma^2_{\rm QPS}\sin^2\left(\frac{\Phi_0 j}{2\tau}\right)\int_{-L/2}^{L/2}{\rm d}x\,{\rm d}x'\\ &\times\int_0^\infty {\rm d}t\,\big(P(x,x';t) + P(x',x;-t)\big)\cos(I\Phi_0 t)\,.\end{aligned} \tag{190}$$

Performing the Fourier transformation

$$P(x,x';\omega) = \int_0^\infty {\rm d}t\,\exp({\rm i}\omega t)P(x,x';t) \tag{191}$$

and introducing

$$\Gamma_{\rm QPS}(\omega)=\frac{\gamma_{\rm QPS}^2}{4}\int_{-L/2}^{L/2}{\rm d}x\,{\rm d}x'\left(P(x,x';\omega)+P^*(x',x;\omega)\right), \tag{192}$$

we find

$$\frac{w(j)}{\tau}=-\frac{{\rm i}j^2}{2\tau^2}\,G_{vv}^{\rm K}(0)+\Gamma_{\rm QPS}(I\Phi_0)\left[\exp\left(\frac{{\rm i}\Phi_0 j}{\tau}\right)-1\right]+\Gamma_{\rm QPS}(-I\Phi_0)\left[\exp\left(-\frac{{\rm i}\Phi_0 j}{\tau}\right)-1\right]. \tag{193}$$

This expression fully describes the statistics of QPS-induced voltage fluctuations in superconducting nanowires in the zero frequency limit.

It follows immediately from Eqn (193) that this statistics is Poissonian in the above limit. In particular, combining Eqns (187) and (193) and evaluating the first and the second derivatives of w with respect to j, we again recover the first two voltage cumulants in Eqns (151) and (161).

Higher voltage cumulants in the zero frequency limit can be found in the same manner. Let us define them as

$$\mathcal{C}_N(I)=(-{\rm i})^N\tau^{N-1}\,\partial_j^N w(j)\Big|_{j\to 0}. \tag{194}$$

After simple algebra, all zero frequency cumulants can be expressed through the current–voltage characteristics for our system. In particular, for odd cumulants, we have

$$\mathcal{C}_{2N+1}(I)=\Phi_0^{2N}V(I), \tag{195}$$

whereas for even ones we obtain

$$\mathcal{C}_{2N}(I)=\Phi_0^{2N-1}V(I)\coth\left(\frac{I\Phi_0}{2T}\right). \tag{196}$$

The above results demonstrate that in the long time limit the effect of interacting QPS reduces to that of independent sharp voltage pulses which occur with the effective rate $\Gamma_{\rm QPS}(I\Phi_0)$ and are described by Poisson statistics. Note that this conclusion holds only for not too thin wires with $\lambda>2$ described by quantum phase slips bound in close pairs.

7.3 Noise power in the short wire limit

At nonzero frequencies, the system behavior becomes more involved and the statistics of voltage fluctuations deviate from Poissonian, as will be demonstrated below. The general expression for the noise power is defined as

$$\mathcal{S}_\omega(I)=-\int{\rm d}t\,\exp({\rm i}\omega t)\,\frac{\delta^2\mathcal{W}[J]}{\delta J(t)\delta J(0)}\Big|_{J\to 0}. \tag{197}$$

Making use of Eqn (182), we find

$$\mathcal{S}_\omega(I)={\rm i}G_{vv}^{\rm K}(\omega)+\frac{\gamma_{\rm QPS}^2}{2}\Bigg[\int_{-L/2}^{L/2}{\rm d}x\,{\rm d}x'\,G_{v\chi}^{\rm K}(x;\omega)G_{v\chi}^{\rm R}(x';\omega)\times\int_0^\infty{\rm d}t\left(P(x,x';t)-P(x',x;-t)\right)\cos(I\Phi_0 t)\times\left[\exp({\rm i}\omega t)-1\right]+\frac{1}{4}\int_{-L/2}^{L/2}{\rm d}x\,{\rm d}x'\,G_{v\chi}^{\rm R}(x;\omega)\times G_{v\chi}^{\rm R}(x';-\omega)\int_{-\infty}^{\infty}{\rm d}t\left(P(x,x';t)+P(x',x;-t)\right)\times\cos(I\Phi_0 t)\exp({\rm i}\omega t)+\{\omega\to-\omega\}\Bigg]. \tag{198}$$

With the aid of the FDT, this result can be transformed into that already derived in Section 6, where we merely addressed the long wire limit. Here, in contrast, we will specify the expression for the noise power for shorter wires. This limit also includes the case of Josephson junctions and other types of short superconducting weak links.

Let us note that each term in the square brackets in Eqn (198) contains a combination of the form factors $P(x,x';t)$ describing the intrinsic dynamics of a superconducting nanowire during the QPS process, as well as two $v\chi$-type Green's functions indicating how the detector 'feels' voltage fluctuations inside the nanowire. Provided the wire is short enough, we can retain only the dependence of these Green's functions on frequency and ignore their spatial coordinates. We then get

$$G_{v\chi}^{\rm R}(x;\omega)\approx\Phi_0(1-{\rm i}\omega\tau_R+\ldots), \tag{199}$$

where τ_R is the effective RC time of the system. Accordingly, we obtain

$$G_{v\chi}^{\rm K}(x,\omega)\approx-{\rm i}\omega\tau_R\coth\left(\frac{\omega}{2T}\right). \tag{200}$$

Employing these approximations, from Eqn (198), we obtain

$$\mathcal{S}_\omega(I)={\rm i}G_{vv}^{\rm K}(\omega)-{\rm i}\Phi_0^2\tau_R\omega\coth\left(\frac{\omega}{2T}\right)\left[\Gamma_{\rm QPS}^{\rm R}(\omega+I\Phi_0)+\Gamma_{\rm QPS}^{\rm R}(\omega-I\Phi_0)+\Gamma_{\rm QPS}^{\rm R}(-\omega+I\Phi_0)+\Gamma_{\rm QPS}^{\rm R}(-\omega-I\Phi_0)-2\Gamma_{\rm QPS}^{\rm R}(I\Phi_0)-2\Gamma_{\rm QPS}^{\rm R}(-I\Phi_0)\right]+\frac{1}{2}\,\Phi_0^2\left[\Gamma_{\rm QPS}(\omega+I\Phi_0)+\Gamma_{\rm QPS}(\omega-I\Phi_0)+\Gamma_{\rm QPS}(-\omega+I\Phi_0)+\Gamma_{\rm QPS}(-\omega-I\Phi_0)\right], \tag{201}$$

where we introduced the function

$$\Gamma_{\rm QPS}^{\rm R}(\omega)=\frac{\gamma_{\rm QPS}^2}{4}\int_{-L/2}^{L/2}{\rm d}x\,{\rm d}x'\left(P(x,x';\omega)-P^*(x',x;-\omega)\right), \tag{202}$$

related to $\Gamma_{\rm QPS}(\omega)$ (192) as

$$\Gamma_{\rm QPS}^{\rm R}(\omega)=\int\frac{{\rm d}z}{2\pi{\rm i}}\,\frac{\Gamma_{\rm QPS}(z)-\Gamma_{\rm QPS}(-z)}{z-\omega-{\rm i}0}. \tag{203}$$

As an illustration, let us consider a short superconducting nanowire embedded in a linear dissipative external circuit modeled by an Ohmic shunt resistor R_S. This situation is equally relevant for resistively shunted Josephson junctions in the limit of large Josephson coupling energies $E_{\rm J}$. In this limit, one has

$$G_{\chi\chi}^{\rm R}(x,x';\omega)\approx-\frac{2\pi{\rm i}\mu}{\omega+{\rm i}0}, \tag{204}$$

where $\mu = R_Q/R_S$ is the shunt dimensionless conductance and $R_Q = \pi/(2e^2)$ is the 'superconducting' resistance quantum. The QPS rate then equals

$$\Gamma_{\rm QPS}(\omega) = \gamma_{\rm QPS}^2 (2\pi T\tau_R)^{2\mu} \exp\left(\frac{\omega}{2T}\right) \times \frac{\Gamma\big(\mu + {\rm i}\omega/(2\pi T)\big)\,\Gamma\big(\mu - {\rm i}\omega/(2\pi T)\big)}{8\pi T\Gamma(2\mu)}\,, \qquad (205)$$

where $\Gamma(y)$ is the Euler gamma function and τ_R^{-1} plays the role of effective high-energy cutoff frequency. Evaluating the corresponding integrals in the short wire limit $\omega, T, I\Phi_0 \ll \tau_R^{-1}$ and also for $1 < \mu < 3/2$, we obtain

$$\Gamma_{\rm QPS}^{\rm R}(\omega) = {\rm const} - {\rm i}\Gamma_{\rm QPS}(\omega) \exp\left(-\frac{\omega}{2T}\right) \times \frac{\sin\big(\pi\mu + {\rm i}\omega/(2T)\big)}{\cos(\pi\mu)}\,. \qquad (206)$$

These expressions can be simplified in certain limits. For example, by setting $0 < \mu - 1 \ll 1$, we get

$$\Gamma_{\rm QPS}(\omega) \approx \frac{\gamma_{\rm QPS}^2 (2\pi T\tau_R)^{2\mu} \exp\left(\dfrac{\omega}{2T} - 2\mathbf{C}(\mu-1)\right)\sqrt{\omega^2 + 4\pi^2T^2(\mu-1)^2}}{16\pi T^2\Gamma(2\mu)\sqrt{\sin\left(\pi\mu + \dfrac{{\rm i}\omega}{2T}\right)\sin\left(\pi\mu - \dfrac{{\rm i}\omega}{2T}\right)}}, \qquad (207)$$

where $\mathbf{C}$ is a Euler–Mascheroni constant. Also, the expressions for both QPS rates get significantly simplified in the limit $|\omega| \gg T$. One has

$$\Gamma_{\rm QPS}(\omega) \approx \pi\gamma_{\rm QPS}^2\theta(\omega)\frac{(\omega\tau_R)^{2\mu}}{2\omega\Gamma(2\mu)}\,, \qquad (208)$$

$$\Gamma_{\rm QPS}^{\rm R}(\omega) \approx {\rm const} + \pi\gamma_{\rm QPS}^2\frac{|\omega\tau_R|^{2\mu}\exp\big(-{\rm i}\pi\mu\,{\rm sign}\,(\omega)\big)}{4\omega\Gamma(2\mu)\cos(\pi\mu)}\,. \qquad (209)$$

Accordingly, in the zero-temperature limit, one finds

$$\mathcal{C}_N(I) = \pi\gamma_{\rm QPS}^2\,{\rm sign}^N(I)\,\frac{\Phi_0^{N+2\mu-1}\tau_R^{2\mu}}{2\Gamma(2\mu)}\,|I|^{2\mu-1}\,. \qquad (210)$$

The above results are consistent with ones previously derived for ultrasmall Josephson junctions [71].

7.4 Higher voltage cumulants

We now turn to higher voltage cumulants at nonzero frequencies. We adopt the following definition for the Nth voltage cumulant:

$$\mathcal{S}_{\omega_1,\ldots,\omega_{N-1}}(I) = \int {\rm d}t_1 \ldots {\rm d}t_{N-1} \exp({\rm i}\omega_1 t_1 + \ldots + {\rm i}\omega_{N-1}t_{N-1})(-{\rm i})^N \frac{\delta^N\mathcal{W}[J]}{\delta J(t_{N-1})\ldots\delta J(t_1)\delta J(0)}\bigg|_{J\to 0}\,. \qquad (211)$$

In the zero frequency limit, this definition yields

$$\mathcal{S}_{\underbrace{00\ldots0}_{N}}(I) = \mathcal{C}_N(I)\,. \qquad (212)$$

Under the condition $T, \omega \ll \tau_R^{-1}$ or, in other words, provided the detector immediately 'feels' QPS-generated voltage fluctuations, one can set $\tau_R \to 0$ and explicitly evaluate all voltage cumulants at nonzero frequencies. In this case, the cumulant generating function takes the form

$$\mathcal{W}[J] \approx -\frac{\rm i}{2}\int {\rm d}t\,{\rm d}t'\,J(t)G_{vv}^{\rm K}(t-t')J(t') - \gamma_{\rm QPS}^2\int_{-L/2}^{L/2}{\rm d}x\,{\rm d}x' \times \int {\rm d}t\int^t {\rm d}t'\big(P(x,x';t-t') - P(x',x;t'-t)\big) \times \sin\big(I\Phi_0(t-t')\big)\sin\left(\frac{\Phi_0 J(t)}{2}\right)\cos\left(\frac{\Phi_0 J(t')}{2}\right) - \frac{\gamma_{\rm QPS}^2}{2} \times \int_{-L/2}^{L/2}{\rm d}x\,{\rm d}x'\int {\rm d}t\int {\rm d}t'\big(P(x,x';t-t') + P(x',x;t'-t)\big) \times \cos\big(I\Phi_0(t-t')\big)\sin\left(\frac{\Phi_0 J(t)}{2}\right)\sin\left(\frac{\Phi_0 J(t')}{2}\right). \qquad (213)$$

One can observe that the second term in Eqn (213) can only contribute to odd cumulants, whereas the last term determines all even cumulants. After some algebra, we arrive at the following expressions for both even and odd voltage cumulants, respectively:

$$\mathcal{S}_{\omega_1,\ldots,\omega_{2M}}(I) = \frac{\Phi_0^{2M+1}}{2^{2M}(2M)!}\sum_{p\in{\rm perm}}\sum_{m=0}^{2M}\binom{2M}{m} \times \Big[\Gamma_{\rm QPS}^{\rm R}\big(I\Phi_0 - (-1)^m(\omega_{p_1} + \ldots + \omega_{p_m})\big) - \Gamma_{\rm QPS}^{\rm R}\big(-I\Phi_0 - (-1)^m(\omega_{p_1} + \ldots + \omega_{p_m})\big)\Big]\,, \qquad (214)$$

$$\mathcal{S}_{\omega_1,\ldots,\omega_{2M+1}}(I) = \frac{\Phi_0^{2M+2}}{2^{2M+1}(2M+1)!}\sum_{p\in{\rm perm}}\sum_{m=0}^{M}\binom{2M+1}{2m+1} \times \Big[\Gamma_{\rm QPS}\big(I\Phi_0 + (\omega_{p_1} + \ldots + \omega_{p_{2m+1}})\big) + \Gamma_{\rm QPS}\big(-I\Phi_0 + (\omega_{p_1} + \ldots + \omega_{p_{2m+1}})\big) + \Gamma_{\rm QPS}\big(I\Phi_0 - (\omega_{p_1} + \ldots + \omega_{p_{2m+1}})\big) + \Gamma_{\rm QPS}\big(-I\Phi_0 - (\omega_{p_1} + \ldots + \omega_{p_{2m+1}})\big)\Big]\,, \qquad (215)$$

where the sum is taken over all permutations of frequencies.

The above results allow us to extend the relation between the voltage cumulants and the current–voltage characteristics of our device to nonzero frequencies. For the odd cumulants, we obtain

$$\mathcal{S}_{\omega_1,\ldots,\omega_{2M}}(I) = \frac{\Phi_0^{2M+2}I}{2^{2M-1}(2M)!}\int\frac{{\rm d}I'}{2\pi{\rm i}}\,V(I')\sum_{p\in{\rm perm}}\sum_{m=0}^{2M}\binom{2M}{m} \times \frac{1}{\big(I'\Phi_0 + (-1)^m(\omega_{p_1} + \ldots + \omega_{p_m}) - {\rm i}0\big)^2 - (I\Phi_0)^2}\,, \qquad (216)$$

while the expression for the even cumulants reads

$$\mathcal{S}_{\omega_1,\ldots,\omega_{2M+1}}(I) = \frac{\Phi_0^{2M+1}}{2^{2M+1}(2M+1)!}\sum_{p\in{\rm perm}}\sum_{m=0}^{M}\binom{2M+1}{2m+1} \times \left[\coth\left(\frac{I\Phi_0 + (\omega_{p_1} + \ldots + \omega_{p_{2m+1}})}{2T}\right) \times V\left(I + \frac{\omega_{p_1} + \ldots + \omega_{p_{2m+1}}}{\Phi_0}\right)\right.$$

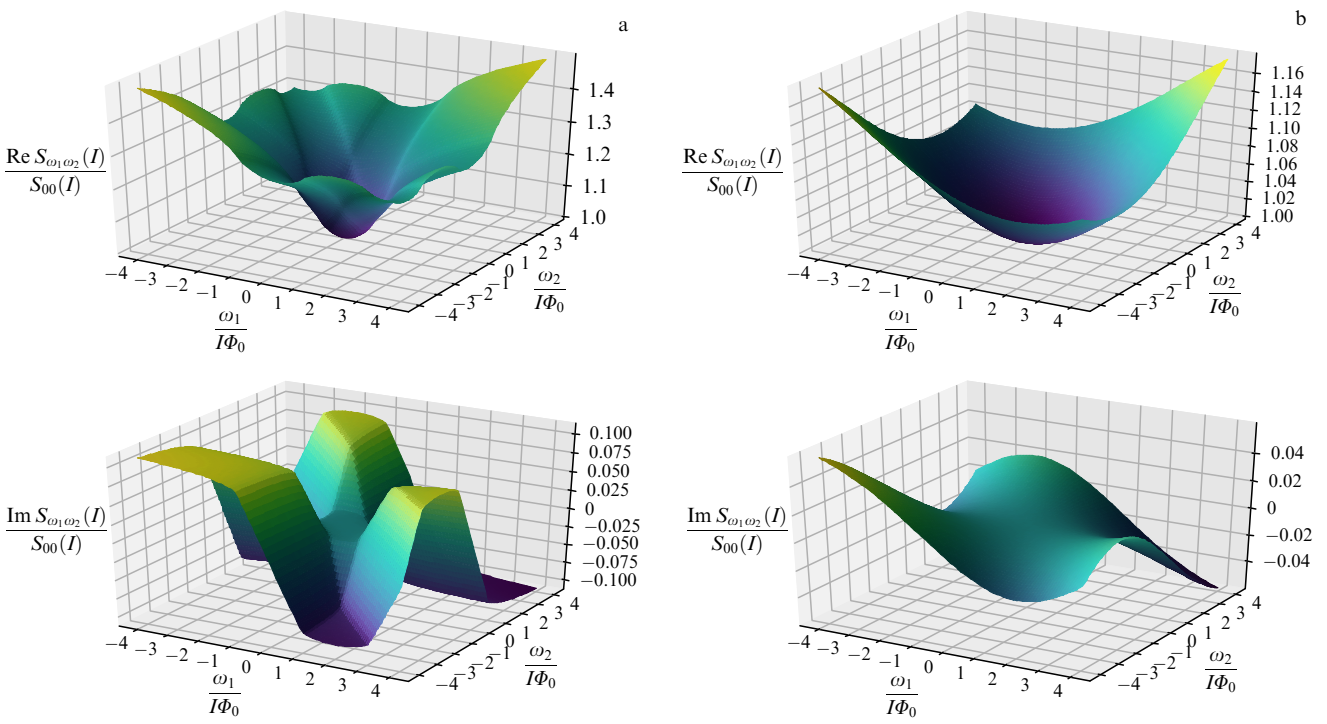

Figure 12. Real and imaginary parts of third voltage cumulant at $T \to 0$ (a) and $T = I\Phi_0$ (b) for $\mu = 1.1$.

$$+ \coth\left(\frac{I\Phi_0 - (\omega_{p_1} + \ldots + \omega_{p_{2m+1}})}{2T}\right) \times V\left(I - \frac{\omega_{p_1} + \ldots + \omega_{p_{2m+1}}}{\Phi_0}\right)\Bigg] . \quad (217)$$

These expressions can be evaluated numerically with the aid of Eqns (205)–(209) for $\Gamma_{\mathrm{QPS}}(\omega)$ and $\Gamma^{\mathrm{R}}_{\mathrm{QPS}}(\omega)$ derived above. The corresponding results for the third voltage cumulant as a function of two frequencies are displayed in Fig. 12 at low and high temperatures. The third voltage cumulant generally consists of real and imaginary parts

$$\mathcal{S}_{\omega_1,\omega_2}(I) = \mathrm{Re}\, \mathcal{S}_{\omega_1,\omega_2}(I) + \mathrm{i}\, \mathrm{Im}\, \mathcal{S}_{\omega_1,\omega_2}(I) . \quad (218)$$

As can be seen in the plots, both these functions become considerably smoother at higher T.

To conclude our analysis of voltage fluctuation statistics in superconducting nanowires, we emphasize again that in the zero-frequency limit this statistics reduces to Poissonian, similarly to the situation encountered in a number of other tunneling-like problems. In this limit, all (symmetrized) cumulants of the voltage operator can be expressed in a simple manner through the current–voltage characteristics of the system $V(I)$ (cf. Eqns (195), (196)). At nonzero frequencies, quantum voltage fluctuations in superconducting nanowires are no longer described by Poisson statistics, because inter-QPS interaction produced by an effective environment (due to the wire itself and/or an external dissipative circuit) starts playing a more important role at shorter time scales, making the whole problem much more involved. Remarkably, in this case, it is also possible to establish a relation between the voltage cumulants and the current-voltage characteristics of our device $V(I)$, though in a much more complicated form than that in the zero frequency limit (cf. Eqns (216), (217)). This observation could be important for possible experimental verification of the above results.

8. Topology-controlled phase coherence in superconducting nanowires

It is by now well established that at $T \to 0$ a long superconducting nanowire suffers a quantum phase transition (QPT) controlled by the wire cross section s or, equivalently, by the parameter $\lambda \equiv g/8$, which we already introduced above and which sets the magnitude of (logarithmic in space–time) interaction among different quantum phase slips [12]. For $\lambda > 2$, this interaction is strong enough, and close QPS–anti-QPS pairs are formed in the wire, which then demonstrates vanishing *linear* resistance $R \propto T^{2\lambda-3}$ (cf. Eqns (154), (155)). Hence, as long as $\lambda > 2$ (or, equivalently, $g > 16$), the ground state of the system can be considered superconducting. In contrast, for $\lambda < 2$, inter-QPS interaction is weak, quantum phase slips are unbound, and the wire acquires nonzero resistance, which tends to *increase* with decreasing T. The last feature allows calling the wire behavior insulating provided $\lambda < 2$. Thus, at $g = 16$ and $T \to 0$, one expects a superconductor-to-insulator quantum phase transition (SIT) to occur in the systems under consideration.

Let us emphasize that possible insulating behavior of superconducting nanowires is essentially linked to a certain type of experiment performed with such nanowires and may not always be realized. For example, an ultrathin superconducting nanowire forming a closed ring does not lose the ability to carry supercurrent even for $\lambda < 2$, as we have already demonstrated in Section 5. In this case, a characteristic length scale (119)

$$R_{\mathrm{c}} \sim L_{\mathrm{c}} \propto \exp\left(\frac{ag_\xi}{2-\lambda}\right) \quad (219)$$

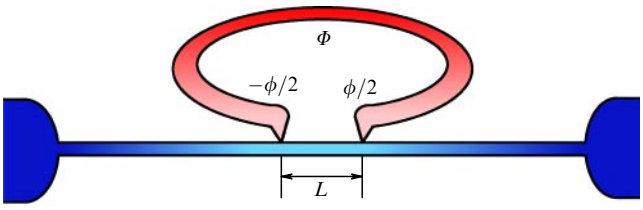

Figure 13. Bulk open superconducting ring attached to a superconducting nanowire via two ultrasmall tunnel barriers located at a distance L from each other. The ring is threaded by the magnetic flux Φ.

emerges, beyond which phase coherence (and, hence, supercurrent) gets exponentially suppressed by QPS. The correlation length (219) diverges at $\lambda \to 2$, thus signaling the transition to the ordered phase $\lambda > 2$ with bound QPS–anti-QPS pairs and more robust superconductivity.

On the other hand, a closed ring geometry seriously restricts the space for phase fluctuations, thereby enhancing the tendency towards superconductivity (see, e.g., Ref. [72] for further discussion of this point). For this reason, it is highly desirable to analyze ground state properties of superconducting nanowires where no fluctuation configurations are suppressed by geometry constraints and/or boundary conditions. An example of a system of that kind is depicted in Fig. 13. A long superconducting nanowire with sufficiently small cross section s, geometric capacitance (per length) C, and kinetic inductance (times length) $\mathcal{L}_{\rm kin}$ is attached to two big superconducting reservoirs at its ends. In order to probe fluctuation effects inside the wire, it is connected to a bulk superconductor forming an open ring by two identical small area tunnel junctions with Josephson energy $E_{\rm J}$ located at a distance L from each other at the points $x = 0$ and $x = L$. External magnetic flux Φ piercing the ring controls the phase difference $\phi = 2\pi\Phi/\Phi_0$ between the bulk sides of the point contacts. As desired, within this setup, fluctuations in the superconducting phase $\varphi(x,\tau)$ remain unrestricted at any point x of the wire.

Below, we will analyze the effect of these fluctuations on the supercurrent $I(\phi)$ flowing through the wire segment of length L between the two Josephson contacts [73]. As $I(\phi)$ is a 2π-periodic function of ϕ, in what follows, it suffices to restrict the phase interval to $|\phi| \leqslant \pi$. Below, we will demonstrate that, in the setup displayed Fig. 13, a 'disordered' phase $\lambda < 2$ (or $g < 16$) for a superconducting nanowire itself consists of two different phases: a nonsuperconducting one with $g < 2$ as well as a 'mixed' one with $2 < g < 16$ characterized by two different correlation lengths, $L_{\rm c}$ (219) and

$$L^* \propto g^{1/(1-2/g)}\,, \quad g \geqslant 2\,. \tag{220}$$

The latter phase is characterized by a nontrivial interplay between supercurrent and quantum fluctuations, resulting in superconducting behavior of the wire at shorter length scales combined with its vanishing superconducting response in the long scale limit.

8.1 Effective action

Low energy processes in the system under consideration can be described by the effective action

$$S[\varphi] = S_{\rm TL}[\varphi] + S_J\big[\varphi(0),\varphi(L)\big]\,, \tag{221}$$

where, as before,

$$S_{\rm TL}[\varphi] = \frac{C}{8e^2}\int_0^{1/T} {\rm d}\tau \int {\rm d}x\,\left[(\partial_\tau\varphi)^2 + v^2(\partial_x\varphi)^2\right] \tag{222}$$

is the low energy effective action for a superconducting nanowire in the φ-representation [12–14] and

$$S_{\rm J}[\varphi_1,\varphi_2] = -E_{\rm J}\int_0^{1/T} {\rm d}\tau\,\left[\cos\left(\varphi_1 + \frac{\phi}{2}\right) + \cos\left(\varphi_2 - \frac{\phi}{2}\right)\right] \tag{223}$$

accounts for the Josephson energy of the contacts, where we set $\varphi_1 = \varphi(0,\tau)$, $\varphi_2 = \varphi(L,\tau)$. For simplicity, in Eqn (223), we do not include the charging energy of the point contacts, which could always be absorbed into the first term of the wire action (222).

As the wire action (222) is Gaussian, it is possible to exactly integrate out the phase variable $\varphi(x)$ at all values of x except for $x = 0, L$. Then, we arrive at the reduced effective action $S_{\rm R}$ which depends on the two phase variables φ_1 and φ_2. The grand partition function $\mathcal{Z}$ reads

$$\begin{aligned}\mathcal{Z} &= \int D\varphi(x)\,\exp\left\{-S_{\rm TL}[\varphi(x)] - S_{\rm J}[\varphi(0),\varphi(L)]\right\}\\ &= \int D\varphi_1 D\varphi_2\,\exp\left\{-S_{\rm R}[\varphi_1,\varphi_2] - S_{\rm J}[\varphi_1,\varphi_2]\right\},\end{aligned} \tag{224}$$

where

$$S_{\rm R}[\varphi_1,\varphi_2] = \frac{1}{2}\,{\rm tr}\left[\begin{pmatrix}\varphi_1 & \varphi_2\end{pmatrix}\begin{pmatrix}G_0(0) & G_0(L)\\ G_0(L) & G_0(0)\end{pmatrix}^{-1}\begin{pmatrix}\varphi_1\\ \varphi_2\end{pmatrix}\right]. \tag{225}$$

Here, the trace also includes integration over imaginary time. The Green's function $G_0 = \langle\varphi(x,\tau)\varphi(0,0)\rangle_{S_0}$ has the form

$$G_0(\omega_n,x) = \frac{4e^2}{C}\int\frac{{\rm d}q}{2\pi}\,\frac{\exp({\rm i}qx)}{\omega_n^2 + v^2q^2} = \frac{4\pi}{g|\omega_n|}\,\exp\left(-\left|\frac{\omega_n x}{v}\right|\right). \tag{226}$$

In order to diagonalize the quadratic part of the action, it is convenient to express $S_{\rm R}$ in terms of the variables $\varphi_\pm = (\varphi_1 \pm \varphi_2)/2$. Then, we obtain

$$\begin{aligned}S_{\rm R} + S_{\rm J} = \frac{1}{2}\sum_{a=\pm}{\rm tr}\left[\varphi_a G_{0,a}^{-1}\varphi_a\right]\\ - 2E_{\rm J}\int_0^{1/T}{\rm d}\tau\,\cos(\varphi_+)\cos\left(\varphi_- - \frac{\phi}{2}\right)\end{aligned} \tag{227}$$

with the propagators

$$G_{0,\pm}(\omega_n) = \frac{2\pi}{g|\omega_n|}\left[1 \pm \exp\left(-\left|\frac{\omega_n L}{v}\right|\right)\right]. \tag{228}$$

Let us stress that phase variables φ_+ and φ_- account for different physics in our problem. The phase $\varphi_- = (\varphi(L) - \varphi(0))/2$ determines the supercurrent flowing between two contacts inside a wire segment of length L. Hence, configurations with nonzero φ_- have nonzero energies due to the kinetic inductance of the wire, and the mode corresponding to φ_- has a mass equal to $gv/2\pi L$. The variable φ_+, in contrast, describes simultaneous shifts of both phases $\varphi(0)$ and $\varphi(L)$ by the same value without producing any phase gradient along the wire. Thus, in the absence of

interactions, the mode corresponding to φ_+ is massless. At the same time, below, we will observe that fluctuations in φ_+ yield renormalization of Josephson coupling energies E_J of the contacts and, as such, should also be taken into account.

8.2 Variational analysis and propagators

Let us make use of the variational perturbation theory as described, for example, in Ref. [74]. The main idea here is to improve the standard perturbation expansion by adding an extra term δS which depends on the variational parameters in the quadratic part of the action S_R. In order to accomplish this goal, partition function (224) can be identically rewritten as

$$\mathcal{Z} = \int D\varphi_1 D\varphi_2 \, \exp(-S_{tr}) \, \exp\left[-(S_J - \delta S)\right] \tag{229}$$

with the trial action $S_{tr} = S_R + \delta S$. The last exponent can then be conveniently expanded in powers of $S_J - \delta S$. Being expanded to *all* orders, partition function (229) obviously remains independent of the choice of δS and the variational parameters. However, such a dependence emerges as long as only a finite number of terms of this expansion are kept. Then, the most accurate approximation is achieved by minimizing the result of the perturbative expansion with respect to the variational parameters.

In what follows, we choose the trial action in the form

$$S_{tr} = \frac{1}{2} \operatorname{tr}\left[\varphi_+ (G_{0+}^{-1} + m_+)\varphi_+\right] + \frac{1}{2} \operatorname{tr}\left[(\varphi_- - \psi)(G_{0-}^{-1} + m_-)(\varphi_- - \psi)\right], \tag{230}$$

which corresponds to effectively performing a self-consistent harmonic approximation (SCHA). Here, the parameters $m_\pm$ represent the interaction-generated effective masses for the modes associated with the phase variables $\varphi_\pm$. The parameter ψ accounts for the average value of the combination $(\varphi(L) - \varphi(0))/2$. We note that a somewhat similar variational calculation with a mass term was proposed in the context of Brownian motion of a quantum particle in a periodic potential with linear Ohmic dissipation [75]. The results obtained within the framework of this variational approach agree with those derived by means of more rigorous techniques [41].

Expanding the last exponent in Eqn (229) in powers of $S_J - \delta S$ and evaluating the integrals, for the free energy $\mathcal{F} = -T \ln \mathcal{Z}$ we get

$$\mathcal{F} = \mathcal{F}_0 + \mathcal{F}_1 + \text{higher order terms}, \tag{231}$$

where

$$\mathcal{F}_0 = \frac{T}{2}\left(\operatorname{tr} \ln G_+^{-1} + \operatorname{tr} \ln G_-^{-1}\right), \quad \mathcal{F}_1 = \left\langle S_{int} - \delta S \right\rangle_{tr}. \tag{232}$$

Neglecting all higher order terms in expansion (231) and evaluating the average in Eqn (232) with respect to S_{tr} (230), we obtain

$$\mathcal{F}_1 = -\frac{m_+}{2} G_+(0) - \frac{m_-}{2} G_-(0) + \frac{1}{2}\psi G_{0-}^{-1}(\omega_n = 0)\psi - 2E_J \cos\left(\psi - \frac{\phi}{2}\right) \exp\left(-\frac{G_+(0) + G_-(0)}{2}\right), \tag{233}$$

where $G_\pm^{-1} = G_{0,\pm}^{-1} + m_\pm$ and $G_\pm(0) = T\sum_{\omega_n} G_\pm(\omega_n)$, with $\omega_n = \pi T(2n+1)$ being the Matsubara frequency. Evaluating variational derivatives of $\mathcal{F}$ with respect to $m_\pm$ and ψ, we readily find

$$\frac{\delta \mathcal{F}_0}{\delta m_\pm} = \frac{G_\pm(0)}{2}, \tag{234}$$

$$\frac{\delta \mathcal{F}_0}{\delta \psi} = 0, \tag{235}$$

$$\frac{\delta \mathcal{F}_1}{\delta m_\pm} = -\frac{G_\pm(0)}{2} - \frac{1}{2}\frac{\delta G_\pm(0)}{\delta m_\pm}\left[m_\pm - 2E_J \cos\left(\psi - \frac{\phi}{2}\right) \times \exp\left(-\frac{G_+(0) + G_-(0)}{2}\right)\right], \tag{236}$$

$$\frac{\delta \mathcal{F}_1}{\delta \psi} = 2E_J \sin\left(\psi - \frac{\phi}{2}\right) \exp\left(-\frac{G_+(0) + G_-(0)}{2}\right) + G_{0-}^{-1}(\omega_n = 0)\psi. \tag{237}$$

Imposing the extremum conditions $\delta\mathcal{F}/\delta m_\pm = \delta\mathcal{F}/\delta\psi = 0$ and making use of Eqns (234)–(237), we arrive at the following set of SCHA equations:

$$m_+ = m_- \equiv m, \tag{238}$$

$$2E_J \cos\left(\psi - \frac{\phi}{2}\right) \exp\left(-\frac{G_+(0) + G_-(0)}{2}\right) - m = 0, \tag{239}$$

$$2E_J \sin\left(\psi - \frac{\phi}{2}\right) \exp\left(-\frac{G_+(0) + G_-(0)}{2}\right) + \frac{gv}{2\pi L}\psi = 0. \tag{240}$$

Note that the mass parameters $m_\pm$ in Eqn (238) remain equal to each other, since the two Josephson junctions involved in our problem are identical. Equation (239) provides the relation between the effective mass m and the fluctuation-induced renormalization of the Josephson coupling energy E_J. Equation (240) represents the equation of motion for ψ. It coincides with the equation of motion for the phase φ_- with E_J renormalized by quantum fluctuations.

As we already pointed out, the wire effective action in the form (222) applied in the low energy limit, i.e., for $\omega, vq \ll \Delta$. Hence, a proper ultraviolet cutoff should be imposed which respects both causality and the fluctuation–dissipation relation. This goal is achieved by modifying the spectral density

$$J_\pm(\omega) = -\frac{1}{\pi} \operatorname{Im} G_\pm^R(\omega),$$

making it decay at $\omega > \Delta$. The retarded Green's function $G_\pm^R(\omega)$ can be obtained from its Matsubara counterpart by means of the standard analytic continuation procedure

$$G_\pm^R(\omega) = -G_\pm(i\omega_n)\big|_{i\omega_n \to \omega + i0}, \quad \omega_n > 0.$$

Then, the Matsubara frequency summation in $G_\pm(0)$ can be performed with the aid of the contour integration in the complex plane. Employing our regularization procedure, we obtain

$$G_\pm(0) = T\sum_{\omega_n} G_\pm(\omega_n) = \frac{2\pi}{g} T\sum_{\omega_n}\left[\frac{|\omega_n|}{1 \pm \exp\left(-|\omega_n L/v|\right)} + \mu\right]^{-1}$$

$$= \frac{1}{4\pi i}\int_{\mathcal{C}} dz\, G_{\pm}(-iz)\coth\frac{z}{2T}$$
$$= \frac{i}{4\pi}\int_{-\infty}^{\infty} d\omega\left(G_{\pm}^{R}(\omega) - G_{\pm}^{A}(\omega)\right)\coth\frac{\omega}{2T}$$
$$= \int_{0}^{\Delta} d\omega\, J_{\pm}(\omega)\coth\frac{\omega}{2T}, \qquad (241)$$

where the spectral density functions $J_{\pm}(\omega)$ read

$$J_{\pm}(\omega) = -\frac{1}{\pi}\,\mathrm{Im}\left[\frac{2\pi}{g}\left(\frac{i\omega}{1\pm\exp(i\omega L/v)} - \mu\right)^{-1}\right], \qquad (242)$$

and we define $\mu = 2\pi m/g$. In the limit $\mu L/v \ll 1$, these expressions reduce to

$$J_{+}(\omega) = \frac{4}{g}\frac{\omega}{\omega^2 + 4\mu^2}, \quad J_{-}(\omega) = 0. \qquad (243)$$

8.3 Quantum phase transition and supercurrent

Let us now evaluate the supercurrent I flowing in a wire segment of length L between two Josephson junctions. This current can be defined as

$$I = -2eT\frac{1}{\mathcal{Z}}\frac{d\mathcal{Z}}{d\phi} = 2e\frac{d\mathcal{F}}{d\phi} = -2eE_J\sin\left(\psi - \frac{\phi}{2}\right)$$
$$\times\exp\left(-\frac{G_{+}(0) + G_{-}(0)}{2}\right) = \frac{gev}{2\pi L}\psi. \qquad (244)$$

Thus, within the framework of our approach, the effect of phase fluctuations is accounted for by effective renormalization of the critical current by the factor $\exp\left[-(G_{+}(0) + G_{-}(0))/2\right]$. In the zero temperature limit $T \to 0$, the solution of Eqn (239) takes the form

$$\mu = \begin{cases} \Delta\left(\dfrac{4\pi E_J\cos(\psi - \phi/2)}{g\Delta}\right)^{g/(g-2)}, & g > 2, \\ 0, & g < 2, \end{cases} \qquad (245)$$

while the renormalized equation of motion (240) can be rewritten as

$$\frac{\mu L}{v}\tan\left(\psi - \frac{\phi}{2}\right) + \psi = 0. \qquad (246)$$

We observe that for $g < 2$ one has $\psi = 0$ and, hence, the supercurrent I inside the wire is completely suppressed by strong quantum fluctuations of the phase. On the other hand, at bigger values of $g > 2$, a nonvanishing supercurrent I can flow across the wire segment between the two Josephson junctions.

We arrive at an important conclusion: a quantum phase transition occurs at $g = 2$ separating two different phases with nonsuperconducting ($g < 2$) and superconducting-like ($g > 2$) behavior. This dissipative QPT belongs to the same universality class as the so-called Schmid phase transition in resistively shunted Josephson junctions [41, 76]. It is curious that this QPT occurs at exactly the same value of the parameter g where the superconducting gap singularity in the local electron density of states gets suppressed due to interaction between electrons and a dissipative bath formed by Mooij–Schön plasmons.

Let us now focus our attention on the superconducting-like phase $g > 2$ and evaluate the supercurrent I affected by quantum fluctuations of the phase φ inside the wire. For this purpose, let us combine the solution of the equation

$$\frac{\Delta L}{v}\left(\frac{4\pi E_J}{g\Delta}\right)^{g/(g-2)}\sin\left(\psi - \frac{\phi}{2}\right)\left[\cos\left(\psi - \frac{\phi}{2}\right)\right]^{2/(g-2)} + \psi = 0 \qquad (247)$$

with Eqn (244). We observe that there is a new length scale L^* in our problem associated with the effective mass m. Making use of the Ambegaokar–Baratoff formula for the Josephson coupling energy $E_J = g_N\Delta/8$ (where g_N is the dimensionless normal state conductance of each tunnel junction), we can express L^* in the form

$$L^* = \frac{v}{\Delta}\left(\frac{2g}{\pi g_N}\right)^{g/(g-2)}. \qquad (248)$$

Here, we are merely interested in the case of small-size tunnel junctions with few conducting channels serving as probes aiming to disturb the superconducting wire as little as possible. Accordingly, we typically have $g_N \ll g$, and L^* diverges at $g \to 2$, remaining much longer than the characteristic length scale v/Δ at any value of $g > 2$.

Length scale (248) separates two different fluctuation regimes. For $L \gg L^*$, the wire kinetic inductance contribution remains small compared to that of the Josephson junctions. Then, the phase difference across the wire segment between the junctions does not fluctuate, being equal to $\varphi(L) - \varphi(0) = \phi$. In this case, we reproduce the standard mean field current–phase relation

$$I(\phi) = \frac{gev}{4\pi L}\phi. \qquad (249)$$

In the opposite limit $L \ll L^*$, the renormalization of E_J becomes important and phase fluctuations tend to suppress the supercurrent flowing inside the wire. In this limit, we arrive at the L-independent result

$$I(\phi) = \frac{gev}{2\pi L^*}\sin\left(\frac{\phi}{2}\right)\left[\cos\left(\frac{\phi}{2}\right)\right]^{2/(g-2)}. \qquad (250)$$

Comparing results (249) and (250), we observe that quantum fluctuations can strongly affect both the supercurrent magnitude and the current–phase relation. The dependence $I(\phi)$ (250) in the presence of fluctuations becomes smoother than in Eqn (249), and the absolute value of the supercurrent is reduced by the factor $\sim L/L^*$. Additional reduction in I originates from the term in the square brackets in Eqn (250). The supercurrent gets suppressed more strongly for bigger values of ϕ. This effect becomes particularly significant for g sufficiently close to 2. For $\phi \to \pi$ and any $g > 2$, the supercurrent tends to zero as $I(\phi) \propto (\pi - \phi)^{g/(g-2)}$.

We also point out that, for L not much smaller than L^*, the supercurrent $I(\phi \to \pi)$ behaves somewhat differently: it vanishes only for $2 < g < 4$, whereas at $g > 4$ we have

$$I(\phi \to \pi) \approx \frac{ge\Delta}{2\pi}\left(\frac{\Delta L}{v}\right)^{2/(g-4)}\left(\frac{\pi g_N}{2g}\right)^{g/(g-4)}, \qquad (251)$$

i.e., for such values of g, the current–phase relation remains discontinuous at $\phi = \pi$. The dependences $I(\phi)$ evaluated for different values of g and L are also displayed in Fig. 14.

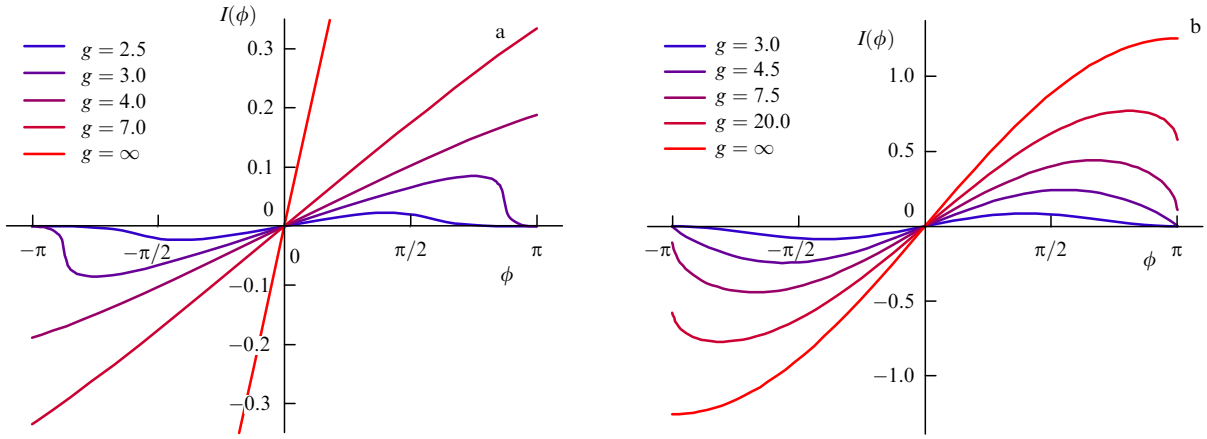

Figure 14. Phase dependent supercurrent $I(\phi)$ (expressed in units of $e\Delta/(2\pi)$) for $E_J/\Delta = 0.1$ and different g. Panels a and b correspond to $\Delta L/v = 20$ and $\Delta L/v = 0.5$, respectively.

Finally, we note that the form of the current–phase relation (250) derived here resembles that obtained for resistively shunted Josephson junctions in the presence of quantum fluctuations of the phase [77].

8.4 Effect of quantum phase slips and localization of Cooper pairs

Let us recall that the effective action $S_{\rm TL}$ (222) employed in the above analysis only accounts for the effect of Gaussian fluctuations of the superconducting phase and does not yet include quantum phase slips. In order to describe QPS effects inside the wire, it is convenient to turn to the dual χ-representation for the wire effective action $S_{\rm eff}[J(\tau) = 0]$ (107) derived in Section 5. As we already discussed, this effective action defines the sine-Gordon model, which has a QPT at $T \to 0$ and $\lambda = 2$ (or $g = 16$) separating two different phases [12]. Provided $g > 16$, 'positive' and 'negative' quantum phase slips are bound in close 'neutral' pairs which do not disrupt phase coherence at any relevant scales exceeding the superconducting coherence length ξ. For such values of g, QPS effects are irrelevant for any of the above results for the supercurrent $I(\phi)$, and all solutions remain applicable without any modifications.

On the other hand, for $g < 16$, quantum phase slips are no longer bound in pairs. In this phase, relevant excitations of our sine-Gordon theory are kinks and anti-kinks (as well as their bound states) with an effective gap in the spectrum [78, 79]

$$\tilde{\Delta} \propto \gamma_{\rm QPS}^{1/(2-\lambda)}. \tag{252}$$

The appearance of this gap for $g < 16$ (or $\lambda < 2$) gives rise to the correlation length $L_c \propto 1/\tilde{\Delta}$, which, similarly to the case of superconducting nanorings, can be evaluated by equating the renormalized QPS amplitude at this length scale $L_c\tilde{\gamma}_{\rm QPS}(L_c)$ (see Eqn (117)) to the inductive energy $\Phi_0^2/(2\mathcal{L}_{\rm kin}L_c) \sim \xi\Delta g_\xi/L_c$ with some numerical prefactor. Keeping track of all relevant prefactors, in the most relevant limit $\xi \ll v/\Delta$, we obtain

$$L_c \approx \left(\frac{\pi}{8\sqrt{2b}}\right)^{1/(1-\lambda/2)} \xi \exp\left(\frac{ag_\xi}{2-\lambda}\right)\left(\frac{\xi\Delta}{v}\right)^{\lambda/(2-\lambda)} \tag{253}$$

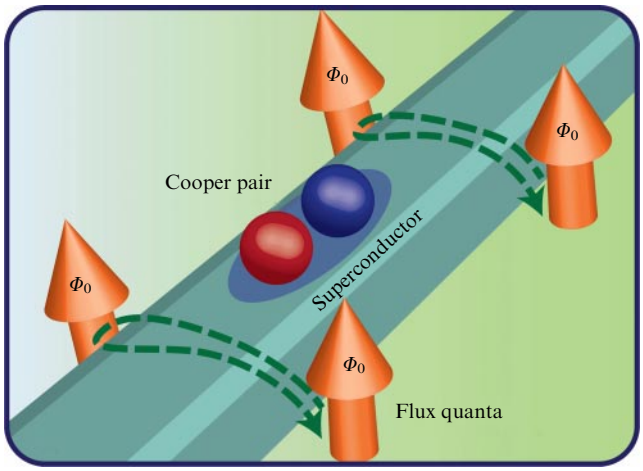

Figure 15. Localization of Cooper pairs in the ground state of a uniform superconducting nanowire due to strong zero-point fluctuations of magnetic flux.

(cf. also Eqn (119)). The appearance of this fundamental length scale in our problem is directly related to the phase–charge (or flux–charge) duality. It can be interpreted as a result of spontaneous tunneling of magnetic fluxons Φ_0 back and forth across the wire, as illustrated in Fig. 15. These strong quantum fluctuations of magnetic flux wipe out phase coherence at distances $\gtrsim L_c$ and yield effective *localization of Cooper pairs* at such length scales. Accordingly, one may interpret the energy

$$\tilde{E} \sim \frac{\xi\Delta g_\xi}{L_c} \propto \tilde{\Delta} \tag{254}$$

as an effective Coulomb gap for a wire segment of length $\sim L_c$. Viewing our nanowire as a chain of $N \approx L/L_c$ independent segments, it may be concluded that its total Coulomb gap in the insulating regime could be as high as $\sim \xi\Delta g_\xi L/L_c^2$.

In the context of the setup considered here, the correlation length (253) is essentially irrelevant for $g < 2$, since, in this case, the supercurrent I is totally suppressed already by smooth phase fluctuations.

On the other hand, for $2 < g < 16$, the length scale (253) becomes important. At such values of g, two correlation lengths exist, L^* and L_c, defined in Eqns (248) and (253), respectively. The first of these two lengths diverges at one of the phase boundaries $g = 2$, whereas the second one tends to infinity at another phase boundary $g = 16$.

Consider the situation with $L^* < L_c$, in which case three regimes exist. At $L < L^*$, the supercurrent is strongly affected only by smooth phase fluctuations and not by quantum phase slips. This regime is accounted for by Eqn (250). At $L^* < L < L_c$, the supercurrent is insensitive to any kind of phase fluctuations and, hence, it is given by a simple mean field formula (249). Finally, for $L > L_c$, the supercurrent gets exponentially suppressed by quantum phase slips and, similarly to Eqn (120), we have

$$I(\phi) \sim \frac{e g_\xi \Delta \sqrt{L}}{\sqrt{\xi}} \left(\frac{v}{L\Delta}\right)^{3\lambda/4} \exp\left(-\frac{3a g_\xi}{4} - \left(\frac{L}{L_c}\right)^{1-\lambda/2}\right) \sin\phi\,. \tag{255}$$

In practical terms, the last regime can be regarded as nonsuperconducting, provided L greatly exceeds L_c. It is also possible to realize the opposite situation with $L^* > L_c$, in particular, for values of g close to 2. In this case, the length L^* becomes irrelevant, and one distinguishes only two regimes: $L < L_c$ and $L > L_c$. The first one is again superconducting with the supercurrent $I(\phi)$ affected by smooth phase fluctuations according to Eqn (250), whereas the second regime corresponds to exponential suppression of the supercurrent due to proliferating QPS (cf. Eqn (255)). No room for the mean field regime (249) exists at $L^* > L_c$.

8.5 Alternative setup

As we already emphasized, the setup displayed in Fig. 13 enables passing an equilibrium supercurrent across a wire segment of an arbitrary length L without restricting phase fluctuations inside the wire by any means. Below, we will consider an alternative setup that allows us to effectively restrict the space available for phase fluctuations by 'pinning' the superconducting phase φ at one point inside the wire [80]. This setup is schematically shown in Fig. 16. As before, it includes a long and thin superconducting nanowire with one of its ends attached to a bulk superconducting reservoir. This reservoir has the form of an open ring whose opposite end is attached to the wire via a small-area tunnel junction at a distance L along the wire. The open ring is pierced by an external magnetic flux Φ which controls the phase difference $\phi = 2\pi\Phi/\Phi_0$ between its ends. Accordingly, the phase at the left end of the wire is pinned by the reservoir and is set equal to zero, i.e., $\varphi(x = 0) = 0$.

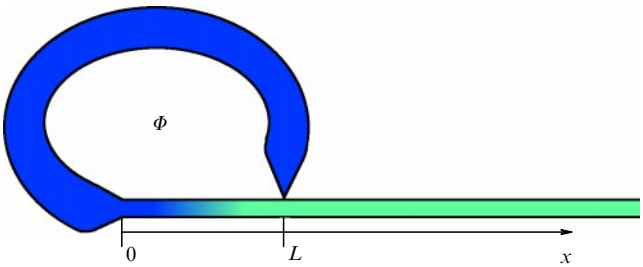

Figure 16. Superconducting nanowire directly attached to a bulk open superconducting ring at its left end. Ring is also attached to the wire via a small-area tunnel junction at distance L from its left end. Open ring is pierced by external magnetic flux Φ.

We will demonstrate that such topology controlled phase pinning severely enhances the ability of the wire to conduct supercurrent. This effect can be interpreted in terms of the absence of a massless mode responsible for the destruction of superconductivity at $g < 2$ in the setup in Fig. 13. Instead, the nanowire embedded in our present setup exhibits a transition between 'more' and 'less' superconducting phases characterized by different types of long-range behavior. Our observable of interest is again the supercurrent $I(\phi)$ flowing through the wire segment of length L between the left wire end and the junction. As before, the phase ϕ is restricted to the interval $|\phi| \leqslant \pi$.

In order to proceed, we will again describe our system with the aid of the effective action (221), where the wire contribution S_{TL} (222) remains the same, whereas the Josephson term S_J now has a somewhat simpler form

$$S_J[\varphi(L)] = -E_J \int_0^{1/T} d\tau \cos\big(\varphi(L) - \phi\big) \tag{256}$$

than Eqn (223). Our further analysis will be fully analogous to that already carried out above for the setup of Fig. 13. Integrating out the phase variable $\varphi(x)$ at all points along the wire except for its value at $x = L$, we arrive at the reduced effective action

$$S_R + S_J = \frac{1}{2}\,\mathrm{tr}\left[\varphi\, G_0^{-1}\varphi\right] - E_J \int_0^{1/T} d\tau \cos(\varphi - \phi)\,, \tag{257}$$

with

$$G_0(\omega_n) = \frac{8\pi}{g\omega_n} \tanh\left(\frac{\omega_n L}{v}\right). \tag{258}$$

We observe that fluctuations in the phase variable are massive with $m_0 = gv/(8\pi L)$. The absence of a massless mode in our setup (in contrast to that in Fig. 13) is a direct consequence of phase pinning at $x = 0$, which prohibits uniform shifts of the phase inside the wire. Again, employing the SCHA-type of analysis, we define the trial action

$$S_{tr} = \frac{1}{2}\,\mathrm{tr}\left[(\varphi - \psi)(G_0^{-1} + m)(\varphi - \psi)\right], \tag{259}$$

where the variational parameter m accounts for the interaction-induced effective mass for the φ-mode and ψ determines the average value of the phase difference. Evaluating the free energy of the system as a function of these two parameters and minimizing it with respect to both m and ψ, we arrive at the following SCHA equations:

$$E_J \cos(\psi - \phi) \exp\left(-\frac{G(0)}{2}\right) - m = 0\,, \tag{260}$$

$$E_J \sin(\psi - \phi) \exp\left(-\frac{G(0)}{2}\right) + \frac{gv}{8\pi L}\,\psi = 0\,, \tag{261}$$

where

$$G(0) = T\sum_{\omega_n} \big(G_0^{-1}(\omega_n) + m\big)^{-1}. \tag{262}$$

As before, the effect of phase fluctuations reduces to effective renormalization of E_J by the factor $\exp(-G(0)/2)$. The

supercurrent I is then found from the equation

$$I = \frac{gev}{4\pi L}\,\psi\,. \tag{263}$$

At $L \lesssim v/\Delta$, phase fluctuations are strongly suppressed and the system remains in the mean-field regime. In the opposite limit of large L, the solution of Eqn (260) exhibits two qualitatively distinct regimes. At $g < 4$, we find $|m| \ll v/L$. Therefore, the emergent mass is negligible, and the effect of fluctuations is purely Gaussian. The equation of motion (261) is then rewritten as

$$E_J \sin(\psi - \phi)\left(\frac{\Delta L}{v}\right)^{-4/g} + \frac{gv}{8\pi L}\,\psi = 0\,. \tag{264}$$

In the limit of small E_J interesting for us, we may readily set $8\pi E_J/(g\Delta) < 1$. In this case, the sine term is renormalized to zero faster than the kinetic inductance contribution $\propto L^{-1}$, and, hence, we obtain

$$I(\phi) = 2eE_J\left(\frac{v}{\Delta L}\right)^{4/g}\sin\phi\,. \tag{265}$$

This expression demonstrates that, for $g < 4$, phase fluctuations (i) modify the current–phase relation, making it sine-like instead of sawtooth-like, and (ii) yield a decrease in supercurrent compared to the standard Josephson formula $I(\phi) = 2eE_J\sin\phi$ that applies in the limit $L \to 0$. In addition, we observe that, in the presence of fluctuations, the supercurrent (265) decays faster with increasing L than the standard mean field dependence $I \propto 1/L$.

Let us now turn to the case $g > 4$. Resolving Eqn (260) in the limit $L \to \infty$, we obtain

$$m = \begin{cases} \left[E_J\cos(\psi-\phi)\left(\dfrac{8\pi}{\Delta g}\right)^{4/g}\right]^{g/(g-4)}, & \cos(\psi-\phi) > 0\,, \\ -\dfrac{gv}{8\pi L} + o\left(\dfrac{1}{L}\right), & \cos(\psi-\phi) < 0\,. \end{cases} \tag{266}$$

This solution remains valid only as long as L exceeds the length scale

$$L^* = \frac{v}{\Delta}\left(\frac{g}{\pi g_N}\right)^{g/(g-4)} \tag{267}$$

(cf. Eqn (248)). This length separates the regime $L > L^*$, where fluctuations yield non-Gaussian renormalization of the interaction potential from the Gaussian regime $L \ll L^*$, where $|m| \ll gv/8\pi L$. As long as $v/\Delta \ll L \ll L^*$, the current is again given by Eqn (265).

For $g > 4$, the renormalized Josephson coupling energy decreases more slowly than $1/L$ and at $L \sim L^*$ it becomes of the same order as the kinetic inductance contribution. At even larger distances, mass renormalization saturates to the value defined in (266). The kinetic inductance contribution, on the contrary, decreases as $1/L$. Therefore, at $L \gg L^*$, the phase is pinned to the lowest minimum of the renormalized Josephson junction potential, i.e., we have $\psi = \phi$. In this case, the current–phase relation reduces to the standard mean field form (249).

Finally, we note that the effects of QPS inside the superconducting nanowire are analyzed in exactly the same manner as was already done above in Section 9.4, except we should now distinguish two phases, $g < 4$ and $4 < g < 16$ (instead of $g < 2$ and $2 < g < 16$), and replace the expression for L^* (248) by Eqn (267).

For $g < 4$, only one correlation length (253) exists in our problem. At $L \ll L_c$, QPS effects are irrelevant, and the supercurrent suppression is merely due to smooth phase fluctuations. In this limit, Eqn (265) applies, and the supercurrent decays as a power law with increasing L. As soon as L exceeds L_c, quantum phase slips come into play, and the supercurrent decay becomes exponential with L according to Eqn (255).

At $4 < g < 16$, there are already two different correlation lengths, L^* and L_c. The first one diverges as $g \to 4$, while the second tends to infinity at $g \to 16$. Depending on the relation between these two lengths, different regimes can occur.

Consider, for example, the limit $L^* \ll L_c$, which can always be realized for sufficiently large values of g_ξ. In this case, at shorter length scales $L < L^*$, only smooth phase fluctuations affect the supercurrent, causing its power-law suppression with increasing L and the sinusoidal current–phase relation (see Eqn (265)). At $L^* < L < L_c$, both smooth phase fluctuations and quantum phase slips are irrelevant, and the supercurrent is defined by the standard mean field result $I \propto 1/L$ (249) describing the sawtooth-shaped current–phase relation. Finally, at $L \gg L_c$, the current is exponentially suppressed, and the current–phase relation again reduces to the sine form (255).

8.6 Discussion

The above analysis demonstrates that superconducting properties of metallic nanowires depend not only on their parameters but also on the topology of the experimental setup and on the way the experiment is performed. The ability of the wire to carry supercurrent also varies at different length scales, being affected by different kinds of fluctuations, including, on the one hand, sound-like collective plasma modes forming a quantum dissipative environment for electrons inside the wire and, on the other hand, quantum phase slips. As the bath of plasma modes is (almost) Ohmic, the low temperature system behavior resembles that involving a Schmid-like dissipative QPT [41, 76] either at $g = 2$ or at $g = 4$, depending on the setup under consideration. The presence of quantum phase slips naturally leads to a BKT-type quantum phase transition at $g = 16$ [12].

While the system displayed in Fig. 13 allows for unrestricted fluctuations in the superconducting phase, the setup in Fig. 16 effectively pins the phase at one of the wire ends. In the former case, a gapless Ohmic mode (associated with uniform phase shifts along the wire) appears at any L. Fluctuations associated with this gapless mode cause a Schmid-like QPT at $g = 2$. As a result, the wire completely loses superconductivity at $g < 2$, whereas the phase with $2 < g < 16$ is mixed, i.e., it is nonsuperconducting in the long length limit and superconducting at shorter scales, even though the gapless mode causes additional suppression of current in the limit $L \to 0$. Comparing this situation with the one encountered for the structure of Fig. 16, we observe that, in the latter case, superconductivity is greatly enhanced as a result of the soft mode suppression due to phase pinning. This effect turns the QPT into a transition between 'less' and 'more' superconducting phases at $g = 4$. Note that a similar phase transition was also discussed in Ref. [81] in the context of superconducting nanorings interrupted by a Josephson junction.

9. Quantum phase slips in capacitively coupled superconducting nanowires

Let us now extend our analysis of QPS-related effects to yet another structure, which consists of capacitively coupled superconducting nanowires. We will demonstrate that quantum fluctuations in one of the two wires effectively 'add up' to those of another one even without any direct electric contact between them, thereby giving rise to a number of interesting effects, such as splitting of plasmon modes and interaction-induced SIT shifting in each of the wires.

9.1 The model

Consider a system of two long superconducting nanowires that are parallel to each other, as schematically shown in Fig. 17. As before, the wires are described by geometric capacitances C_1 and C_2 (per unit wire length) and kinetic inductances $\mathcal{L}_1$ and $\mathcal{L}_2$ (times length) effectively representing the two transmission lines. Capacitive coupling between these two nanowires is accounted for by the mutual capacitance C_m. Generalizing our analysis in Section 4.1 to the above structure, we arrive at the contribution to the system Hamiltonian that keeps track of both electric and magnetic energies in these coupled transmission lines. It reads [82, 83]

$$\hat{H}_\mathrm{TL} = \frac{1}{2}\sum_{i,j=1,2}\int \mathrm{d}x \left[\mathcal{L}_{ij}^{-1}\hat{\Phi}_i(x)\hat{\Phi}_j(x) + \frac{1}{\Phi_0^2}\, C_{ij}^{-1}\left(\partial_x\hat{\chi}_i(x)\partial_x\hat{\chi}_j(x)\right)\right], \tag{268}$$

where x is the coordinate along the wires, and $\mathcal{L}_{ij}$ and C_{ij} denote the matrix elements of the inductance and capacitance matrices

$$\check{\mathcal{L}} = \begin{pmatrix} \mathcal{L}_1 & 0 \\ 0 & \mathcal{L}_2 \end{pmatrix}, \quad \check{C} = \begin{pmatrix} C_1 & C_\mathrm{m} \\ C_\mathrm{m} & C_2 \end{pmatrix}. \tag{269}$$

As before, Hamiltonian (268) is expressed in terms of the dual operators $\hat{\chi}(x)$ and $\hat{\Phi}(x)$ which obey the canonical commutation relation

$$\left[\hat{\Phi}_i(x), \hat{\chi}_j(x')\right] = -\mathrm{i}\delta_{ij}\Phi_0\delta(x-x'). \tag{270}$$

Provided the wires are thick enough, the low energy Hamiltonian in Eqn (268) is sufficient. However, for thinner wires, one should also account for the effect of quantum phase slips. The corresponding contribution to the total Hamiltonian for our system can be expressed in the form (cf. Eqn (79))

$$\hat{H}_\mathrm{QPS} = -\sum_{j=1,2}\gamma_j\int \mathrm{d}x\, \cos\left(\hat{\chi}_j(x)\right), \tag{271}$$

where

$$\gamma_j \sim \frac{g_{j\xi}\Delta}{\xi}\exp\left(-a g_{j\xi}\right), \quad a\sim 1, \quad j=1,2 \tag{272}$$

are the QPS amplitudes per unit wire length, Δ is the superconducting order parameter in each of the wires, $g_{j\xi} = R_q/R_{j\xi}$, and $R_{j\xi}$ is the normal state resistance of the jth wire segment equal in length to the superconducting coherence length ξ. The total Hamiltonian for the system under consideration equals the sum of the two terms in Eqns (268) and (271),

$$\hat{H} = \hat{H}_\mathrm{TL} + \hat{H}_\mathrm{QPS}, \tag{273}$$

representing an effective sine-Gordon model, which will be treated below.

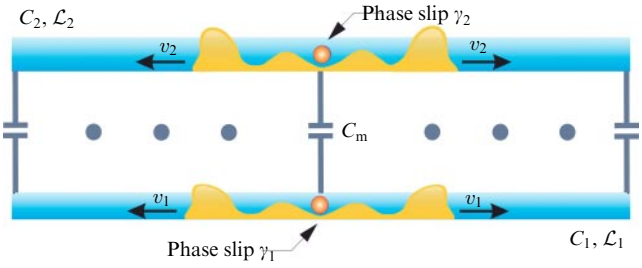

Figure 17. Two capacitively coupled superconducting nanowires.

9.2 Plasma mode splitting

Any QPS event causes a redistribution of charges inside the wire and generates a pair of voltage pulses propagating simultaneously in opposite directions along a wire with velocity v (see also Fig. 18a). In a single wire, this process is controlled, e.g., by wave equation (188) for the operator $\hat{\chi}$. In the case of two capacitively coupled wires, a QPS event in one of the wires generates voltage pulses in *both wires*. The corresponding generalization of wave equation (188) for the operators $\hat{\chi}_{1,2}$ in each of the two wires follows directly from system Hamiltonian (268), and the corresponding voltage operators $\hat{V}_{1,2}$ read

$$\hat{V}_i(t) = \frac{1}{\Phi_0}\sum_{j=1,2} C_{ij}^{-1}\left(\partial_x\hat{\chi}_j(x_1,t) - \partial_x\hat{\chi}_j(x_2,t)\right). \tag{274}$$

It will be convenient for us to move to the phase representation and express the corresponding equation of motion for the phases $\varphi_{1,2}$ in both wires in the form (cf., e.g., Eqn (86))

$$\left(\check{1}\partial_t^2 - \check{\mathcal{V}}^2\partial_x^2\right)\begin{pmatrix}\varphi_1(x,t)\\ \varphi_2(x,t)\end{pmatrix} = 0, \tag{275}$$

where $\check{\mathcal{V}} = (\check{C}\check{\mathcal{L}})^{-1/2}$ is the velocity matrix that accounts for plasmon modes propagating along the wires. Assume now that a QPS event occurs at the initial time moment $t=0$ at the point $x=0$ inside the first wire. As we just discussed, at $t>0$, voltage pulses originating from this QPS event will propagate in both wires. Resolving Eqn (275) together with the proper initial condition corresponding to a QPS event (cf., e.g., Eqn (87)), we arrive at the following picture.

In the first wire, each of the two voltage pulses propagating in opposite directions turns out to be split into two pulses of the same sign propagating with different velocities v_+ and v_-, as also illustrated in Fig. 18b. Each of the voltage pulses generated in the second wire by a QPS event in the first one is also split into two, and they also propagate with two different velocities v_+ and v_-; however, the signs of these voltage pulses are now opposite to each other (Fig. 18c). The velocities of these split plasmon modes are determined by the eigenvalues

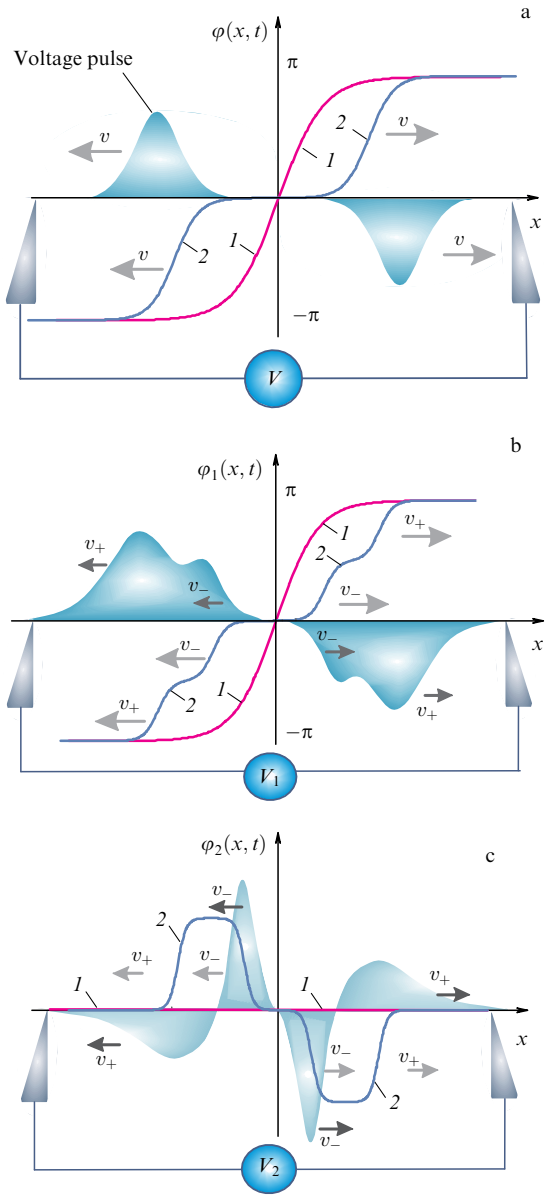

Figure 18. (Color online.) Time-dependent phase configurations describing a QPS event at $t = 0$ (red curve *1*) and $t > 0$ (blue curve *2*) together with propagating voltage pulses generated by this QPS event in a single superconducting nanowire (a) and in the first of two capacitively coupled superconducting nanowires (b). In the case of two wires, each of the voltage pulses is split into two propagating with different velocities $v_\pm$. (c) Time-dependent phase configurations at $t = 0$ (red curve *1*) and $t > 0$ (blue curve *2*) together with propagating voltage pulses in the second of two capacitively coupled superconducting nanowires generated by a QPS event in the first one.

of the velocity matrix $\check{\mathcal{V}}$. They read [84]

$$v_\pm = \frac{1}{2\kappa}\left[\sqrt{v_1^2 + v_2^2 + 2v_1v_2\kappa} \pm \frac{\sqrt{(v_1^2 - v_2^2)^2 + 4C_m^2 v_1^2 v_2^2/(C_1C_2)}}{\sqrt{v_1^2 + v_2^2 + 2v_1v_2\kappa}}\right], \tag{276}$$

where $\kappa = \sqrt{1 - C_m^2/(C_1C_2)}$ and $v_i = 1/\sqrt{C_i\mathcal{L}_i}$ $(i = 1, 2)$ is the velocity of the Mooij–Schön modes in the ith wire for $C_m \to 0$. In the case of identical wires with $C_1 = C_2 = C$ and $\mathcal{L}_1 = \mathcal{L}_2 = \mathcal{L}$, result (276) reduces to a particularly simple form:

$$v_\pm = \frac{1}{\sqrt{\mathcal{L}(C \mp C_m)}}\,. \tag{277}$$

This expression indicates that one of these velocities may strongly increase, provided the wires are located close enough to each other, in which case the cross-capacitance C_m may become of order C. In the absence of inter-wire interaction, we have $\kappa = 1$, and Eqn (276) obviously yields $v_+ = v_1$ and $v_- = v_2$.

9.3 Quantum phase transitions: renormalization group analysis

Let us now turn to the issue of a superconductor–insulator QPT in capacitively coupled superconducting nanowires with proliferating quantum phase slips. As we just demonstrated, the presence of capacitive coupling between nanowires may significantly affect plasmon propagation in our system and, hence, alter the interaction between quantum phase slips. In this case, the SIT in each of the wires is controlled not only by the parameters of the corresponding wire but also by those of the neighboring one, as well as by mutual capacitance. Interestingly enough, superconducting nanowires with properly chosen parameters may turn insulating once they are brought sufficiently close to each other [83].

In order to quantitatively describe QPT in coupled superconducting nanowires, we will employ the renormalization group (RG) analysis. This approach is well developed and has been successfully applied to a variety of problems in condensed matter theory, e.g., the problem of weak Coulomb blockade in tunnel [41, 85–87] and non-tunnel [88–90] barriers between normal metals or that of a dissipative phase transition in resistively shunted Josephson junctions [41, 76, 91, 92]. In the case of superconducting nanowires, QPT was described in [12] with the aid of RG equations equivalent to those initially developed for two-dimensional superconducting films [11] which exhibit classical BKT phase transition driven by temperature. In contrast, as we already discussed above, the quantum SIT in quasi-one dimensional superconducting wires is controlled by the parameter λ, proportional to the square root of the wire cross section s.

Provided the two superconducting wires depicted in Fig. 17 are decoupled from each other, i.e., for $C_m \to 0$, one should expect two independent QPTs to occur in these two wires at $\lambda_1 = 2$ and at $\lambda_2 = 2$, respectively, where $\lambda_{1,2} = (R_q/8)\sqrt{C_{1,2}/\mathcal{L}_{1,2}}$. In the presence of capacitive coupling between the wires, these two QPTs get modified. In order to account for these modifications, let us express the grand partition function of our system $\mathcal{Z} = \mathrm{tr}\,\exp(-\hat{H}/T)$ in terms of the path integral

$$\mathcal{Z} = \int D\chi_1 \int D\chi_2 \exp\left(-S[\chi_1, \chi_2]\right), \tag{278}$$

where

$$S = \frac{1}{2\Phi_0^2}\sum_{i,j=1,2}\int \mathrm{d}x\,\mathrm{d}\tau\left(\xi\Lambda\mathcal{L}_{ij}\partial_\tau\chi_i\partial_\tau\chi_j + \frac{1}{\xi\Lambda}\,C_{ij}^{-1}\partial_x\chi_i\partial_x\chi_j\right) - \sum_{i=1,2} y_i\int \mathrm{d}x\,\mathrm{d}\tau\,\cos\chi_i \tag{279}$$

is the effective action corresponding to Hamiltonian (273) and $y_i = \gamma_i \xi/\Lambda$ denotes the effective fugacity for the gas of quantum phase slips in the ith wire. For the sake of convenience, in Eqn (279), we rescaled the spatial coordinate in units of x_0, i.e., $x \to x\xi$, and the time coordinate in units of τ_0, i.e., $\tau \to \tau/\Lambda$.

As usual, let us divide the χ-variables into fast and slow components $\chi_i = \chi_i^{\rm f} + \chi_i^{\rm s}$, where

$$\chi_i^{\rm f}(x,\tau) = \int_{\Lambda<\omega^2+q^2<\Lambda+\delta\Lambda} \frac{{\rm d}\omega\,{\rm d}q}{2\pi}\,\chi_{\omega,q}\exp\left({\rm i}\omega\tau + {\rm i}qx\right),$$

$$\chi_i^{\rm s}(x,\tau) = \int_{\omega^2+q^2<\Lambda} \frac{{\rm d}\omega\,{\rm d}q}{2\pi}\,\chi_{\omega,q}\exp\left({\rm i}\omega\tau + {\rm i}qx\right).$$

Assuming $\delta\Lambda/\Lambda \ll 1$, expanding in $\chi_i^{\rm f}$, and integrating these fast variables out, we employ the perturbation theory in $y_{1,2}$ and observe that, in order to account for the leading order corrections, it suffices to evaluate the following matrix Green's function at coincident points

$$\check{G}^f(0,0) = \Phi_0^2 \int \frac{{\rm d}\omega\,{\rm d}q}{(2\pi)^2}\left(\xi\Lambda\check{\mathcal{L}}\omega^2 + \frac{1}{\xi\Lambda}\,\check{C}^{-1}q^2\right)^{-1} = 2\,\frac{\delta\Lambda}{\Lambda}\,\check{\lambda}\,, \tag{280}$$

where $\check{\lambda} = (R_q/8)\check{\mathcal{V}}\check{C}$. The matrix $\check{\lambda}$ reads

$$\check{\lambda} = \frac{1}{\sqrt{1/v_1^2 + 1/v_2^2 + 2\kappa/(v_1 v_2)}} \times \begin{pmatrix} \lambda_1\left(\dfrac{1}{v_1} + \dfrac{\kappa}{v_2}\right) & \dfrac{R_q C_{\rm m}}{8} \\ \dfrac{R_q C_{\rm m}}{8} & \lambda_2\left(\dfrac{1}{v_2} + \dfrac{\kappa}{v_1}\right) \end{pmatrix}. \tag{281}$$

Following the standard analysis [11] and proceeding to bigger and bigger scales Λ, we eventually arrive at the following RG equations for the QPS fugacities y_1 and y_2:

$$\frac{{\rm d}y_i}{{\rm d}\log\Lambda} = (2-\lambda_{ii})\,y_i\,, \quad i = 1,2\,, \tag{282}$$

where λ_{11} and λ_{22} are diagonal elements of the matrix $\check{\lambda}$. Note that, here, we restrict our RG analysis to the lowest order in $y_{1,2}$, in which case other parameters of our problem remain unrenormalized. It follows immediately from Eqns (282) that our system exhibits two BKT-like QPTs at $\lambda_{11} = 2$ and $\lambda_{22} = 2$. For the first wire, the corresponding phase transition point is fixed by the condition [83]

$$\lambda_1 = 2\,\frac{\sqrt{1 + v_1^2/v_2^2 + 2\kappa\, v_1/v_2}}{1 + \kappa\, v_1/v_2}\,. \tag{283}$$

The same condition for the second wire is derived from Eqn (283) simply by interchanging the indices $1 \leftrightarrow 2$.

These results allow the conclusion that, in the presence of capacitive coupling, quantum fluctuations in one of these wires tend to decrease the superconducting properties of the other one. As a result, the SIT in both wires occurs at larger values of $\lambda_{1,2}$ than in the absence of such coupling. Equation (283) demonstrates that the magnitude of this effect depends on the ratio of the plasmon velocities in the two wires v_1/v_2 and on the strength of the capacitive coupling

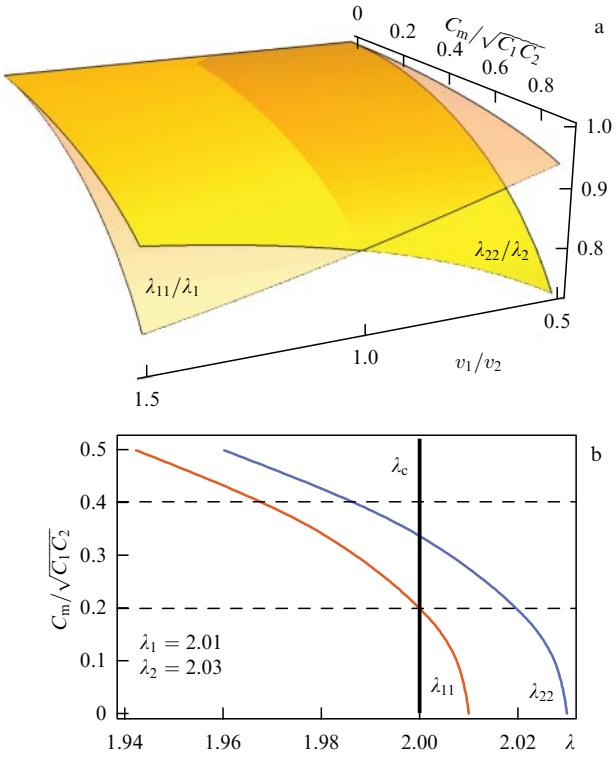

Figure 19. (a) Critical surfaces corresponding to SIT at $\lambda_{11} = 2$ and $\lambda_{22} = 2$. (b) Phase diagram for two capacitively coupled superconducting nanowires with $\lambda_1 = 2.01$ and $\lambda_2 = 2.03$. Both curves $\lambda_{11}(C_{\rm m})$ and $\lambda_{22}(C_{\rm m})$ decrease and cross critical line $\lambda_{\rm c} = 2$ with increasing mutual capacitance $C_{\rm m}$.

controlled by $C_{\rm m}$. Provided the wire cross sections s_1 and s_2 differ strongly, the plasmon velocities $v_i \propto \sqrt{s_i}$ also differ considerably. Provided, for example, the first wire is much thinner than the second one, we have $v_1 \ll v_2$, and, hence, the QPT condition (283) in the first wire remains almost unaffected for any capacitive coupling strength. If, on the contrary, the first wire is much thicker than the second one, then we have $v_1 \gg v_2$, and condition (283) reduces to $\lambda_1 \simeq 2/\sqrt{1 - C_{\rm m}^2/(C_1 C_2)}$, implying that the critical value λ_1 can considerably exceed 2 for sufficiently large values of $C_{\rm m}$.

It is fairly obvious that capacitive coupling depends on the distance between the wires. While at large distances this coupling is negligible, as the wires get closer to each other, the value of $C_{\rm m}$ increases, and, hence, their mutual influence increases as well. Let us choose the wire parameters in such a way that for $C_{\rm m} = 0$ both λ_1 and λ_2 slightly exceed 2, i.e., the wires remain in the superconducting phase, being relatively close to the SIT. Moving the wires closer to each other, we 'turn on' capacitive coupling between them and, hence, decrease both values λ_{11} and λ_{22} to below 2. As a result, two superconducting wires become insulating as soon as they are brought sufficiently close to each other. This remarkable physical phenomenon is illustrated by the phase diagram in Fig. 19.

We can also add that transport properties can be investigated in exactly the same manner as in the case of a single nanowire. Generalization of the technique [12] is straightforward and yields

$$R_i(T) \propto \gamma_i^2 T^{2\lambda_{ii}-3}\,, \quad i = 1,2\,, \tag{284}$$

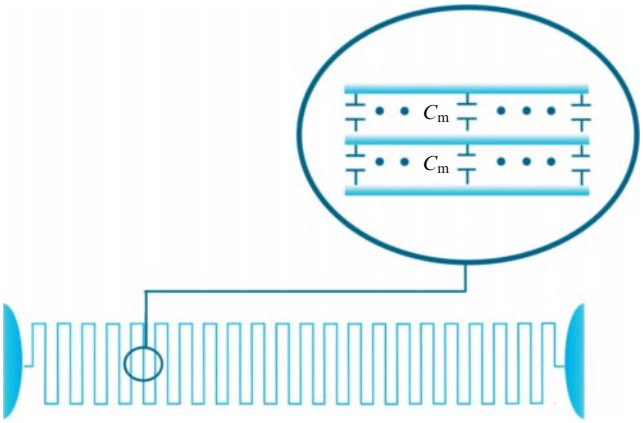

Figure 20. Superconducting nanowire in the form of a meander.

where $R_i(T)$ is the linear resistance of the ith wire. This result remains applicable either for $\lambda_{ii} > 2$ or for any λ_{ii} at sufficiently high temperatures.

The effects discussed here can be observed in a variety of structures involving superconducting nanowires. For instance, superconducting nanowires in the form of a meander are quite frequently employed in experiments (see, e.g., Ref. [93]). Different segments of such a wire remain parallel to each other, being close enough to develop electromagnetic coupling. One can expect, therefore, that the wire of such a geometry should be 'less superconducting' than the same wire that has the form of a straight line.

Let us first mimic the behavior of the wire depicted in Fig. 20 by considering three identical capacitively coupled superconducting nanowires that are parallel to each other. For simplicity we will assume the nearest neighbor interaction, i.e., the second (central) nanowire is coupled to both the first and the third nanowires via the mutual capacitance C_m, whereas the latter two are decoupled from each other. The quantum properties of this system are described by the same effective action (279), where the inductance and capacitance matrices now read

$$\check{\mathcal{L}} = \begin{pmatrix} \mathcal{L} & 0 & 0 \\ 0 & \mathcal{L} & 0 \\ 0 & 0 & \mathcal{L} \end{pmatrix}, \qquad \check{C} = \begin{pmatrix} C & C_m & 0 \\ C_m & C & C_m \\ 0 & C_m & C \end{pmatrix}, \tag{285}$$

and the summation runs over the indices $i, j = 1, 2, 3$. Proceeding along the same lines as above, we again arrive at Eqn (280), where the diagonal elements of the matrix $\check{\lambda}$ now read [83]

$$\lambda_{22} = \frac{\lambda}{2}\left(\sqrt{1 - \frac{\sqrt{2}\,C_m}{C}} + \sqrt{1 + \frac{\sqrt{2}\,C_m}{C}}\right), \tag{286}$$

$\lambda_{11} = \lambda_{33} = \lambda/2 + \lambda_{22}/4$, and $\lambda = g/8$ with g defined in (3). We again recover the RG equations (282), now with $i = 1, 2, 3$. When combined with Eqn (286), these RG equations demonstrate that, in the presence of capacitive coupling between nanowires, the SET in the central nanowire occurs at $\lambda_{22} = 2$, implying $\lambda > 2$, similarly to the case of two coupled nanowires.

The RG equation (282) for $i = 2$ combined with (286) also accounts for the QPT in the wire having the form of a meander, displayed in Fig. 20. In this case, within the approximation of the nearest neighbor, when capacitive interaction is only between the wire segments, the QPT occurs at

$$\lambda = \frac{4}{\sqrt{1 - \sqrt{2}\,C_m/C} + \sqrt{1 + \sqrt{2}\,C_m/C}}, \tag{287}$$

i.e., the critical value of the parameter λ exceeds 2 for any $C_m \neq 0$. The approximation of the nearest neighbor interaction appears to be well justified in the limit $C_m \ll C$. For stronger interactions with $C_m \sim C$, this approximation becomes insufficient for a quantitative analysis. Qualitatively, our key observations should also remain applicable in this case: a nanowire in the form of a straight line with λ slightly exceeding the critical value 2 should demonstrate superconducting-like behavior with $R(T) \propto T^{2\lambda-3}$ [12], whereas the wire with exactly the same parameters may turn insulating, provided it has the form of a meander with capacitive coupling between its segments.

10. Concluding remarks

In this review, we have made an effort to cover a number of recent developments related to the quantum properties of superconducting nanowires, emphasizing fundamental aspects of the theory of such systems. Unlike the case of bulk superconductors, the low temperature physics of quasi-one-dimensional nanowires and nanorings is essentially determined by quantum fluctuations, which are, in turn, controlled by two different parameters, the dimensionless normal state conductance of wire segment g_ξ (2) and dimensionless wire admittance g (3). Both these parameters decrease with decreasing wire cross section, making quantum fluctuations progressively more pronounced.

Provided parameter g_ξ remains very large, the low temperature behavior of the system is determined by small (Gaussian) quantum fluctuations in the phase of the order parameter which, for not very large values of g, significantly affect the electron density of states in superconducting nanowires and cause supercurrent noise in superconducting nanorings. As soon as dimensionless conductance g_ξ becomes not too large, quantum phase slips come into play. As a result, current-biased superconducting nanowires acquire a nonzero resistance and exhibit shot noise of the voltage. These phenomena can be conveniently interpreted in terms of tunneling of quantum fluxons (i.e., the flux quanta Φ_0) across the nanowire. In the context of phase–charge duality, these fluxons can be treated as effective quantum 'particles' exactly dual to Cooper pairs with charge $2e$. Such 'particles' obey complicated full counting statistics which, however, reduces to Poissonian one in the zero frequency limit.

Quantum phase slips may strongly affect both the supercurrent and its fluctuations in superconducting nanorings. This effect can be particularly pronounced if QPSs remain unbound, i.e., for $g < 16$ or, equivalently, for $\lambda < 2$. In this case and provided the ring radius exceeds the critical value R_c (119), even at $T \to 0$, strong quantum fluctuations essentially 'dephase' and suppress supercurrent that could flow across the ring.

The same nonperturbative length scale L_c (253) emerges in superconducting nanowires. For $g < 16$ and $T \to 0$, such nanowires do show an insulating behavior at scales exceeding the typical size of a 'superconducting domain' L_c, whereas at shorter length scales they may exhibit superconducting properties, albeit possibly affected by quantum fluctuations

in the phase. Hence, L_c can be interpreted as the *localization length for Cooper pairs*.

Direct experimental evidence of this kind of behavior and of the presence of this localization length was very recently observed in nominally uniform titanium nanowires [94]. Moreover, reanalyzing similar data reported previously in [22, 23, 95] for a large number of MoGe nanowires, we conclude that these data are also consistent with the above physical picture involving the correlation length L_c (253), i.e., the superconducting MoGe samples [22, 23, 95] obey the condition $L \lesssim L_c$, whereas the nonsuperconducting ones typically have a length L exceeding L_c. It is also important to emphasize that the nanowires employed in all these experiments did not contain any grains or dielectric barriers. Hence, similarly to normal metallic structures [1], these observations can be interpreted as a manifestation of a *weak Coulomb blockade* of Cooper pairs that may occur even in the absence of any tunnel barriers.

Further nontrivial properties of superconducting nanowires may be sensitive to the specific topology of the experimental setup under consideration. A number of interesting phenomena associated with quantum phase slips also occur in capacitively coupled superconducting nanowires.

Finally, it is worthwhile to point out that the nontrivial quantum properties of superconducting nanowires and nanorings open up plenty of possibilities for their applications in nanoelectronics, metrology, and quantum information technology. Various devices, such as single-charge transistors [51] and charge quantum interference devices [52] have already been demonstrated. Superconducting nanowires can also be employed as central elements for QPS flux qubits [55] as well as for creating a QPS-based standard of electric current [48, 53] and single photon detectors [93]. We are confident that intensive investigations of the intriguing fundamental properties of quasi-one-dimensional superconducting structures, as well as their technological applications, will continue in the near future.

Acknowledgements

We would like to thank K Yu Arutyunov, A Radkevich, and A Latyshev for their stimulating discussions and collaboration on a number of issues touched upon in this review. Our work was supported by the Russian Foundation for Basic Research, grant no. 19-12-50260.

References

1. Zaikin A D, Golubev D S *Dissipative Quantum Mechanics of Nanostructures*: *Electron Transport, Fluctuations, and Interactions* (Singapore: Jenny Stanford, Publ., 2019)
2. Arutyunov K Yu, Golubev D S, Zaikin A D *Phys. Rep.* **464** 1 (2008)
3. Larkin A, Varlamov A *Theory of Fluctuations in Superconductors* (Oxford: Clarendon Press, 2005)
4. Bezryadin A *J. Phys. Condens. Matter* **20** 043202 (2008)
5. Zaikin A D, in *Handbook of Nanophysics*: *Nanotubes and Nanowires* (Ed. K D Sattler) (Boca Raton, FL: CRC Press. Taylor and Francis Group, 2010) p. 40-1
6. Bezryadin A *Superconductivity in Nanowires*: *Fabrication and Quantum Transport* (Weinheim: Wiley-VCH Verlag, 2013)
7. Mermin N D, Wagner H *Phys. Rev. Lett.* **17** 1133 (1966)
8. Hohenberg P C *Phys. Rev.* **158** 383 (1967)
9. Berezinskii V S *Sov. Phys. JETP* **32** 493 (1971); *Zh. Eksp. Teor. Fiz.* **59** 907 (1971); *Sov. Phys. JETP* **34** 610 (1972); *Zh. Eksp. Teor. Fiz.* **61** 1144 (1971)
10. Kosterlitz J M, Thouless D J *J. Phys. C* **6** 1181 (1973)
11. Kosterlitz J M *J. Phys. C* **7** 1046 (1974)
12. Zaikin A D et al. *Phys. Rev. Lett.* **78** 1552 (1997)
13. van Otterlo A, Golubev D S, Zaikin A D, Blatter G *Eur. Phys. J. B* **10** 131 (1999)
14. Golubev D S, Zaikin A D *Phys. Rev. B* **64** 014504 (2001)
15. Golubev D S, Zaikin A D *Phys. Rev. B* **78** 144502 (2008)
16. Mooij J E, Schön G *Phys. Rev. Lett.* **55** 114 (1985)
17. Little W A *Phys. Rev.* **156** 396 (1967)
18. Langer J S, Ambegaokar V *Phys. Rev.* **164** 498 (1967)
19. McCumber D E, Halperin B I *Phys. Rev. B* **1** 1054 (1970)
20. Lukens J E, Warburton R J, Webb W W *Phys. Rev. Lett.* **25** 1180 (1970)
21. Newbower R S, Beasley M R, Tinkham M *Phys. Rev. B* **5** 864 (1972)
22. Bezryadin A, Lau C N, Tinkham M *Nature* **404** 971 (2000)
23. Lau C N et al. *Phys. Rev. Lett.* **87** 217003 (2001)
24. Zgirski M et al. *Phys. Rev. B* **77** 054508 (2008)
25. Lehtinen J S et al. *Phys. Rev. B* **85** 094508 (2012)
26. Baumans X D A et al. *Nat. Commun.* **7** 10560 (2016)
27. Radkevich A, Semenov A G, Zaikin A D *Phys. Rev. B* **96** 085435 (2017)
28. Usadel K D *Phys. Rev. Lett.* **25** 507 (1970)
29. Belzig W et al. *Superlatt. Microstruct.* **25** 1251 (1999)
30. Dynes R C, Narayanamurti V, Garno J P *Phys. Rev. Lett.* **41** 1509 (1978)
31. Panyukov S V, Zaikin A D *J. Low Temp. Phys.* **73** 1 (1988)
32. Arutyunov K Yu et al. *J. Magn. Magn. Mater.* **459** 356 (2018)
33. Camarota B et al. *Phys. Rev. Lett.* **86** 480 (2001)
34. Semenov A G, Zaikin A D *Phys. Rev. B* **88** 054505 (2013)
35. Semenov A G, Zaikin A D *J. Phys. Condens. Matter* **22** 485302 (2010)
36. Scalapino D J, White S R, Zhang S *Phys. Rev. B* **47** 7995 (1993)
37. Resta R *J. Phys. Condens. Matter* **30** 414001 (2018)
38. Zaikin A D, Panyukov S V *Phys. Lett. A* **120** 306 (1987)
39. Averin D V, Odintsov A A *Phys. Lett. A* **140** 251 (1989)
40. Zaikin A D *J. Low Temp. Phys.* **80** 223 (1990)
41. Schön G, Zaikin A D *Phys. Rep.* **198** 237 (1990)
42. Mooij J E, Nazarov Yu V *Nat. Phys.* **2** 169 (2006)
43. Semenov A G, Zaikin A D *Low Temp. Phys.* **43** 805 (2017); *Fiz. Nizk. Temp.* **43** 1011 (2017)
44. Barone A, Paternò G *Physics and Applications of the Josephson Effect* (New York: Wiley, 1982)
45. Astafiev O V et al. *Nature* **484** 355 (2012)
46. Peltonen J T et al. *Phys. Rev. B* **88** 220506 (2013)
47. Lehtinen J S, Zakharov K, Arutyunov K Yu *Phys. Rev. Lett.* **109** 187001 (2012)
48. Shaikhaidarov R S et al. *Nature* **608** 45 (2022)
49. Il'ichev E V, Ryazanov V V, Astafiev O V *Phys. Rev. Lett.* **128** 159701 (2022)
50. Arutyunov K Yu, Lehtinen J S *Phys. Rev. Lett.* **128** 159702 (2022)
51. Hongisto T T, Zorin A B *Phys. Rev. Lett.* **108** 097001 (2012)
52. de Graaf S E et al. *Nat. Phys.* **14** 590 (2018)
53. Wang Z M, Lehtinen J S, Arutyunov K Yu *Appl. Phys. Lett.* **114** 242601 (2019)
54. Semenov A G, Zaikin A D *Phys. Scr.* **2012** (T151) 014022 (2012)
55. Mooij J E, Harmans C J P M *New J. Phys.* **7** 219 (2005)
56. Semenov A G, Zaikin A D *Phys. Rev. B* **84** 045416 (2011)
57. Averin D, Imam H T *Phys. Rev. Lett.* **76** 3814 (1996)
58. Martín-Rodero A, Levy Yeyati A, García-Vidal F J *Phys. Rev. B* **53** R8891 (1996)
59. Galaktionov A V, Zaikin A D *Phys. Rev. B* **82** 184520 (2010)
60. Blanter Ya M, Büttiker M *Phys. Rep.* **336** 1 (2000)
61. Semenov A G, Zaikin A D *Phys. Rev. B* **94** 014512 (2016)
62. Weiss U *Quantum Dissipative Systems* (Singapore: World Scientific, 2008) p. 207
63. Semenov A G, Zaikin A D *Fortschr. Phys.* **65** 1600043 (2017)
64. Controzzi D, Essler F H L, Tsvelik A M *Phys. Rev. Lett.* **86** 680 (2001)
65. Semenov A G, Zaikin A D *J. Supercond. Nov. Magn.* **30** 139 (2017)
66. Semenov A G, Zaikin A D *J. Supercond. Nov. Magn.* **31** 711 (2018)
67. Golubev D S et al. *Phys. Rev. B* **81** 184516 (2010)
68. Žonda M, Belzig W, Novotný T *Phys. Rev. B* **91** 134305 (2015)
69. Semenov A G, Zaikin A D *Phys. Rev. B* **99** 094516 (2019)
70. Galaktionov A V, Golubev D S, Zaikin A D *Phys. Rev. B* **68** 235333 (2003)

71. Averin D V, Nazarov Yu V, Odintsov A A *Physica B* **165–166** 945 (1990)
72. Bobbert P A, Fazio R, Schön G, Zaikin A D *Phys. Rev. B* **45** 2294 (1992)
73. Radkevich A, Semenov A G, Zaikin A D *Phys. Rev. B* **100** 014520 (2019)
74. Kleinert H *Electron. J. Theor. Phys.* **8** (25) 57 (2011)
75. Fisher M P A, Zwerger W *Phys. Rev. B* **32** 6190 (1985)
76. Schmid A *Phys. Rev. Lett.* **51** 1506 (1983)
77. Panyukov S V, Zaikin A D *Physica B* **152** 162 (1988)
78. Lukyanov S, Zamolodchikov A *Nucl. Phys. B* **493** 571 (1997)
79. Gogolin A O, Nersesyan A A, Tsvelik A M *Bosonization and Strongly Correlated Systems* (Cambridge: Cambridge Univ. Press, 1998)
80. Radkevich A, Semenov A G, Zaikin A D *J. Supercond. Nov. Magn.* **33** 2335 (2020)
81. Hekking F W J, Glazman L I *Phys. Rev. B* **55** 6551 (1997)
82. Latyshev A, Semenov A G, Zaikin A D *J. Supercond. Nov. Magn.* **33** 2329 (2020)
83. Latyshev A, Semenov A G, Zaikin A D *Beilstein J. Nanotechnol.* **11** 1402 (2020)
84. Latyshev A, Semenov A G, Zaikin A D *Beilstein J. Nanotechnol.* **13** 292 (2022)
85. Guinea F, Schön G *Europhys. Lett.* **1** 585 (1986)
86. Panyukov S V, Zaikin A D *Phys. Rev. Lett.* **67** 3168 (1991)
87. Hofstetter W, Zwerger W *Phys. Rev. Lett.* **78** 3737 (1997)
88. Kindermann M, Nazarov Yu V *Phys. Rev. Lett.* **91** 136802 (2003)
89. Golubev D S, Zaikin A D *Phys. Rev. B* **69** 075318 (2004)
90. Bagrets D A, Nazarov Yu V *Phys. Rev. Lett.* **94** 056801 (2005)
91. Bulgadaev S A *JETP Lett.* **39** 315 (1984); *Pis'ma Zh. Eksp. Teor. Fiz.* **39** 264 (1984)
92. Guinea F, Hakim V, Muramatsu A *Phys. Rev. Lett.* **54** 263 (1985)
93. Delacour C et al. *Nano Lett.* **12** 3501 (2012)
94. Arutyunov K Yu et al. *Commun. Phys.* **4** 146 (2021)
95. Bollinger A T et al. *Phys. Rev. Lett.* **101** 227003 (2008)